# Electrons in model nanostructures

Matthew James Paul Hodgson

Doctor of Philosophy

University of York
Physics

September 2016

# Abstract

For calculating the properties of solids and molecules, density functional theory (DFT) has become extremely popular because of its inherent computational efficiency. However, despite being in principle exact, an approximation must be introduced into DFT in practice. The accuracy of DFT has been key to its popularity; however, even for some of the simplest systems, using common approximations to the exchange-correlation (xc) functional may give inaccurate results. Therefore, we aim to contribute to the development of improved approximate xc functionals.

It is logical to begin by studying the most elementary of systems where the common approximate xc functionals require improvement, as one can model these systems exactly by solving the many-electron Schrödinger equation. By allowing us to study DFT and time-dependent DFT (TDDFT) in the absence of approximations for prototype systems, this approach provides insight into the fundamental principles of the theory, informing the development of new approximations.

We show that steps arise in the level of the exact xc potential: steps are known to be important for giving accurate electron and current densities, yet little about their origin is understood. We show that steps form due to a change in the 'local effective ionisation energy' of the electrons: this concept is well defined for strongly localised electrons. We find that the tendency of an electron to exclude others from its vicinity (electron localisation) is surprisingly high in our finite systems; hence, we develop an approximate functional that uses a measure of localisation as an ingredient, with the analytical form of the Kohn-Sham potential in the limit of complete localisation. Our functional, termed the mixed localisation potential, gives accurate electron and current densities for our test systems where local approximations are less valid. The approximation's success stems in part from its ability to reproduce steps in the xc potential.

# Contents

# List of Figures

# List of Tables

# List of Algorithms

# Acknowledgements

I'd like to thank, most of all, my supervisor Rex Godby and colleague James Ramsden, for their unique insight, excellent teaching and guidance.

I would also like to thank Piers Lillystone for his involvement with the very start of what would become iDEA, as well as Jack Wetherell, James Ramsden, Jacob Chapman, Tom Durrant, Mike Entwhistle, Matt Smith, Bradley Longstaff and Richard Lynn for their development of iDEA.

For helpful discussions I thank Phil Hasnip, James Ramsden and Jack Wetherell.

I thank Tom Durrant, Bradley Longstaff and Mike Entwistle for the work they did alongside me (please see the declaration for more detail); Mike led the work outlined in Chapter 5 following from Bradley, and Tom led the work outlined in Sections 7.2 and 7.3.

I thank Lizzie Brookes for her many hours of proofreading. Finally, I acknowledge funding from the Engineering and Physical Sciences Research Council (EPSRC).

# Declarations

I declare that the work presented in this thesis, except where otherwise stated, is based on my own research and has not been submitted previously for a degree in this or any other university. Parts of the work reported in this thesis have been published in: Physical Review B Rapid Communications and Physical Review B

Sections 4.1.1 describes collaborative work that has been submitted for publication: M. J. P. Hodgson, J. D. Ramsden, J. B. J. Chapman, P. Lillystone and R. W. Godby, 'Exact time-dependent density-functional potentials for strongly correlated tunneling electrons', *Physical Review B (Rapid Communications)* **88**, 241102(R) (2013). I participated fully in the development of the code and the formulation and analysis of the research and executed the calculations shown in the paper, and prepared the first draft of the paper.

Chapter 5 describes collaborative work that has been submitted for publication: M. T. Entwistle, M. J. P. Hodgson, J. Wetherell, B. Longstaff, J. D. Ramsden and R. W. Godby, 'Local density approximations from finite systems', submitted (2016). Sections 5.1-5.4 are adapted from that paper. I participated fully in the formulation and analysis of the research, and in the collaborative writing of the paper. Mike Entwistle executed most of the calculations shown in the paper, and prepared the first draft of the paper.

Chapter 6 describes collaborative work that has been published: M. J. P. Hodgson, J. D. Ramsden, J. B. J. Chapman, P. Lillystone and R. W. Godby, 'Exact time-dependent density-functional potentials for strongly correlated tunneling electrons', *Physical Review B (Rapid Communications)* **88**, 241102(R) (2013). Sections 6.1-6.3 are adapted from that paper. I participated fully in the formulation and analysis of the research and executed the calculations shown in the paper, and prepared the first draft of the paper.

Chapter 7 describes collaborative work that has been published: M. J. P. Hodgson, J. D. Ramsden, T. R. Durrant and R. W. Godby, 'Role of electron localization in density functionals', *Physical Review B (Rapid Communications)* **90**, 241107(R) (2014). Sections 7.4-7.7.1, 7.7.3, 7.7.4 and 7.7.6 are adapted from that paper. I participated fully in the formulation and analysis of the research and executed the calculations shown in the paper, and prepared the first draft of the paper. I also give thank to Daniele Torelli for his assistance with some of the calculations in this chapter.

Chapter 8 describes collaborative work that has been published: M. J. P. Hodgson, J. D. Ramsden and R. W. Godby, 'Origin of static and dynamic steps in exact Kohn-Sham potentials', *Physical Review B* **93**, 155146 (2016). Sections 8.1-8.7 are adapted from that paper. I participated fully in the formulation and analysis of the research and executed the calculations shown in the paper, and prepared the first draft of the paper.

# Chapter 1

# Introduction

Over the course of the past half-century, simulations have become one of the most important aspects of scientific research. The vast majority of *ab intio* material, chemical, and solid-state simulations use density functional theory (DFT) [1, 2] – an exact reformulation of many-body quantum mechanics – which owes its popularity to the computational benefits it has over other methods. DFT is even being applied to systems as large and complex as DNA. DFT works by mapping a real world system of interacting electrons onto an equivalent auxiliary system of noninteracting electrons. In principle, one can use the latter system to reproduce the densities of the former system exactly, for a minute fraction of the computational cost. In fact, in most cases, without these computational savings the calculation would not be possible. However, the success of DFT hinges on *approximating* one central unknown – to which various approximations exist. It is the aim of the work set out in this thesis to inform the development of improved approximations in DFT, in order for the theory to be used accurately to model a broader scope of phenomena.

As it stands, DFT can be used to accurately model a wide range of ground-state (lowest energy state) systems. However, experimental observations and theoretical evidence have shown that the approximations made within the theory become much less secure in the presence of strong correlation [3, 4, 5, 6, 7] and/or current flow [8, 9, 10, 11]. In particular, when applied to the flow of electrons through molecules, the approximations made in time-dependent DFT (TDDFT) [12, 13] lead to a particularly poor description of electronic properties.

Accurate approximations within (TD)DFT allow for more accurate simulations of chemicals and materials. Recent technological advancements mean the need for a fully quantum mechanical description of electronic properties in molecules has become critical.

## 1.1 Our strategy

We identify why the common approximations to the xc functional break down in certain circumstances, with the goal of contributing to the development of improved approximate density functionals, hence increasing the accuracy of the theory for challenging situations. We model simple systems, consisting of a few electrons, using many-body quantum me-

chanics in order to find the exact electron density[1]. The aim here is to study TDDFT in the absence of approximation for these elementary, but *broad*, scenarios. Each system studied is designed to either test or illustrate important *general* phenomena that are representative of the behaviour of electrons in realistic finite systems.

In order to carry out our investigations, we have developed a code that models electrons in one dimension[2]. We can choose any external potential, as well as any static perturbing field, and propagate the electrons through time. Our code, named iDEA[3] [14], is used for generating all computational results in this thesis (unless otherwise stated).

## 1.2 Outline

The following chapter outlines the fundamental aspects of quantum mechanics and (TD)DFT and the approximations made within these theories. Chapter 3 details in which situations these approximations disagree with experimental evidence – presenting the motivation for the work set out in the rest of the thesis. Chapter 4 gives a full description of our code and method.

Chapter 5 details our development of the simplest approximation to the xc functional – a local density approximation (LDA) [2]. We construct our LDAs from finite, one-dimensional systems with regions of homogenous density; they are used throughout the thesis as the benchmark for what local approximations can, and cannot, achieve, and as a means of determining which features of the exact xc potential are important for yielding accurate densities and currents.

Following on from the conclusions we reached in Chapter 5, Chapter 6 is an investigation of many-electron tunnelling using *exact* TDDFT. We find universal 'step' features in the Kohn-Sham potential that are missing from local approximations, as well as a large self-interaction correction (SIC), both due to strong electron localisation. We give insight into how approximate functionals, which aim to include steps and other 'non-LDA' features, can be constructed.

The prominent SIC of the exact xc potential stems from the tendency of our model electrons to exclude others from their local vicinity. We find that electron localisation is common in our finite systems, and that the electron localisation function (ELF), used in DFT calculations, is a useful indicator of this characteristic. Chapter 7, where we introduce our density functional – the mixed localisation potential (MLP), builds on our understanding of localisation. The MLP, used in the Kohn-Sham scheme, gives accurate electron densities for situations where the usual approximations do not, *e.g.*, systems that require steps in the Kohn-Sham potential, even in the time-dependent regime, such as disassociated molecules, charge transfer, electron tunnelling, to name a few. Furthermore, we indicate how the MLP, and the approximations made to construct the potential, can be progressed, capitalising on the promising performance of the method.

[1] By calculating the exact electron density, we can 'reverse engineer' TDDFT, *i.e.*, work backwards, starting with the electron density, and inspect differences between approximate and exact TDDFT (detail on this is given throughout the thesis).

[2] We detail the exact characteristics of what the code can model in Chapter 4.

[3] Interacting dynamic electrons approach.

Finally, Chapter 8 details the origin of steps, as well as other features in the exact Kohn-Sham potential from fundamental concepts in DFT, and to a lesser extent TDDFT. Here our aim is to offer an understanding of features of the exact Kohn-Sham potential, that can aid the development of further improved density functionals.

# Chapter 2

# Established theory

## 2.1 Many-body quantum mechanics

Quantum mechanics is undoubtably one of the most successful theories ever devised. As the theory is concerned with the nature of the most elementary building blocks of the universe, it is considered to be a fundamental description of nature. Hence, many phenomena and laws of physics, which describe the macroscopic world, can be derived from quantum mechanics.

Louis de Broglie first proposed the wave nature of matter in 1924 [15]. This idea was later combined with work done on quantisation by Planck and Einstein [16, 17] (among others) about two decades prior. This revolution in thinking would eventually lead to a new theory of matter, replacing the idea of particles with definite positions in space, with a view of waves and positional uncertainty. This theory, which became known as quantum mechanics, quickly established itself within physics by describing nature with unprecedented accuracy. Below we outline the concepts that underpin many-body quantum mechanics today and discuss the unavoidable approximations made when using the theory to describe complex systems. Then we introduce density functional theory, which in principle is equivalent to many-body quantum mechanics in its description of certain observables, namely electron densities and currents, but which differs in its level of approximation and cost of simulation.

### 2.1.1 Schrödinger's equation

The Schrödinger equation,

$$\hat{H}\Psi(\{\mathbf{r}\},\{\mathbf{R}\};t) = i\hbar\frac{\partial}{\partial t}\Psi(\{\mathbf{r}\},\{\mathbf{R}\};t), \tag{2.1}$$

describes, in theory, all material properties, provided certain limits (*i.e.*, non-relativistic speeds), where the many-body Hamiltonian is given by

$$\hat{H} = \sum_{j=1}^{N}\left[-\frac{\hbar^2}{2m_e}\nabla_j^2 + v_{\text{ext}}(\mathbf{r}_j,t)\right] + \sum_{j=1}^{N'}\left[-\frac{\hbar^2}{2M_j}\nabla_j^2 + v_{\text{ext}}(\mathbf{R}_j,t)\right] + \frac{e^2}{4\pi\varepsilon_0}\left[\sum_{j=1}^{N}\sum_{k>j}\frac{1}{|\mathbf{r}_j-\mathbf{r}_k|} + \sum_{j=1}^{N'}Z_j\left(\sum_{k>j}\frac{Z_k}{|\mathbf{R}_j-\mathbf{R}_k|} - \sum_{k=1}^{N}\frac{1}{|\mathbf{R}_j-\mathbf{r}_k|}\right)\right].$$

Equation (2.1) is the governing equation within the theory[1]. Here, $v_{\text{ext}}$ is the external potential applied to the system, $m_e$ and $M_j$ represent the electron and nucleus mass respectively, and $Z_j$ is the atomic number for a given atomic nucleus. From Eq. (2.1) one can, in theory, acquire the many-body wavefunction ($\Psi$; where $\mathbf{r}$ denotes the co-ordinates of an electron, and $\mathbf{R}$ denotes the co-ordinates of a nucleus), from which all the properties of the system can be derived. However, in practice Eq. (2.1) cannot be solved for *most* systems, even given certain approximations (see below). The difficulties lie with the interaction terms, which make solving Eq. (2.1) a computational problem that scales exponentially with the number of electrons ($N$) and nuclei ($N'$). It is therefore vital to make approximations which eliminate, or at the very least alleviate, this scaling problem in order for quantum mechanics to be a practical theory.

### 2.1.2 The Born-Oppenheimer approximation

Within electronic structure calculations, one of the most common approximations made is the Born-Oppenheimer approximation (BOA) [18]. The BOA assumes that, within a given molecule or atom, the motion of the nuclei and electrons are separable, owing to the mass of the proton being about 1836 times that of the electron. Therefore, when applying the BOA, one may consider the interaction of the nuclei with the electrons, and any interactions between nuclei, to be accounted for by the external potential. Hence, the electron's response to changes in the position of the nuclei are instantaneous – this is generally known as the *adiabatic* approximation. This simplification is well justified for most systems, and in particular the systems we study. Therefore, this approximation is used throughout all of the work set out in this thesis.

A correct application of the BOA allows one's focus to be on the quantum description of the electrons. As our goal is an accurate description of *electronic* properties, we choose the BOA as the starting point for our *ab initio* study of electrons within single molecules. However, while the BOA eliminates approximately half the number of variables on which the many-body wavefunction depends, the scaling problem persists owing to the electron-electron interaction.

## 2.2 Density functional theory

Density functional theory (DFT) is an exact reformulation of many-body quantum mechanics. DFT is a practical theory for calculating the ground-state density and energy of a quantum system by using the electron density to minimise the energy opposed to the many-body wavefunction. Below we outline the basic concepts of DFT, and detail what methods we use in our own investigations of finite molecules.

### 2.2.1 The Hohenberg-Kohn theorem

We have already established that the many-body wavefunction depends on the position of every electron within a given system. Realistically this could correspond to, of the order of,

[1] Here we are using Système Internationale units (S.I.). Henceforth we use atomic units (a.u.); $\hbar = 4\pi\varepsilon_0 = m_e = e^2 = 1$.

$10^{23}$ variables. As this problem scales exponentially with system variables, this level of complexity makes solving the Schrödinger equation for realistic systems impossible. Hohenberg and Kohn (HK) made a revolution in this matter in 1964 [1] – an innovation that would later earn Walter Kohn the 1998 Nobel Prize for Chemistry. They showed that stationary ground-state systems are fully described by the electron density – a function with only one variable $n(\mathbf{r})$.

As the system is uniquely defined by the electron density, we can define an energy functional $E[n]$, which when minimised yields the ground-state energy ($E_0$) and density ($n$), with $\int n(\mathbf{r})\ \mathrm{d}^3r = N$ as an enforced constraint ($N$ is the integer number of electrons, and the integral, with no limits, is over all space – this convention is used throughout the thesis, unless otherwise stated). The functional may be written as [19]:

$$E[n] \equiv F[n] + V[n] = \min \left\langle \Psi \left| \hat{T} + \hat{V}_{\mathrm{ee}} \right| \Psi \right\rangle + \int n(\mathbf{r})\, v(\mathbf{r})\ \mathrm{d}^3r, \tag{2.2}$$

where the internal-energy functional $F[n]$ is independent of the external potential $v$, $\hat{T}$ is the many-body kinetic energy operator, $\hat{V}$ is the external potential operator, and $\hat{V}_{\mathrm{ee}}$ is the electron-electron interaction operator.

The ground-state wavefunction can be considered as that which minimises $F[n]$, whilst reproducing the ground-state density. For a non-degenerate ground-state, this definition uniquely determines the ground-state wavefunction in terms of $n$, without explicitly specifying $v$. Hence, the density, opposed to the many-body wavefunction, can be used to determine the ground-state energy of the system. Furthermore, as the HK theorem shows that the potential uniquely determines the ground-state wavefunction, we can further infer that two different potentials *cannot* yield the same ground-state electron density.

As the density defines the system, one can acquire the ground-state energy and density from minimising the energy functional with respect to the density, as such

$$\frac{\delta E[n]}{\delta n} = 0. \tag{2.3}$$

### 2.2.2 Kohn-Sham theory

In 1965 Kohn and Sham developed a practical application of DFT using a single-particle theory [2], where the system of interacting electrons is mapped onto an auxiliary system of noninteracting electrons. The advantages of the Kohn-Sham approach over other formulations of quantum mechanics originate from this mapping. In theory one can acquire all densities exactly from the noninteracting system owing to the exchange and correlation potential (usually abbreviated as the correlation or xc potential), which we define below. The xc potential (an effective external potential experienced by the noninteracting electrons) ensures that the many-electron effects are taken into account in the noninteracting system. In fact, if the xc potential is known without any approximation, the many-body effects are reproduced exactly. In practice, however, the xc potential is seldom known, and certainly for most systems of interest the xc potential *must* be approximated.

In detailing the Kohn-Sham approach we will begin with the single-particle kinetic energy,

which can be found exactly from

$$T_s[\{\phi_i[n]\}] = -\tfrac{1}{2}\sum_{i=1}^{N}\int \phi_i^*(\mathbf{r})\nabla^2\phi_i(\mathbf{r})\,\mathrm{d}^3r, \tag{2.4}$$

where $\phi_i$ is the $i^{\text{th}}$ single-particle wavefunction (known as a Kohn-Sham orbital), found from solving the single-particle Schrödinger equations [known as the Kohn-Sham equations; see Eq. (2.10)]. Evidently Eq. (2.4) is an explicit orbital functional, and as these orbitals are functionals of the density, it is therefore an implicit density functional. We now rewrite the exact energy functional of Eq. (2.2) as

$$E[n] = T[n] + V_{\text{ee}}[n] + V[n] = T_s[\{\phi_i[n]\}] + U[n] + V[n] + E_{\text{xc}}[n], \tag{2.5}$$

where $E_{\text{xc}}[n]$ is the xc energy and $U[n]$ is the Hartree energy (which is known analytically; see below). Clearly from Eq. (2.5) the xc energy is compensating for the difference between the many-electron and single-electron kinetic energies, as well as the difference between the Coulomb energy and Hartree energy.

Using Eq. (2.5) one can rewrite the minimisation procedure for finding the ground-state density and energy as

$$0 = \frac{\delta E[n]}{\delta n} = \frac{\delta T_s[n]}{\delta n} + \frac{\delta U_{\text{H}}[n]}{\delta n} + \frac{\delta V[n]}{\delta n} + \frac{\delta E_{\text{xc}}[n]}{\delta n} = \frac{\delta T_s[n]}{\delta n} + v_{\text{s}}[n]. \tag{2.6}$$

This minimisation procedure is for a system of noninteracting electrons in an external potential $v_{\text{s}}$, which yields the same ground-state density and energy as the many-electron system provided

$$v_{\text{s}}(\mathbf{r}) = v_{\text{ext}}(\mathbf{r}) + v_{\text{H}}(\mathbf{r}) + v_{\text{xc}}(\mathbf{r}), \tag{2.7}$$

where $v_{\text{ext}}(\mathbf{r})$ is the external potential for the many-electron system, $v_{\text{H}}(\mathbf{r})$ is the Hartree potential, given by

$$v_{\text{H}}(\mathbf{r}) = \frac{\delta U_{\text{H}}[n]}{\delta n} = \int \frac{n(\mathbf{r}')\,\mathrm{d}^3r'}{|\mathbf{r}-\mathbf{r}'|}, \tag{2.8}$$

and $v_{\text{xc}}(\mathbf{r})$ is the xc potential, found from

$$v_{\text{xc}}(\mathbf{r}) = \frac{\delta E_{\text{xc}}[n]}{\delta n}. \tag{2.9}$$

Of these potentials only the xc potential is unknown, hence, *the accuracy of the method hinges on approximating this term*.

We have so far established that Kohn-Sham theory uses an effective external potential ($v_{\text{s}}$), known as the Kohn-Sham potential, which reproduces the same electron density as solving the many-electron Schrödinger equation for the same external potential. This is the only potential that the noninteracting Kohn-Sham electrons experience, hence, the Kohn-Sham equations can be written as

$$\left(-\tfrac{1}{2}\nabla^2 + v_{\text{s}}[n]\right)\phi_i = \varepsilon_i\phi_i, \tag{2.10}$$

where $\varepsilon_i$ is the $i^{\text{th}}$ eigen-energy corresponding to $\phi_i$. The electron density can be calculated

using the individual single-particle electron densities, as follows

$$n(\mathbf{r}) = \sum_{i=1}^{N} |\phi_i(\mathbf{r})|^2, \tag{2.11}$$

and the energy of the system can be found from

$$E[n] = \sum_{i=1}^{N} \varepsilon_i + E_{\mathrm{xc}} - \int n(\mathbf{r}) \left[ v_{\mathrm{xc}}(\mathbf{r}) + \tfrac{1}{2} v_{\mathrm{H}}(\mathbf{r}) \right] \mathrm{d}^3 r. \tag{2.12}$$

### 2.2.3 The exchange-correlation functional

We will now look more closely at the xc energy functional ($E_{\mathrm{xc}}[n]$), and some of the common approximations used for it. The xc energy can be broken up into two terms; the first ($E_{\mathrm{x}}$) is the energy corresponding to the exchange of particles adhering to Pauli's exclusion principle. An analytical form for this energy is known in terms of the Kohn-Sham orbitals (Fock term; see Section 2.3 on page 24):

$$E_{\mathrm{x}}[\{\phi_i[n]\}] = -\tfrac{1}{2} \sum_{j,k} \int \mathrm{d}^3 r \int \mathrm{d}^3 r' \frac{\phi_j^*(\mathbf{r}) \phi_k^*(\mathbf{r}') \phi_j(\mathbf{r}) \phi_k(\mathbf{r}')}{|\mathbf{r} - \mathbf{r}'|}, \tag{2.13}$$

however, no such expression is known explicitly in terms of the electron density. The second term is the correlation energy ($E_{\mathrm{c}}$), for which no analytic term is known. The exchange term, in the Kohn-Sham approach, accounts for the decrease in total energy of the interacting system due to the antisymmetrisation of the many-body wavefunction (as electrons are spin-half fermions, they obey Pauli's exclusion principle, meaning no two *same-spin* electrons can occupy the same state). And the correlation term accounts for the decrease in repulsive energy required to account for the overestimation of the repulsive Hartree energy between any electron pair. (Note, the correlation term also accounts for the difference between the noninteracting and interacting kinetic energies.)

The concept of exchange holes was introduced as an interpretation of the way that both exchange and correlation tend to exclude electrons from the vicinity of other electrons. This has the effect of causing same-spin electrons to 'avoid' each other; a concept we refer to as electron localisation later on. This gives rise to the definition of the xc hole $n_{\mathrm{xc}}(\mathbf{r}, \mathbf{r}')$, which describes the *decrease* in probability of finding an electron at position $\mathbf{r}'$ due to the presence of an electron at $\mathbf{r}$. The energy associated with this can be calculated from this Hartree-like expression between the electron density and the hole density:

$$E_{\mathrm{xc}}[n] = \tfrac{1}{2} \int \mathrm{d}^3 r \int \mathrm{d}^3 r' \frac{n(\mathbf{r}) n_{\mathrm{xc}}(\mathbf{r}, \mathbf{r}')}{|\mathbf{r} - \mathbf{r}'|}. \tag{2.14}$$

Equation (2.14) defines $n_{\mathrm{xc}}(\mathbf{r}, \mathbf{r}')$, and because there is always one electron in total excluded from the vicinity of $\mathbf{r}$ (owing to Pauli's exclusion principle), we can infer the sum rule $\int n_{\mathrm{xc}}(\mathbf{r}, \mathbf{r}') \, \mathrm{d}^3 r = -1$ [20].

#### 2.2.3.1 Exact properties

While the form of the universal xc functional is unknown, a few exact properties have been derived; these can be important when one is considering the effectiveness of approximate xc functionals. We note, however, that when developing approximate xc functionals the focus of one's efforts to ensure that their functional satisfies certain exact limits should not supersede insight which will lead to improved accuracy in the density, even if said insight violates the known exact properties.

We begin by considering a one electron system; the Kohn-Sham potential must be equal to the external potential [$v_{\mathrm{s}}^{(1)} = v_{\mathrm{ext}}$], as both the many-electron system and the Kohn-Sham system are identical. Hence, from Eq. (2.7) it must follow that $v_{\mathrm{xc}}^{(1)} = -v_{\mathrm{H}}^{(1)}$. By substituting this result into Eq. (2.12), we obtain $E_{\mathrm{xc}}^{(1)} = -E_{\mathrm{H}}^{(1)}$. This result, which is not satisfied by some common approximations (discussed below), is necessary for correct cancellation of the erroneous self-interaction of the electrons. There are many issues that arise when an electron interacts with itself (see Chapter 3), and hence it is an important constraint to consider.

One of the most elusive properties of the exact xc functional is the derivative discontinuity of the xc energy with respect to electron number $N$. Perdew *et al.* [21] showed that when applying HK theory to a system that is *not* constrained by integer numbers of electrons, the gradient of the xc energy with respect to electron number is discontinuous when passing through an integer value of $N$. If one replaces the number-conserving variations (mentioned before) with a Lagrange multiplier $\mu$, one obtains

$$\frac{\delta}{\delta n}\left(E_v[n] - \mu \int n(\mathbf{r})\mathrm{d}^3 r\right) = 0. \tag{2.15}$$

The Euler-Lagrange equation is therefore $\delta E_v/\delta n(\mathbf{r}) = \mu (= \partial E/\partial N)$. This discontinuity in the xc energy corresponds to a 'jump' in the xc potential – which, to date, has not been successfully reproduced by any approximate explicit xc functionals, as its form would need to be non-analytic. The jump in the potential ($\Delta_{\mathrm{xc}}$) is a constant shift which occurs as one passes through an integer value of $N$, and can be calculated as follows:

$$\Delta_{\mathrm{xc}} = v_{\mathrm{xc}}(\mathbf{r})|_{N+\delta} - v_{\mathrm{xc}}(\mathbf{r})|_{N-\delta} = \left.\frac{\delta E_{\mathrm{xc}}[n]}{\delta n(\mathbf{r})}\right|_{N+\delta} - \left.\frac{\delta E_{\mathrm{xc}}[n]}{\delta n(\mathbf{r})}\right|_{N-\delta} = \left.\frac{\partial E_{\mathrm{xc}}}{\partial N}\right|_{N+\delta} - \left.\frac{\partial E_{\mathrm{xc}}}{\partial N}\right|_{N-\delta},$$

where $\delta$ is an infinitesimal amount of an electron.

Next, consider an electron far from any atom, the external potential decays as $Z/r$, and the Hartree potential decays as $-(N-1)/r$. The Kohn-Sham potential decays as $(Z-N)/r$, hence, we can infer that the xc potential must decay as $-1/r$, as shown for finite systems in Refs. [22] and [23]. This form of the xc potential can be important for edges of 'molecule-like' systems, as it partially determines the confinement of the electron density. Thus this property of $v_{\mathrm{xc}}$ is important for accurate chemical modelling.

It is known that the exchange energy is always negative. A further constraint on the xc energy was derived by Lieb and Oxford [24], they showed that

$$E_{\mathrm{x}} \geq E_{\mathrm{xc}} \geq -1.68 \int \mathrm{d}^3 r\, n(\mathbf{r})^{\frac{4}{3}}. \tag{2.16}$$

However, we note that as our calculations are in 1D, some constraints, such as this one, may

take a slightly different mathematical form.

Our list of exact properties could go on, but as stated before, exact constraints are useful for testing approximate functionals but are by no means crucial.

#### 2.2.3.2 The local density approximation

Below we discuss the common approximations to the xc functional. The most simple approximation to the xc energy is the local density approximation (LDA). It was first proposed by Kohn and Sham in their original 1965 paper [2], and has since proven to be one of the most important and popular approximations to the xc functional. To understand the concept of the LDA, one must first consider a *homogenous electron gas* (HEG). The exchange energy per unit volume for a HEG in 3D is known analytically:

$$\varepsilon_{\mathrm{x}}^{\mathrm{HEG}} = -\tfrac{3}{4}\left(\tfrac{3}{\pi}\right)^{\frac{1}{3}} n^{\frac{4}{3}}. \tag{2.17}$$

By integrating over all space one acquires the total exchange energy, and when applying Eq. (2.17) to systems that are *inhomogeneous*, the exchange energy is approximated as

$$E_{\mathrm{x}} \approx E_{\mathrm{x}}^{\mathrm{LDA}} = -\tfrac{3}{4}\left(\tfrac{3}{\pi}\right)^{\frac{1}{3}} \int \mathrm{d}^3 r\, n(\mathbf{r})^{\frac{4}{3}}. \tag{2.18}$$

When it comes to the correlation term the procedure is not so simple, as the form of $E_{\mathrm{c}}$ is not known. The breakthrough came from Ceperley and Adler with their Quantum Monte Carlo (QMC) simulation of the HEG [25], which gave rise to an accurate expression for $\varepsilon_{\mathrm{c}}^{\mathrm{HEG}}$, parameterised from this calculation [25, 26].

The use of the LDA has been hugely successful for ground-state calculations. This can be partially explained by a systematic cancellation of errors, owing to the fact that the LDA satisfies the sum rule of the xc hole – $E_{\mathrm{c}}$ is underestimated and $E_{\mathrm{x}}$ is overestimated.

The LDA has given reliable results for decades, for total energy and geometrical structure calculations within solid-state physics [27]. However, its performance is far less impressive for quantum chemistry as the LDA tends to over-bind atoms [28]. In order for quantum chemistry calculations to be practical, the error in the energy is required to be no worse than about 0.1 kcal/mol – this is not achievable using the LDA. However, approximate functionals have been developed that perform better in these scenarios [28] (see below). (Chapter 3 gives an overview of some of the failings of the LDA, among other approximations.)

#### 2.2.3.3 Beyond local approximations

The LDA is concerned only with the electron density at point $\mathbf{r}$, which is a fair assumption when the density is approximately uniform. However, for molecules the density can be far from homogenous. As the exact xc functional has a nonlocal dependence on the density, the gradient of the density must be considered in order to improve the xc energy for inhomogeneous systems. This is usually done using the reduced density gradient $s = |\nabla n|\, n^{-\frac{4}{3}}$, which is dimensionless by necessity. Hence, the LDA xc functional can be improved by considering

$$E_{\mathrm{xc}}[n] = \int \varepsilon_{\mathrm{xc}}^{\mathrm{LDA}}(n)[1 + \mu(n)s^2 + ...]\mathrm{d}^3 r, \tag{2.19}$$

where $\mu(n)$ is a function that gives a constant for the exchange component. Approximations of this type are known as density-gradient expansion functionals. However, there are problems associated with this approach; one such problem is the divergence of the xc potential far from any atom. This can be shown by considering the form of the density in said region, which was shown by Perdew to asymptotically decay [$n(\mathbf{r}) \propto e^{-cr}$] [21, 29]. Hence we substitute this form into $s$ and find that $s = |\nabla n|\, n^{-\frac{4}{3}} = ce^{\frac{cr}{3}}$ which tends to infinity as $r \to \infty$.

Perdew, Burke and others remedied this unphysical behaviour by replacing the truncated series expansion in Eq. (2.19) with a dampening term $F_{\mathrm{xc}}[n, s]$. Density approximations of this form are know as generalised gradient approximations (GGAs). The form of $F_{\mathrm{xc}}$ varies, but the most popular was proposed by Perdew, Burke and Ernzerhof (PBE) [30];

$$F_{\mathrm{x}}^{\mathrm{PBE}}(s) = 1 + \frac{as^2}{1 + bs^2}, \tag{2.20}$$

where $a$ and $b$ are functions which are either calculated by considering exact constraints of $E_{\mathrm{xc}}$ or from experimental results. GGAs have been successful in extending the applicability of DFT [31, 32], specifically in chemistry due to the increase in accuracy that the improved approximation provides. However, GGAs do not always yield reliable electron densities; see Chapter 3.

## 2.3 Hartree-Fock approximation

While the Hartree-Fock (HF) method [33, 34] is not a density functional approach, it is an approximate method for solving Eq. (2.1) (although here we are only considering the ground state) that has similarities with the DFT approach. The HF approach assumes that the many-electron wavefunction $\Psi(\mathbf{r}_1, ...\mathbf{r}_N)$ can be represented by a Slater determinant of *single-particle wavefunctions* $\Phi_{1...N}$ (in a similar fashion to Kohn-Sham theory). And hence the density is calculated by summing over the single-particle HF densities, like Eq. (2.11). However, unlike Kohn-Sham theory, HF theory is inherently approximate because the wavefunction is constructed from single-particle wavefunctions. These single-particle wavefunctions are known as HF orbitals. Working with this assumption, when one minimises the energy $E_{\mathrm{HF}} = \langle \Phi_{1...N} | \hat{H} | \Phi_{1...N} \rangle$ using the Slater determinant $\Phi_{1...N}$ opposed to the full many-electron wavefunction $\Psi(\mathbf{r}_1, ...\mathbf{r}_N)$, one obtains the HF equations

$$-\tfrac{1}{2}\nabla^2 \phi_i^{\mathrm{HF}}(\mathbf{r}) + \int \mathrm{d}^3 r'\, v^{\mathrm{HF}}(\mathbf{r}, \mathbf{r}') \phi_i^{\mathrm{HF}}(\mathbf{r}') = \varepsilon^{\mathrm{HF}} \phi_i^{\mathrm{HF}}(\mathbf{r}), \tag{2.21}$$

where $\{\phi_i^{\mathrm{HF}}\}$ are the set of $N$ single-particle wavefunctions, and $v^{\mathrm{HF}}(\mathbf{r}, \mathbf{r}')$ is a nonlocal effective potential given by

$$v^{\mathrm{HF}}(\mathbf{r}, \mathbf{r}') = v_{\mathrm{x}}^{\mathrm{HF}}(\mathbf{r}, \mathbf{r}') + v^{\mathrm{H}}(\mathbf{r}) = -\frac{1}{|\mathbf{r} - \mathbf{r}'|} \sum_{j=1}^{N} \phi_j^{\mathrm{HF}}(\mathbf{r}) (\phi_j^{\mathrm{HF}}(\mathbf{r}'))^* + \int \mathrm{d}^3 r' \frac{1}{|\mathbf{r} - \mathbf{r}'|} \sum_{j=1}^{N} \left| \phi_j^{\mathrm{HF}}(\mathbf{r}') \right|^2.$$

This potential is comprised of two terms; the nonlocal Fock operator (first term) and the Hartree potential (second term) [see Eq. (2.8)]. [Note that we have neglected spin from Eq. (2.21) and above; to include spin, one would simply need to sum over the spin index.]

As the HF potential is nonlocal, the method is more computationally expensive than DFT.

In HF theory exchange is treated exactly, and hence we use HF calculations on some of our systems as a means of identifying systems with appreciable correlation[2]. As exchange is exact, the self-interaction is exactly cancelled. If we set $v_x^{\mathrm{HF}}(\mathbf{r}, \mathbf{r}') = 0$ and solve Eq. (2.21) self-consistently, we obtain the Hartree approximation, which can also be used to test the performance of approximate functionals in DFT, *i.e.*, the effectiveness of the self-interaction correction.

## 2.4 Summary

Density-functional calculations have become prominent in condensed-matter physics because of the ability to treat the electrons as noninteracting in the Kohn-Sham approach, while in principle reproducing the exact electron density of the real interacting system via an effective potential. However, in practice the exchange-correlation part of this potential must be approximated. Approximations based on the local density [2], or the local density and its gradient [30] (among others), are often used to calculate the electron density with success, however, they are known to break down in a number of important cases [8, 35]; see Chapter 3.

## 2.5 Time-dependent density functional theory

Time-dependent DFT (TDDFT) has made it possible for excited states, and truly time-dependent systems to be studied, which opens up *many* possibilities in terms of system modelling [36]. Of course, one such example of these types of systems is the transport of electrons through single molecules [37]. In the following section we outline the theories that underpin TDDFT.

### 2.5.1 Runge-Gross theorem

Just as for DFT, in order to construct a time-dependent density functional theory (TDDFT) we need to show that the time-dependent density $n(\mathbf{r}, t)$ is a variable that completely determines the dynamics of a system without the need for the wavefunction. This was initially shown to be possible by Runge and Gross [12]. They showed, in a similar fashion to Hohenberg and Kohn, that for a given initial state, two different potentials (different by more than a time-dependent constant) will yield different densities. However, when it comes to using TDDFT for practical calculations, we would like to replace the interaction with an auxiliary system of noninteracting electrons, akin to the Kohn-Sham theory in DFT. This was proven to be possible by van Leeuwen [13].

[2]From a practical chemistry point of view, correlation is defined as anything beyond the capability of the Hartree-Fock (HF) approximation. Of course, this means, by definition the HF approximation is completely missing correlation.

### 2.5.2 Time-dependent Kohn-Sham theory

The van Leeuwen theorem [13] shows that the time-dependent density $n(\mathbf{r},t)$, evolving from an initial state $\Psi_0$, can be exactly reproduced by an auxiliary system of noninteracting electrons. And, like for Kohn-Sham theory, the electrons experience an effective potential (*time-dependent* Kohn-Sham potential) $v_\mathrm{s}[n,\Psi_0,\Phi_0](\mathbf{r},t)$, which is a functional of the initial states of the interacting and noninteracting systems ($\Psi_0$ and $\Phi_0$ respectively), and the time-dependent density.

Commonly the initial state is the ground state, and hence the Hohenberg-Kohn theorem applies. In this case both the initial state of the interacting and noninteracting systems are functionals of the ground-state density, thus the functional form of the time-dependent Kohn-Sham potential can be simplified to $v_\mathrm{s}[n](\mathbf{r},t)$.

The noninteracting, time-dependent Kohn-Sham electrons now obey the time-dependent Kohn-Sham equations

$$i\frac{\partial}{\partial t}\phi_j(\mathbf{r},t) = \left(-\tfrac{1}{2}\nabla^2 + v_\mathrm{s}[n](\mathbf{r},t)\right)\phi_j(\mathbf{r},t)\,. \tag{2.22}$$

And the electron density is calculated via the noninteracting single-particle densities, as such

$$n(\mathbf{r},t) = \sum_{k=1}^{N}\left|\phi_j(\mathbf{r},t)\right|^2. \tag{2.23}$$

The time-dependent Kohn-Sham potential is comprised of three terms, just like the ground-state [see Eq. (2.7)],

$$v_\mathrm{s}[n](\mathbf{r},t) = v_\mathrm{ext}(\mathbf{r},t) + v_\mathrm{H}[n](\mathbf{r},t) + v_\mathrm{xc}[n](\mathbf{r},t), \tag{2.24}$$

where $v_\mathrm{ext}$ is the external potential, which is the same as the external potential experienced by the system of interacting electrons. $v_\mathrm{H}$ is the Hartree potential at time $t$, and $v_\mathrm{xc}$ is the time-dependent exchange-correlation (xc) potential. As for the ground-state system, the only unknown term is $v_\mathrm{xc}[n](\mathbf{r},t)$.

### 2.5.3 Time-dependent exchange-correlation functional

While the exact time-dependent xc functional is universal and can reproduce the electron and current density of a system exactly via a system of noninteracting electrons, the form is not known and hence must be approximated. The accuracy of TDDFT in simulating realistic systems hence hinges on these approximations.

Below we outline some of the known exact properties of the time-dependent xc potential. We also give a brief account of the most common approximations for the time-dependent xc potential.

#### 2.5.3.1 Exact properties

The ground-state xc potential is known to require a self-interaction correction to prevent the Kohn-Sham electrons from interacting with themselves via the Hartree potential, this is

also required in the time-dependent regime. Hence, it must follow that for a one electron system the xc potential must cancel exactly with the Hartree potential at all times, thus $v_{\mathrm{xc}}^{(1)}(\mathbf{r},t) = -v_{\mathrm{H}}^{(1)}(\mathbf{r},t)$.

The total momentum of a system is $\langle \mathbf{p}(t) \rangle = \int \mathrm{d}^3 r\ \mathbf{j}(\mathbf{r},t) = \int \mathrm{d}^3 r\ \mathbf{r}\ \frac{\partial}{\partial t} n(\mathbf{r},t)$, where $j$ is the current density, and since the densities of the interacting and noninteracting systems are the same, the total momentum for the Kohn-Sham system must match that of the many-body system. Thus

$$0 = \frac{\mathrm{d}}{\mathrm{d}t} \left( \langle \mathbf{p}(t) \rangle - \langle \mathbf{p}_{\mathrm{s}}(t) \rangle \right) = \int \mathrm{d}^3 r\ n(\mathbf{r},t) \nabla [v_{\mathrm{H}}(\mathbf{r},t) + v_{\mathrm{xc}}(\mathbf{r},t)],$$

and as $\int \mathrm{d}^3 r\ n(\mathbf{r},t) \nabla v_{\mathrm{H}}(\mathbf{r},t) = 0$ it must follow that

$$\int \mathrm{d}^3 r\ n(\mathbf{r},t) \nabla v_{\mathrm{xc}}(\mathbf{r},t) = 0. \tag{2.25}$$

This is known as the zero-force theorem [38].

In a similar fashion we consider the expectation value of the Kohn-Sham Hamiltonian,

$$H_{\mathrm{s}} = T_{\mathrm{s}} + V_{\mathrm{s}}, \tag{2.26}$$

where $\langle \hat{H}_{\mathrm{s}} \rangle \equiv H_{\mathrm{s}}$, $T_{\mathrm{s}}$ is the expectation value of the single-particle kinetic energy and $V_{\mathrm{s}}$ is the expectation value of the Kohn-Sham potential. Likewise the many-electron Hamiltonian can be expressed in terms of the kinetic energy and potential operators:

$$H = T + V_{\mathrm{ee}} + V_{\mathrm{ext}}, \tag{2.27}$$

where $V_{\mathrm{ee}}$ is the expectation value of the Coulomb interaction, $V_{\mathrm{ext}}$ is the expectation value of the external potential and $T$ is the expectation value of the many-electron kinetic energy operator.

Hessler *et al.* [39] apply Heisenberg's equation of motion to the single-particle Hamiltonian ($\hat{H}_{\mathrm{s}}$), as such

$$\dot{H}_{\mathrm{s}} = -i \left\langle \left[ \hat{H}_{\mathrm{s}}, \hat{H}_{\mathrm{s}} \right] \right\rangle + \left\langle \frac{\partial \hat{H}_{\mathrm{s}}}{\partial t} \right\rangle = \left\langle \frac{\partial v_{\mathrm{s}}}{\partial t} \right\rangle, \tag{2.28}$$

where $v_{\mathrm{s}}$ is the Kohn-Sham potential, and the many-electron Hamiltonian ($\hat{H}$);

$$\dot{H} = -i \left\langle \left[ \hat{H}, \hat{H} \right] \right\rangle + \left\langle \frac{\partial \hat{H}}{\partial t} \right\rangle = \left\langle \frac{\partial v_{\mathrm{ext}}}{\partial t} \right\rangle, \tag{2.29}$$

where $v_{\mathrm{ext}}$ is the external potential.

Hessler *et al.* use the Hohenberg-Kohn theorem [1]

$$T + V_{\mathrm{ext}} + V_{\mathrm{ee}} = T_{\mathrm{s}} + U + V_{\mathrm{ext}} + E_{\mathrm{xc}}, \tag{2.30}$$

and take the time derivative of each side. Hence, $\dot{E}_{\mathrm{xc}} = \dot{T} - \dot{T}_{\mathrm{s}} + \dot{V}_{\mathrm{ee}} - \dot{U}$. By substituting in the above, we find that the evolution of the xc energy only depends on the evolution of the density:

$$\frac{\mathrm{d}E_{\mathrm{xc}}}{\mathrm{d}t} = \int \mathrm{d}^3 r\ \frac{\mathrm{d}n}{\mathrm{d}t} v_{\mathrm{xc}}. \tag{2.31}$$

There are more exact properties of the time-dependent xc potential/functional that we have not listed here. As for the ground-state, these rules are useful for developing approximate functionals, but should not be enforced at the cost of the accuracy of an approximation, and hence are not central to our development of improved functionals.

#### 2.5.3.2 Adiabatic approximation

The exact xc potential is dependent on the entire history of the Kohn-Sham system. Despite this, the most common approximation implemented in time-dependent models is the adiabatic approximation, which assumes only local dependence on the density in time, *i.e.*, $v_{\mathrm{xc}}[n](\mathbf{r},t) = v_{\mathrm{xc}}[n(t)](\mathbf{r})$. This approximation becomes exact in the limit that $\frac{\partial n}{\partial t} \to 0$.

The adiabatic approximation is often used in conjunction with the LDA (ALDA), meaning that the ALDA is local in both space and time. This level of approximation usually proves to be inadequate to describe highly correlated systems; see Chapter 3 and 5.

## 2.6 Linear response

When the perturbing field is weak, which is usually the case for spectroscopic experiments, perturbation theory can be used. In this case the change to the potential is small, hence $n(\mathbf{r},t) = n_0(\mathbf{r},t) + \delta n(\mathbf{r},t)$, where $n_0(\mathbf{r},t)$ is the ground-state electron density. Therefore one can write the xc potential as

$$v_{\mathrm{xc}}[n_0+\delta n](\mathbf{r},t) = v_{\mathrm{xc}}[n_0](\mathbf{r}) + \int \mathrm{d}t' \int \mathrm{d}^3r' f_{\mathrm{xc}}[n_0](\mathbf{r},\mathbf{r}',t-t')\delta n(\mathbf{r}',t'). \tag{2.32}$$

Here, $f_{\mathrm{xc}}$ is the xc kernel, given by

$$f_{\mathrm{xc}}[n_0](\mathbf{r},\mathbf{r}',t-t') = \left.\frac{\delta v_{\mathrm{xc}}(\mathbf{r},t)}{\delta n(\mathbf{r}',t')}\right|_{n=n_0},$$

when evaluated on the ground-state density.

While the kernel is still a highly complicated entity, it is still more accessible than the full time-dependent xc potential because it is only a functional of the ground-state density. $\chi[n_0]$ is defined as the response of the ground-state, many-electron system to a change in the external potential, given by

$$\delta n(\mathbf{r},t) = \int \mathrm{d}t' \int \mathrm{d}^3r'\, \chi[n_0](\mathbf{r},\mathbf{r}',t-t')\, \delta v_{\mathrm{ext}}(\mathbf{r}',t').$$

This can also be done in a similar fashion for the Kohn-Sham system. Both the many-electron and the Kohn-Sham response function must yield the same response in the density. Hence

$$\chi(\mathbf{r},\mathbf{r}',\omega) = \chi_{\mathrm{s}}(\mathbf{r},\mathbf{r}',\omega) + \int \mathrm{d}^3r_1 \int \mathrm{d}^3r_2 \chi_{\mathrm{s}}(\mathbf{r},\mathbf{r}_1,\omega)\left[\frac{1}{|\mathbf{r}_1-\mathbf{r}_2|} + f_{\mathrm{xc}}(\mathbf{r}_1,\mathbf{r}_2,\omega)\right]\chi_{\mathrm{s}}(\mathbf{r}_2,\mathbf{r}',\omega). \tag{2.33}$$

Equation (2.33) is the central equation within time-dependent linear response theory. From Eq. (2.33) the response of the density can be found from a perturbation of the external potential, then, for example, the Fourier transform of the first-order response of $n$ to $\delta v_{\mathrm{ext}}$ yields the excitation energies of the ground-state system.

The successes and failures of linear response theory are outlined in the following chapter. We also asses the limits of the commonly used approximations within (TD)DFT.

## 2.7 Summary

The extension of density functional theory (DFT) to a system evolving from (typically) its ground state – time-dependent DFT – requires an exchange-correlation potential that depends on the entire history of the electron density. Despite this, in practice, the system's history and initial state are neglected because most time-dependent calculations today use an adiabatic approximation, which assumes dependence only on the instantaneous electron density [40].

# Chapter 3

# Limitations of the established theory

The type of electronic processes we are concerned with simulating happen on a time scale of attoseconds ($10^{-18}$ seconds) to femtoseconds ($10^{-15}$ seconds), and on an energy scale of electron-volts (eV). These events are far too fast and small to see with the human eye and, until recently, even with the most advanced experimental equipment. In this chapter we focus, mainly, on situations where the usual approximations used in density functional theory (DFT) and time-dependent DFT (TDDFT) fail, and hence where improved approximate density functionals are required. It is important to note that this failure is not a problem with the theory, but rather of the approximations used for the exchange-correlation (xc) functional. Cohen *et al*. write 'a possible path forward is to have a deeper look at the errors embedded in currently used functionals to determine the origin of their pathologies at the most basic level' [7]. This idea is at the heart of our approach; see Section 1.1 on page 14.

## 3.1 Problems within density functional theory

Commonly used approximate functionals, like those discussed in the previous chapter, have major failings when it comes to estimating the energy barriers of chemical reactions [41, 42, 43, 44, 45], the band gaps of materials [46, 47, 48] and the energy of dissociating molecular ions [49, 50, 51], among others. Hence, theoretical chemistry and calculations of excited states/band structures are inaccurate when using DFT. This is a serious problem for the theory. While various methods exist to overcome *some* of these problems [52, 53, 54, 55, 56, 57, 58], they can be computationally expensive and difficult to implement. The most simple, organic and efficient means of improvement is to develop more accurate density functionals (see Section 3.3 on page 34).

The above failings of the commonly used approximate functionals can be understood in terms of the various errors. The two leading contributions are the delocalisation error [59] and the static correlation error [60]. The delocalisation error is the tendency of the electron density to artificially spread out. Whereas the static correlation error stems from the poor description of correlation by local density approximations (LDAs).[1]

Both of these errors are associated with the incorrect distribution of fractional charges predicted by local and semi-local approximations, and can be observed for systems as simple

[1] This is most prominent for strongly correlated systems, *i.e.*, systems that cannot be modelled using Hartree-Fock theory [61] (by our definition).

as $H_2^+$ [62]. Commonly used functionals [*e.g.*, the LDA and generalised gradient approximations (GGAs); see Chapter 2], are known to fail as the $H_2^+$ molecule is stretched (reaches the disassociation limit) [21, 49, 50, 51, 63], *i.e.*, local functionals localise the incorrect amount of charge on each atom; see Fig. 3.1(A) and (B) from Ref. [7]. The LDA, for example, does not cancel the spurious self interaction of the electrons (see Chapter 2), thus the electron density spreads out too much and the Hartree potential prevents the electron from localising correctly (more detail is given on this in Chapter 5).

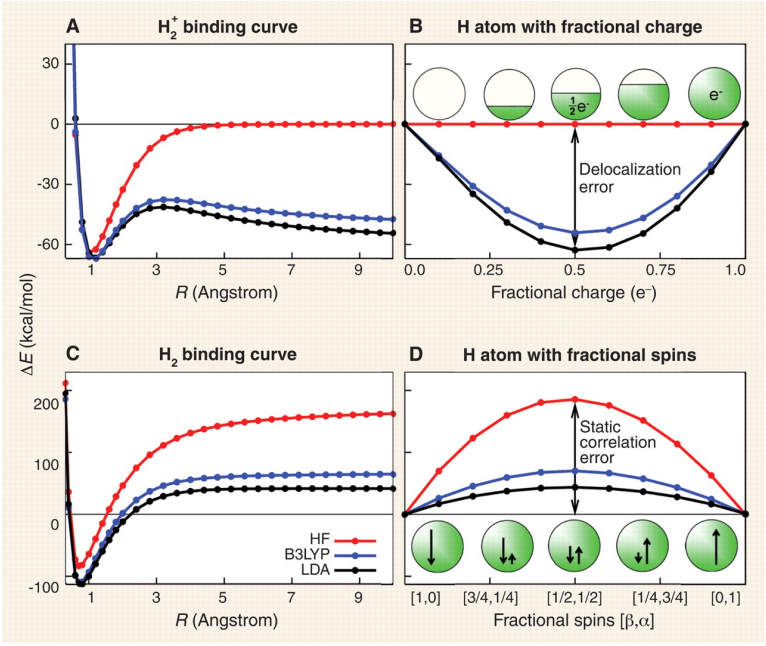


Figure 3.1: DFT approximations fail. The dissociation of $H_2^+$ molecule (A) and $H_2$ molecule (C) are shown for calculations with approximate functionals: Hartree-Fock (HF), local density approximation (LDA), and B3LYP. Although DFT gives good bonding structures, errors increase with the bond length. The huge errors at dissociation of $H_2^+$ exactly match the error of atoms with fractional charges (B), and for $H_2$ they exactly match the error of atoms with fractional spins (D). The understanding of these failures leads to the characterisation of the delocalisation error and static correlation error that are pervasive throughout chemistry and physics, explaining a host of problems with currently used exchange-correlation functionals. (From [Aron J Cohen, Paula Mori-Sánchez, and Weitao Yang. Science, 321(5890):792–794, 2008]. Reprinted with permission from AAAS.)

Hence for disassociated $H_2^+$, various approximate functionals give an energy that is too low when the electron is delocalised; see Fig. 3.1(B). Several features of the exact Kohn-Sham potential are missing from the usual approximations that are associated with these errors, *e.g.*, the self-interaction correction [64]; discussed in Chapter 2.

Approximations also suffer from the lack of a derivative discontinuity in the xc energy with respect to the electron number [53], again discussed in Chapter 2, which also relates to incorrect charge distribution for separated molecules; see Fig. 3.2(A). The behaviour of a system due to adding or removing an electron is very difficult for approximate functionals to reproduce, due, partially to the distribution of the electron being over estimated. This error grows with the system size because of the increase in delocalisation error [7].

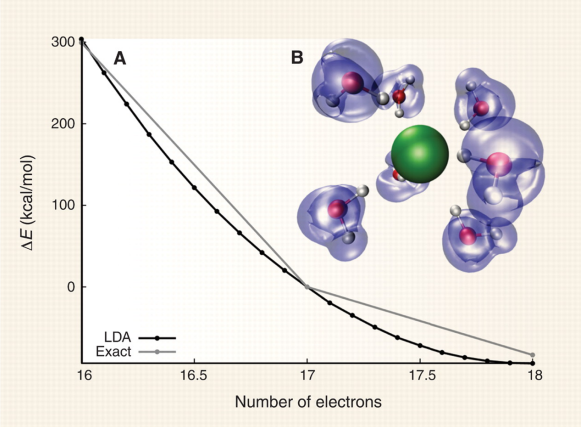


Figure 3.2: Seeing the delocalisation error. The incorrect convex behaviour of the LDA energy is seen for the Cl atom with fractional numbers of electrons (A). Despite good agreement with the exact values at the integer points, the convex behaviour means that a lower energy can be achieved with fractional charges. This leads to an unphysical delocalisation of the electrons in a simulation of the solvated anion, as shown (in blue) by the difference of the LDA density between the solvated Cl and solvated $Cl^-$ (B). (From [Aron J Cohen, Paula Mori-Sánchez, and Weitao Yang. Science, 321(5890):792–794, 2008]. Reprinted with permission from AAAS.)

Owing to the incorrect xc energy predicted by the LDA for systems with fractional charges (Fig. 3.2), the lowest energy state of the system, like the disassociated molecule, predicted by using the LDA localises non-integer amounts of charge on each atom, when there should be integer amounts of total charge on each site.

In order for DFT to become accurate for a wider range of systems, these problems with the usual approximations in DFT must be overcome.

While DFT based calculations suffer from inaccuracies (above), DFT has been hugely successful in describing materials [65]. However, major improvement is required for TDDFT, which, while it has had major successes [36], fails to describe common situations like electron excitations, transport and other strongly perturbed, or correlated, systems. Hence, the rest of this chapter focuses on the limitations of TDDFT.

## 3.2 Electron transport

Throughout the 1990s improved experimental techniques allowed the flow of electronic current through single-layer molecular films between two electrodes to become possible [66, 67, 68], like that shown in Fig. 3.3.

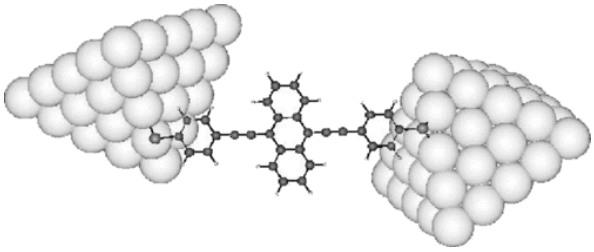

Figure 3.3: Schematic representation for a conductance measurement of the molecule (9,10-Bis((2–paramercaptophenyl)-ethinyl)-anthracene): between gold contacts (Ref. [66]). (Reprinted Figure with permission from [F. Evers, F.Weigend, and M. Koentopp. Phys. Rev. B, 69:235411, Jun 2004.] Copyright 2016 by the American Physical Society.)

As the integrated circuit (IC) becomes ever more miniature, the need for a fully quantum description of the flow of electronic currents becomes increasingly important for improving technology. Below we discuss why the commonly used theories break down for describing such scenarios.

The story of conductance begins with Ohm's law, $V = IR$ where $R$ is the resistance, $I$ is the current and $V$ is the voltage. Ohm's law describes the 'classical' conductance ($G = I/V = 1/R$) of a current carrying wire. However, experimental evidence [69, 70] has shown that the conductance of a lead increases in discrete steps of $4\pi$ as the width of the contact is increased (a two-atom contact has $G = 2G_0$, whereas a one-atom contact has $G = G_0$) [8]. This is due to the quantised nature of electrons. Hence the computational and theoretical difficulties associated with modelling electron transport increase for systems where this quantised nature of the electrons is important, such as nano-sized ICs.

### 3.2.1 Landauer formulation

The Landauer formulation [71] predicts quantised conductance. In this approach electrons are modelled to flow along a wire, connected, at each end, to an ideal lead. For this simple picture the formula reads $G(\mu) = G_0 \sum_n T_n(\mu)$, where $G$ and $G_0$ are defined above, $T_n$ is the transmission eigenvaule of the $n^{\text{th}}$ channel in the conductor, and $\mu$ is the chemical potential.

The model is crude in that the electrons are considered to be *noninteracting*, *i.e.*, they only interact with the wire [72]. For a many-electron problem, like the transport of electrons, the Coulomb interaction can have a large effect on conductance [73], and hence the Landauer formulation often fails to reproduce low-conductance experimental results .

The Landauer formulation can be implemented in a more sophisticated way by using the ground-state Kohn-Sham potential at $t = 0$, then perturbing the system and allowing the electrons to evolve in time, eventually reaching a steady state. Hence, some information about the interaction is included, but by no means are the dynamic interactions of the electrons fully described. Thus, this approach fails when those interactions are of the order of the other forces in the dynamics of the system (a common situation for transport systems; see Section 5.5 on page 65), because the interaction is not included in the Hamiltonian directly (as it is in the many-electron Schrödinger equation), nor is it represented by updating the time-dependent local effective potential (as for TDDFT). Furthermore, the approach also suffers from the need to use an approximation for the ground-state Kohn-Sham potential at $t = 0$.

## 3.3 Problems within time-dependent density functional theory

As for DFT, the inaccuracies of TDDFT are a result of the approximation of the time-dependent xc functional, and not a break down of the theory itself. We discussed, in the previous chapter, the most common time-dependent approximation, the adiabatic LDA (ALDA). While approximations beyond the adiabatic approximation exist [74, 75], there are still many scenarios for which improvement is required [35, 76, 77, 78, 79, 80]. The use of these common approximations lead to an inaccurate description of charge transfer excitations and the response of a system to an applied electric field [7, 59].

Analysis of the failures of the usual approximations implemented in TDDFT and ways of improving them exist [36, 81]. Generally, however, these approximations are least secure in the following circumstances. Firstly, when correlation is strong in the dynamics of the system: the description of correlation of approximate functionals is known to be poor for ground-state DFT, and this issue is exacerbated for time-dependent systems. This is because correlation is generally much stronger once the system becomes dynamic [82] (many-electron excited states are mixed into the evolving many-electron wavefunction). One such example of this is double excitations [83, 84]. A simple thought experiment can be used to understand why approximations struggle to describe such a situation: in a many-body system when the correlation between two electrons is strong, a photon, with sufficient energy to excite an electron, may cause the other, strongly correlated electron to excite (double excitation). In order for this to happen for two noninteracting electrons, two photons would be required. Hence, in the noninteracting Kohn-Sham approach, the time-dependent Kohn-Sham potential must be highly nonlocal, and with a good description of correlation in the xc potential. This type of nonlocality, and accuracy of correlation, is far beyond the scope of local and adiabatic approximations.

Secondly, another common physical scenario where the approximations made in TDDFT struggle to perform well is molecular conductance [84]. Above we briefly discussed the use of static-DFT within the Landauer formulation, which is common for modelling quantum transport but gives poor agreement with experiment. There are also inherent issues with the DFT approach, namely when using an LDA or GGA the incorrect band gap leads to poor conductance characteristics [80, 85]; see Fig. 3.4. For instance, the current-voltage ($I$-$V$) characteristics of organic molecules (including their conductance) often differ from experiment by 1-2 orders of magnitude [9, 35, 86, 87, 88].

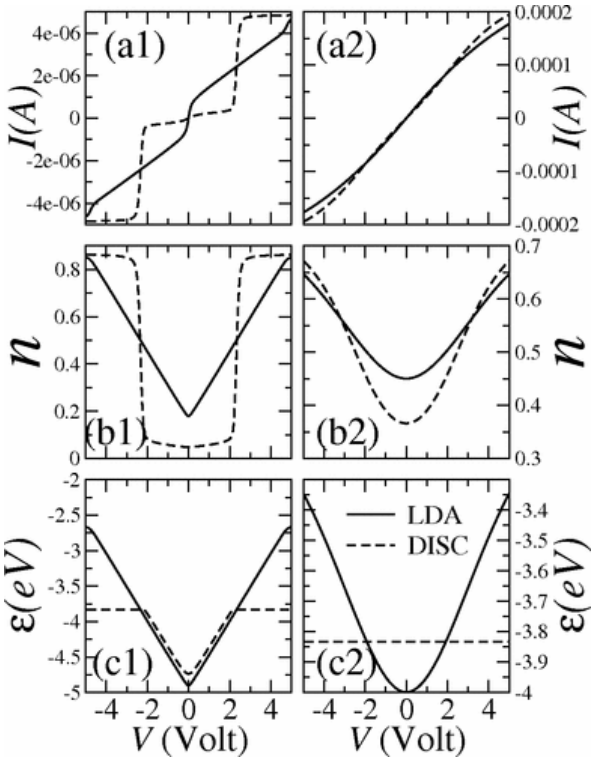


Figure 3.4: (a) Current $I$, (b) occupation $n$, and (c) position of the energy level $\epsilon$ as a function of bias $V$. The parameters used here are $\epsilon(0) = -5.5$ eV, $U = 5$ eV, $E_F = -5.0$ eV, and $T = 300^\circ$K . The curves on the left-hand side are obtained in the weak coupling limit ($\Gamma = 0.02$ eV) and those on the right-hand side in the strong coupling limit ($\Gamma = 1.2$ eV). (Reprinted Figure with permission from [C. Toher, A. Filippetti, S. Sanvito, and Kieron Burke. Phys. Rev. Lett., 95:146402, Sep 2005.] Copyright 2016 by the American Physical Society.)

Hence further improved approximate xc functionals are required, as the usual approximations are missing crucial features of the exact xc potential [89]. Two notable examples being the formation of pronounced spatial steps demonstrated for a quasiparticle wavepacket added to a model semiconductor [10], and for a one-dimensional He atom in the presence of a weak oscillatory electric field [11].

Burke *et al.* offer four sources of error in a typical TDDFT calculation [36]. The errors are described as follows:

Er. 1 The error in the ground-state: if the starting point of the time-dependent calculation is poor, then, of course, one would expect the rest of the time-dependent simulation to be poor.

Er. 2 The lack of nonlocality in one's approximate xc functional: the exact xc functional can depend highly nonlocally on the density, hence local and semi-local functionals lack information needed for potentials that yield accurate densities.

Er. 3 The memory issues with temporally local approximations: adiabatic approximations suffer from a lack of memory effects, *i.e.*, a local dependence on time.

Er. 4 The many-electron wavefunction diverging too much from the Kohn-Sham wavefunction: even if the exact time-dependent xc potential is known, the many-electron wavefunction may be so different to the Slater determinant of the Kohn-Sham single-particle wavefunction, that observables calculated from the Kohn-Sham wavefunction will still be wrong (other than, of course, the electron densities and currents, and certain other observables).

As we are primarily interested in the electron and current densities, we are least concerned with Er. 4. However, that is not to say it is unimportant; the work of D'Amico *et al.* [90] and Sharp *et al.* [91] focuses on how the many-electron wavefunction differs from the Kohn-Sham wavefunction, and the connection with DFT.

The other three points (above) are relevant to the work presented in this thesis, namely they affect the electron density directly. Our approach to the problem (see Section 1.1 on page 14) addresses the above three errors in the following ways:

1. Error 1 is addressed by modelling the ground-state system first, and finding the exact Kohn-Sham potential, so we can observe nonlocal features missing from the common approximations. The importance of these features in the time-dependent regime can then be determined by evolving the system using only the ground-state Kohn-Sham potential and any external field (*i.e.*, we purposely do not use the time-dependent Kohn-Sham potential). Hence this allows us to see which *time-dependent* features of the exact Kohn-Sham potential are important; see Section 5.5 on page 65.

2. We address Er. 2 in a similar way to Er. 1. By having access to the exact Kohn-Sham potential, important nonlocalities can be identified in the exact Kohn-Sham potential. It is then a case of determining approximations to $v_{\mathrm{xc}}$ that capture these nonlocalities (nonetheless, still a difficult task).

3. Finally we address Er. 3 in the same way as Er. 2, as we have access to the fully *time-dependent* Kohn-Sham potential.

### 3.3.1 Rydberg and charge transfer excitations

The linear response approximation is often used within TDDFT (see Section 2.6 on page 28), despite the above issues. [This includes the calculation of excited states and energies, which, as an excited electron can escape the molecule, includes the ionisation energy ($I$) of the system.] A Rydberg atom is an atom that is highly excited and is extremely sensitive to electric/magnetic fields [92, 93], and hence the Rydberg exited states are exceedingly difficult to calculate using linear response. Due to the high energy of Rydberg atoms, some of their electrons are very close be being unbound, and hence can have an energy that is almost the ionisation energy. They have many remarkable properties, including the experimentally detectible radius of the atom which can be of the order of millimetres [93].

The energy of the highest occupied molecular orbital (HOMO) of the exact Kohn-Sham system is minus the ionisation energy of the many-electron system [$\varepsilon_{\mathrm{s}}^{N}(N) = -I$]. However, this is extremely difficult for approximate functionals to get right, in part because of the derivative discontinuity of the xc energy with respect to electron number (discussed above). The problem arises from the non-anayltical behaviour of the exact Kohn-Sham potential with the addition of an infinitesimal amount of an electron through an integer value. Without the correction of the derivative discontinuity the energy gap between the ionisation energy and the electron affinity will be wrong. Furthermore, local approximate xc potentials decay far too rapidly to zero (opposed to the exact which decays as $-1/r$), and hence under-bind the electrons by as much as 5eV (for $N_2$) [94]. Thus, when the system is excited, the high energy states (such as Rydberg states) become unbound far too quickly. Correcting the decay of the xc potential in the ground state would fix this problem for TDDFT to some degree [95, 96] – this stresses Er. 1 above. One should note that error associated with inaccurate ground-state potentials is by no means unique to the problem of Rydberg states [97, 98].

The failure of TDDFT in describing charge transfer excitations is demonstrated in Ref. [99]. They show how TDDFT cannot give correct charge transfer with local xc functionals – stressing Er. 2 above.

### 3.3.2 Beyond linear response

While TDDFT has many successes within the linear response regime (see Section 2.6 on page 28) [100, 101], there are many physical scenarios beyond the scope of this approximation, namely when the system explores many excited states, *e.g.*, double excitation [75] (discussed above).

In theory, with an accurate xc functional, TDDFT is very well suited to this kind of problem. However for TDDFT to be a powerful tool for modelling such things as laser pulses, the approximate functional must have a good description of correlation. Developing approximate functionals with a good description of correlation is therefore an important goal for us, and hence modelling and understanding systems where correlation is significant is crucial. Casida writes 'response theory still depends upon the perturbed system being initially in the ground stationary state. Real-time TDDFT not only opens the possibility to go to infinite order in response theory, but also means that the perturbed system can be taken well beyond the initial ground stationary state [102]. Indeed the simplicity of TDDFT calculations makes

it difficult for other methods to compete in this type of application' [94].

## 3.4 Summary

While density functional theory, and its time-dependent extension, have had great success in modelling useful materials, there remain many, important scenarios where the approximations used within the theories become less secure and hence yield inaccurate electron densities and currents. One possible way forward is to improve the approximations to the exchange-correlation functional by identifying which features of the exact potential are missing from the usual approximations and developing methods to incorporate these features in future improved approximate functionals.

In the following chapter we introduce our code, which we use to study the nature of many-electron systems. These systems are designed to inform the development of improved approximate functionals.

# Chapter 4

# Method

## 4.1 The iDEA code

All of the results presented in this thesis were calculated using our iDEA code [14]. Below we outline the details of the code, and how it can be used to explore the nature of interacting electrons in molecules, and assist with our investigation into the approximations within time-dependent density functional theory (TDDFT). iDEA is a 'reverse engineering' code, that calculates exact Kohn-Sham potentials by first calculating the exact electron density in real space (this can also be done for simpler models like the Hubbard model [103, 104, 105]; not using iDEA).

### 4.1.1 Structure of iDEA[1]

We first solve the many-electron Schrödinger equation for our chosen system[2] (*e.g.*, defined by our external potential and number of electrons), which, by necessity, must consist of two or three electrons[3]. The interacting ground-state many-electron wavefunction $[\Psi_0(x_1, ..., x_N)]$, including full correlation effects, is calculated by first evolving an arbitrary, exchange-antisymmetric trial wavefunction through imaginary time [106] in the chosen external potential, including the interaction term. The amount of imaginary time required to fully converge the ground-state wavefunction (see Appendix A.3.1 on page 122) is dependent on the chosen external potential. However, typically, the amount of imaginary time is of the order of $10^2$ a.u. The wavefunction remains antisymmetric after the imaginary time propagation – this is essential for a fermionic system. The antisymmetry is maintained by the use of our 'cut-down' matrices[4]. These matrices exploit the antisymmetry of the wavefunction in order to compress how it is stored in the computer. As a result, we can use a more accurate spatial grid for the same computational effort, as well as maintaining the antisymmetry of the wavefunction.

[1] This section is based on collaborative work that has been submitted for publication: M. J. P. Hodgson, J. D. Ramsden, J. B. J. Chapman, P. Lillystone and R. W. Godby, 'Exact time-dependent density-functional potentials for strongly correlated tunneling electrons', *Physical Review B (Rapid Communications)* **88**, 241102(R) (2013). Matt Hodgson participated fully in the development of the code and the formulation and analysis of the research and executed the calculations shown in the paper, and prepared the first draft of the paper.

[2] Computationally solving the Schrödinger equation was originally implemented in iDEA by Piers Lillystone, modified by Jacob Chapman and Matt Hodgson, then optimised by Jack Wetherell.

[3] It is not possible, with present computational power, for us to model more than 3 electrons exactly.

[4] Created by James Ramsden.

Our electrons are *spinless* and obey Pauli's exclusion principle, hence each Kohn-Sham electron will occupy its own distinct Kohn-Sham orbital. In this way, we can maximise the richness of exchange and correlation in our systems for a given computational effort, allowing our model to represent a system consisting of as many electrons as is feasible. For example, two spin-half electrons form a spin singlet, and therefore only *one* Kohn-Sham orbital is occupied; whereas our spinless electrons *each* occupy an orbital.

Our many-body spinless electrons interact via the softened Coulomb term $\left(\left|x_i - x_j\right| + \gamma\right)^{-1}$ [107], as is appropriate in one dimension. This form of the Coulomb interaction most faithfully represents three dimensional electrons in a one-dimensional lead, where $\gamma$ is determined by the width of the nanowire; see Appendix A.2 on page 121.

We then apply any static perturbing potential and evolve the ground-state wavefunction through real time. The Crank-Nicolson method [108] is used for both imaginary- and real-time propagation. The Crank-Nicolson equation is

$$\left(\hat{I} + \tfrac{i}{2}\delta t\hat{H}\right)\phi(t+\delta t) = \left(\hat{I} - \tfrac{i}{2}\delta t\hat{H}\right)\phi(t), \tag{4.1}$$

where $\hat{I}$ is the unity operator, $\delta t$ is the time step and $\phi$ can be any wavefunction. We find that this method is numerically stable, provided one abides by $\delta t \lesssim \frac{1}{N}\delta x^N$, where $N$ is the number of electrons (1, 2 or 3). In imaginary time $t \to -it$; generally we find that the algorithm is faster and more stable for imaginary-time propagation. We partly attribute this to the fact that complex numbers (used for real-time propagation) are more computationally taxing to manipulate than real numbers (used for imaginary-time propagation).

The interacting density is

$$n'(x,t) = N\int \mathrm{d}x_2 ... \mathrm{d}x_N \left|\Psi\left(x, x_2 ..., x_N, t\right)\right|^2. \tag{4.2}$$

Once calculated, we 'reverse engineer' $n'(x,t)$ to find the exact ground-state, and subsequently time-dependent Kohn-Sham potential for our system. We do this by solving the noninteracting Kohn-Sham equations, while iteratively correcting the Kohn-Sham potential until the exact many-electron density matches the noninteracting density; see Fig. 4.1.[5]

[5]This reverse engineering algorithm was implemented in iDEA by Matt Hodgson.

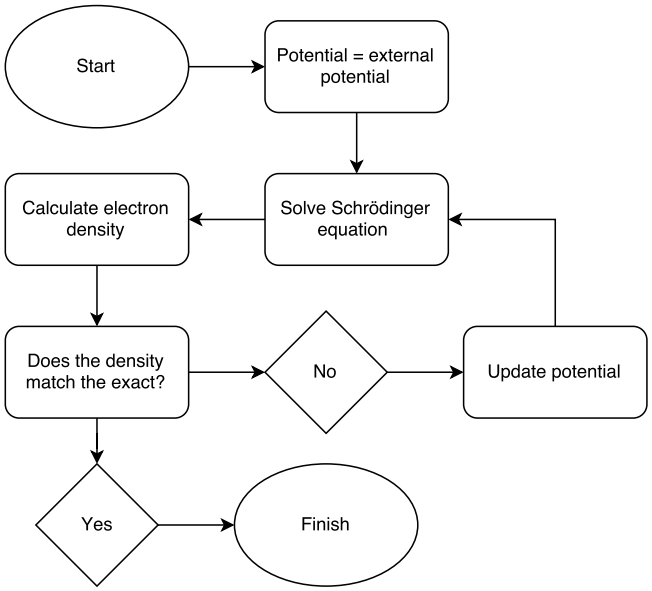


Figure 4.1: The algorithm used in iDEA to reverse engineer the exact Kohn-Sham potential for a given system.

At $t = 0$, before the system becomes dynamic, the ground-state Kohn-Sham potential describes the system. We determine this by iteratively correcting a trial potential using

$$v_{\mathrm{s}} \to v_{\mathrm{s}} + \mu \left[ n\left(x\right)^{p} - n'\left(x\right)^{p} \right], \tag{4.3}$$

where $0 < \mu \leq 1$, $n\left(x\right)$ is the ground-state density produced by $v_{\mathrm{s}}$, and $n'\left(x\right)$ is the target ground-state density (in this case the exact many-electron density). This iterative procedure, which builds on that set out in Ref. [109], clearly has the correct fixed point $n = n'$ for any $p$ and $\mu$, and we find especially rapid convergence when $p \approx 0.05$ and $\mu = 1$; see Appendix A.1.1 on page 120. We monitor the convergence using the integrated absolute error in the density,

$$f_n = \int_{-\infty}^{\infty} \left| n\left(x\right) - n'\left(x\right) \right| \mathrm{d}x. \tag{4.4}$$

The use of a small value of $p$ focuses the emphasis of the iterative procedure on the low-density regions, where substantial adjustments to the potential are needed, while avoiding oscillatory instabilities arising from unduly large adjustments to the potential in the high-density regions. Reducing $f_n$ below $10^{-11}$ a.u. is rapid, requiring around 1500 iterations. We have found this method to be robust, accurate and fast, for a variety of systems.

We use the same numerical methods, where appropriate, for the noninteracting and interacting calculations, to minimise numerical error. The time-dependent Kohn-Sham potential allows the dynamics of the density to be completely described by the single-particle Kohn-Sham orbitals, which obey the 1D version of Eq. (2.22), on page 26, and yield the electron density through the 1D version of Eq. (2.23), on page 26.

When our system becomes dynamic we implement a variant of the reverse-engineering algorithm of Ramsden and Godby [10], where we iteratively correct a time-dependent Kohn-Sham vector potential, $A_{\mathrm{s}}$, at each time step; see Fig. 4.2.[6]

[6]This reverse engineering algorithm was implemented in iDEA by Matt Hodgson.

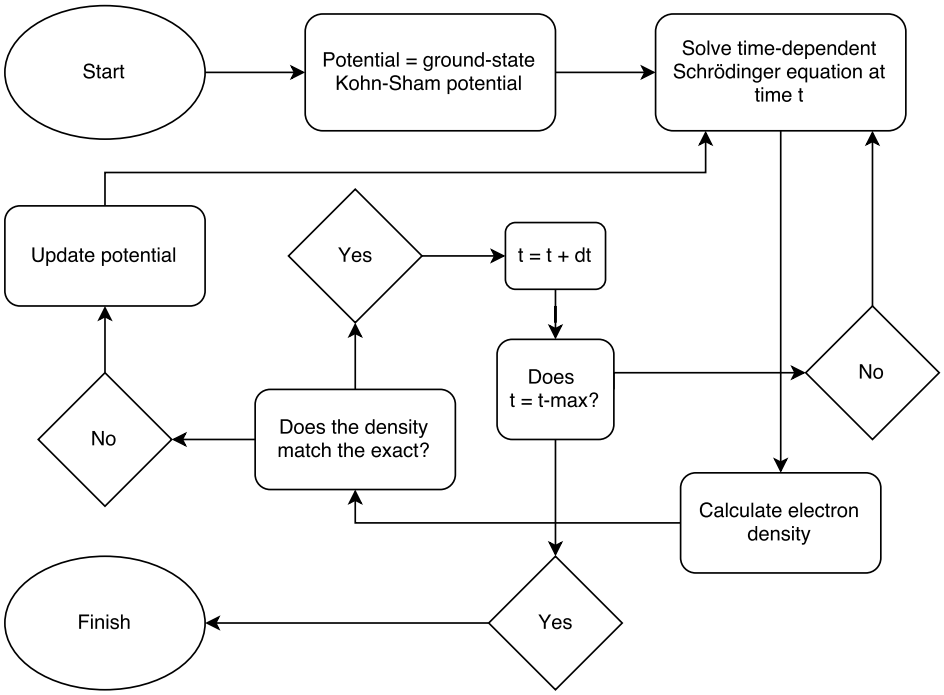


Figure 4.2: The algorithm used in iDEA to reverse engineer the exact *time-dependent* Kohn-Sham potential for a given system.

For this method we temporarily switch to an electromagnetic gauge in which the time-dependent Kohn-Sham potential is split into a *static* scalar potential (the ground-state Kohn-Sham potential plus the external applied field) and a time-dependent vector potential

$$v'_{\mathrm{s}}(x, t > 0) = v_{\mathrm{ext}}(x) + v_{\mathrm{Hxc}}(x, 0)$$
$$A'_{\mathrm{s}}(x, t > 0) = \int_{0^+}^{t} \mathrm{d}t' \, \frac{\partial}{\partial x} v_{\mathrm{Hxc}}(x, t' > 0),$$

where the notation $0^+$ denotes integrating from a time infinitesimally after zero; see Appendix A.1.2.1 on page 120. The vector potential is introduced into the Hamiltonian by adding it to the momentum operator in the usual way. Working in this gauge reduces computational cost by eliminating the need for a spatial integration in every iteration of the algorithm, as well as improving numerical stability. The vector potential is obtained using the iterative procedure

$$A_{\mathrm{s}} \to A_{\mathrm{s}} + \nu \, \frac{j\,(x,t) - j'\,(x,t)}{n'\,(x,t)}, \tag{4.5}$$

where (typically) $\nu = 0.5$, which causes the noninteracting current density, $j$, produced by $A_{\mathrm{s}}$, to converge towards the interacting current density, $j'$. We calculate $j$ and $j'$ directly from their respective time-dependent charge densities, via the continuity equation, $\partial_t n + \partial_x j = 0$, using a numerical time derivative of the charge density and a numerical integration. This use of the continuity equation guarantees that the two densities $n$ and $n'$ automatically match at each time, in addition to $j$ and $j'$, as required.

Having calculated these potentials we transform them to the gauge where the vector potential is zero, so that the time-dependent Kohn-Sham potential is represented completely by a time-dependent scalar potential, as is conventional for finite systems.

The main functions of iDEA are shown in Algorithm 1 below.

**Algorithm 1** This algorithm describes the main function of iDEA. (Italics represents time-dependence, hence not required for a ground-state calculation.)

1: Define the system by the choice of external potential
2: Evolve a trial antisymmetric wavefunction through imaginary time to find the ground-state, fully correlated many-electron wavefunction
3: *Apply our choice of perturbing field*
4: *Evolve the many-electron wavefunction through real time*
5: Calculate the exact electron density (*and current*) from the many-electron wavefunction
6: Reverse-engineer the exact electron density to find the exact ground-state Kohn-Sham potential
7: *Reverse-engineer the exact time-dependent electron and current densities to find the time-dependent Kohn-Sham potential*

### 4.1.2 Testing iDEA

Having written the code, testing is of the utmost importance. Below we outline some of the tests carried out to check iDEA. We generally rely on analytic results to test that our code is correct, as a result we note that no single test can be done to ensure that all aspects of the code work.

#### 4.1.2.1 Ground-state density and energy test

As there exists an analytical solution for noninteracting electrons in a harmonic oscillator, we test iDEA using a potential of the form $v_{\text{ext}} = \frac{1}{2}\omega^2 x^2$. It is straightforward to calculate the ground-state density and energy for $N$ noninteracting electrons in this potential well. This serves as a test of iDEA, as the energy is readily available from the imaginary-time propagation of the wavefunction; see Appendix A.3.1, on page 122, for more detail. Figure 4.3 shows the energy as the trial wavefunction converges towards the ground-state wavefunction for a system of two noninteracting electrons in the harmonic potential above. (Generally we find converged results for $\delta x \leq 0.1$.)

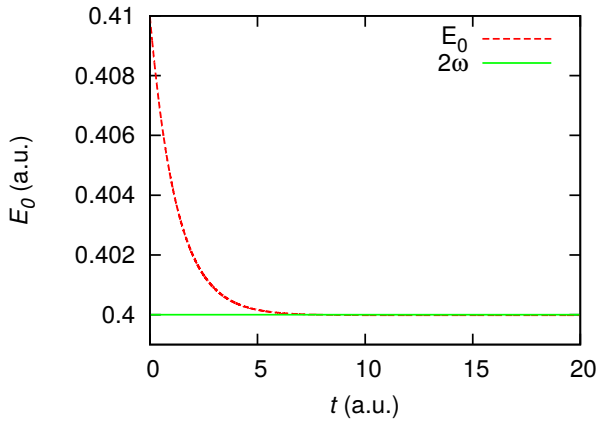


Figure 4.3: The many-body ground-state energy ($E_0$) for two *noninteracting* electrons in a harmonic well ($\frac{1}{2}\omega^2 x^2$) calculated using iDEA with the interaction term set to zero (red dotted). The analytically known energy is $2\omega = 0.4$ (solid green). $E_0$ converges exponentially towards the correct answer as the trial wavefunction is propagated through imaginary time ($t' = -it$).

The energy correctly converges to the analytical value, given by $E_0 = \omega \sum_{n=0}^{1} \left(n + \frac{1}{2}\right) = 2\omega$. The ground-state density for this system is also very accurate compared to the exact solution,

which is of the form $n(x) = \sqrt{\frac{\pi}{\omega}}\left(2x^2+1\right)e^{-\omega x^2}$. However this does not allow us to test the interaction between the electrons nor the time-dependent aspects of the code, nor does it test the reverse engineering.

#### 4.1.2.2 Time-dependent density test

To test the time-dependent code we continue to use the harmonic potential (stated before), but now for a time-dependent system. Consider *three noninteracting* electrons in a harmonic well, where the external potential is $v_{\text{ext}} = \frac{1}{2}\omega^2x^2 - \varepsilon_0 x$ (a harmonic potential with a linear electric field). We can express this external potential as a 'shifted' harmonic well, because $\frac{\omega^2}{2}\left(x - \frac{\varepsilon_0}{\omega^2}\right)^2 - \frac{\varepsilon_0^2}{2\omega^2} = \frac{1}{2}\omega^2x^2 - \varepsilon_0 x = v_{\text{ext}}$. Hence by considering the ground-state solution of the shifted potential as the starting excited state of the non-shifted well, we can time-evolve the system using $\psi_k(x,t) = \sum_n c_{k,n}\phi_n(x)e^{-i\varepsilon_n t}$, where $\psi_k(x,t)$ is the wavefunction of the $k^{\text{th}}$ electron in the shifted well, $\phi_n(x)$ is the $n^{\text{th}}$ eigenfunction of the Hamiltonian of the non-shifted system and $\varepsilon_n$ is the corresponding eigenenergy; see Appendix A.3.2, on page 123, for detail. Figure 4.4 shows the electron density calculated using iDEA and our analytical solution.

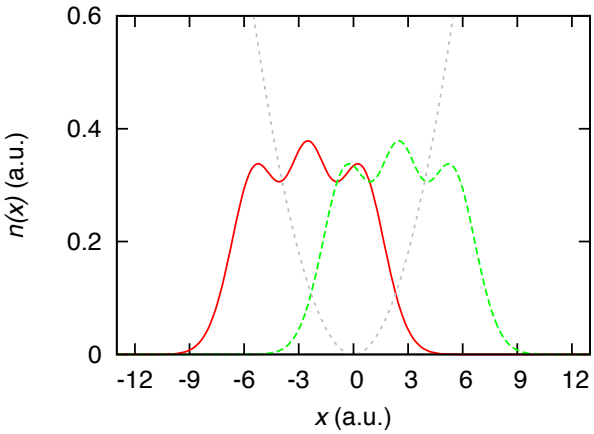


Figure 4.4: The electron density of three noninteracting electrons in a harmonic well with an applied linear electric field, calculated using iDEA at $t = 0$ (red solid, left-hand density) and for $t = \pi/\omega$ (dashed green, right-hand density). The analytical densities overlap exactly with the iDEA densities. Grey dotted line represents the external potential.

These noninteracting densities also obey the harmonic potential theorem (HPT) [110] (incidentally, interacting electrons also obey the HPT, but that is not being tested here) and oscillate with the correct frequency (calculated classically; see Appendix A.3.2 on page 123).

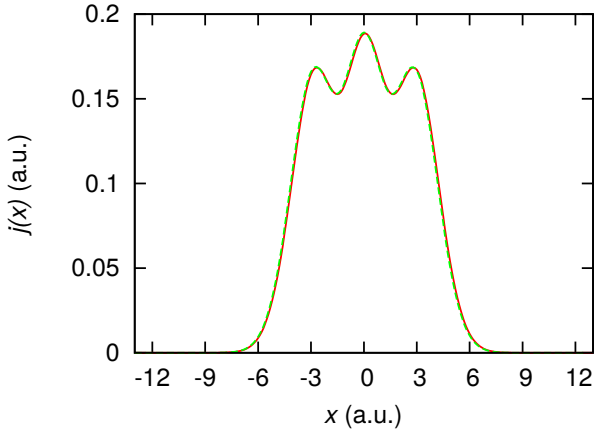


Figure 4.5: The current density of three noninteracting electrons moving a harmonic well, calculated using iDEA (solid red) and also from our analytic wavefunctions (dashed green). They match well at all times [$t = \pi/(2\omega)$ shown; the time corresponding to the maximum current].

The analytical current here is calculated via a different numerical procedure (from the wavefunction) compared to iDEA (which uses the electron density); see Appendix A.3.2 on page 123 – both currents match well for all times as required.

#### 4.1.2.3 Coulomb interaction test

We further test iDEA by comparing the ground-state of two *interacting*, spinless electrons in a harmonic well (same external potential as above) to that given by the analytical solution of the same system, known as Hooke's atom [111]. We find that the two electron densities correspond; see Fig. 4.6.

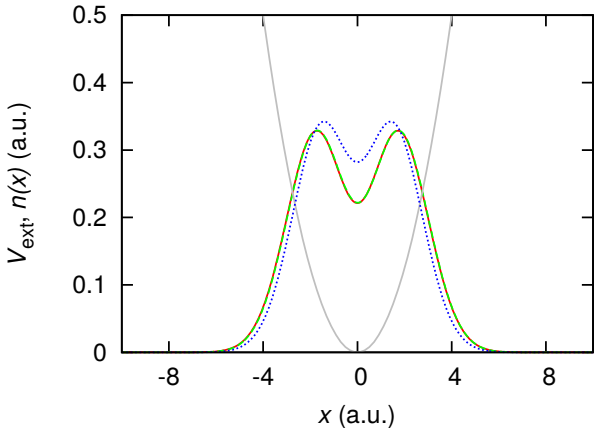


Figure 4.6: Two interacting, spinless electrons in a harmonic well. The red solid line is the many-electron density from iDEA, and the green dashed line is the analytical density [111], they overlap exactly. The blue dotted line is the noninteracting density; the interaction acts to 'push' the peaks in the electron density apart. (The grey line is the external potential.)

#### 4.1.2.4 Reverse engineering test

For our final test we artificially set the interaction strength to zero. Hence, as the Kohn-Sham system and the many-electron system are identical, the Hartree-exchange-correlation potential must be zero. This may serve as a test for our reverse-engineering code. We choose

to study a system of three electrons, that, once again, do not interact with each other and correctly find that $v_{\mathrm{xc}}(x,t) = 0$. While this test is necessary for the code to be correct it is not sufficient to prove that it is. Therefore, we also reverse engineer the electron density corresponding to a spin-singlet, *i.e.*, two *spin-half* electrons in one Kohn-Sham orbital, as, in this case, the Kohn-Sham potential can be analytically found [11, 82, 112, 113]. Once again, we find that the reverse engineering algorithm correctly finds the exact Kohn-Sham potential.

We also note that as our reverse engineered densities (for any system) are accurate ($f_n < 10^{-11}$ a.u.), and the Hohenberg-Kohn theorem states that no two potentials can yield the same ground-state density, we can be confident that the reverse engineering algorithm finds the exact Kohn-Sham potential. (This is also true for the time-dependent Kohn-Sham potential, however, numerical error grows as the density evolves through time.) However, we note that as tiny variations in the density (possibly smaller than our $10^{-11}$ error) may lead to large features in the Kohn-Sham potential, our results must be converged with respect to grid spacing.

## 4.2 Our approach to improving density functionals

We propose to study simple systems, consisting of a few electrons, in order to derive a fundamental understanding of the Kohn-Sham potential in scenarios where the common approximations become less secure (see above). For example, by identifying what is missing from the common approximations in prototype systems we have the opportunity to develop improved approximations to the xc potential that *do* incorporate important features of the exact xc potential that are absent from common approximations, and hence give improved densities.

Table 4.2 shows our proposed classes of systems for our investigations, and the purpose of each class of system.

| **Class of system** | **Purpose** |
|---|---|
| Homogenous 'slab' systems | To find a local density approximation |
| Tunnelling electrons | Examine exact time-dependent KS potential |
| Localised electrons | The role in approximate density functionals |
| Molecules | Study origin of steps in KS potential |

Table 4.1: Table to show the class of system studied in the thesis and the purpose for studying such a class of system. (KS stands for Kohn-Sham.)

# Chapter 5

# Local density approximation from finite systems[1]

In this chapter we develop the simplest approximation to the exchange-correlation (xc) functional – a one dimensional local density approximation [2] (LDA). The LDA is a common approximation for density-functional calculations, however it is usually constructed from the homogenous electron gas (HEG). As an alternative approach, below we construct a set of three LDAs from *finite* systems consisting of a few electrons (one, two and three electrons).

Fully self-consistent density-functional calculations, using our LDAs, serve as a means of determining the scenarios where local approximations struggle to capture exchange and correlation accurately, hence providing the required systems needed to develop improved approximate functionals.

## 5.1 Introduction

The LDA [2] is the most common approximation to the xc potential $v_{\text{xc}}$. The LDA is traditionally based on knowledge of the energy of the infinite three-dimensional (3D) homogeneous electron gas [114] (HEG), in which the electrons are commonly viewed as delocalised. Although local approximations have had major success in many cases [115, 116], they fail in other situations. A notable failing is the inability to correctly cancel the spurious electron self-interaction [3, 96, 99] (discussed in Chapter 3), an error introduced by the Hartree potential. Also, the xc potential far from a finite system decays exponentially in an LDA [3, 23], rather than following the Coulomb-like $-1/r$ decay present in the exact $v_{\text{xc}}$ [22, 23]; see Section 2.5.3.1 on page 26. These failings lead to errors in the Kohn-Sham orbitals [20]. Many time-dependent density functional theory (TDDFT) calculations are performed by applying the LDA adiabatically (ALDA), which further ignores the dependence of $v_{\text{xc}}$ on a system's history and initial state, focusing instead on the instantaneous electron density. Local approximations are known to break down in a number of cases [36, 54, 117, 118, 119, 120, 121, 122, 123, 124, 125], in particular where there is strong correla-

[1] This chapter describes collaborative work that has been submitted for publication: M. T. Entwistle, M. J. P. Hodgson, J. Wetherell, B. Longstaff, J. D. Ramsden and R. W. Godby, 'Local density approximations from finite systems', submitted (2016). Sections 5.1-5.4 are adapted from that paper. Matt Hodgson participated fully in the formulation and analysis of the research, and in the collaborative writing of the paper. Mike Entwistle executed most of the calculations shown in the paper, and prepared the first draft of the paper.

tion in ground-state systems and/or strong current flow when extended to time-dependent systems; see Section 3.3 on page 34.

In this chapter we introduce a set of LDAs constructed from systems of one, two and three electrons. In contrast to a conventional LDA which is constructed through accurate (but not exact) quantum Monte Carlo (QMC) simulations of the HEG approaching the thermodynamic limit [114], our approach is to obtain a set of LDAs constructed from exact *finite* systems resembling the HEG. We refer to these finite systems as 'slabs' to emphasise that the electron density is dominated by a region of homogeneity, but decays exponentially to zero near the edges. We compare these LDAs with one another and with conventional HEG-based LDAs. We illustrate our approach in one dimension (1D), complementing other 1D LDAs that have been constructed through QMC calculations, either with a softened Coulomb interaction [126] or a specified transverse confining potential [127, 128], or through other approaches [129, 130].

We employ our iDEA code [14] – described in Chapter 4 – which determines the exact, fully-correlated, many-body wavefunction for a finite system of electrons interacting via the appropriately softened Coulomb repulsion [107] $(|x-x'|+1)^{-1}$; see Appendix A.2, on page 121, for more detail. We then find the corresponding exact Kohn-Sham system through our reverse engineering algorithm [14]. The electrons are treated as *spinless* to more closely approach the nature of exchange and correlation in many-electron systems. We then apply the LDAs to a variety of ground-state systems and find that they yield accurate densities for systems dominated by either the exchange energy or by the self-interaction correction. We demonstrate that the LDAs break down as correlation becomes strong, including when applied adiabatically to a time-dependent system.

## 5.2 Constructing the LDAs

### 5.2.1 The finite model homogeneous systems

We choose a set of *finite* locally homogeneous systems in order to replicate the HEG from which traditional LDAs are usually constructed. To generate these slab systems we use our optimisation code which uses iDEA to find the correct *external* potential $v_{\text{ext}}$ for a target interacting system with a desired electron density $n_{\text{T}}(x)$. After making an initial guess for the system, the exact many-body wavefunction is calculated and $v_{\text{ext}}$ is refined iteratively, following the method used for the Kohn-Sham potential in iDEA; see Eq. (4.3) in Subsection 4.1.1 on page 39.

The slab systems are chosen such that the majority of the density is approximately uniform over a plateau region of value $n_0$ with the edges of the system decaying rapidly to zero [Fig. 5.1(a)]. We therefore choose a target density of the form $n_{\text{T}}(x) = n_0 e^{-10^{-11}(mx)^{12}}$, where $m$ is a scaling factor chosen so that the density integrates to the appropriate number of electrons (1, 2 or 3). The external potential required to obtain the desired density profile has a non-trivial spatial dependence [Fig. 5.1(b)]. A set is created from both two and three-electron slab systems and the densities cover a typical range (up to 0.6 a.u.) that will be encountered when the LDAs are applied to test systems.

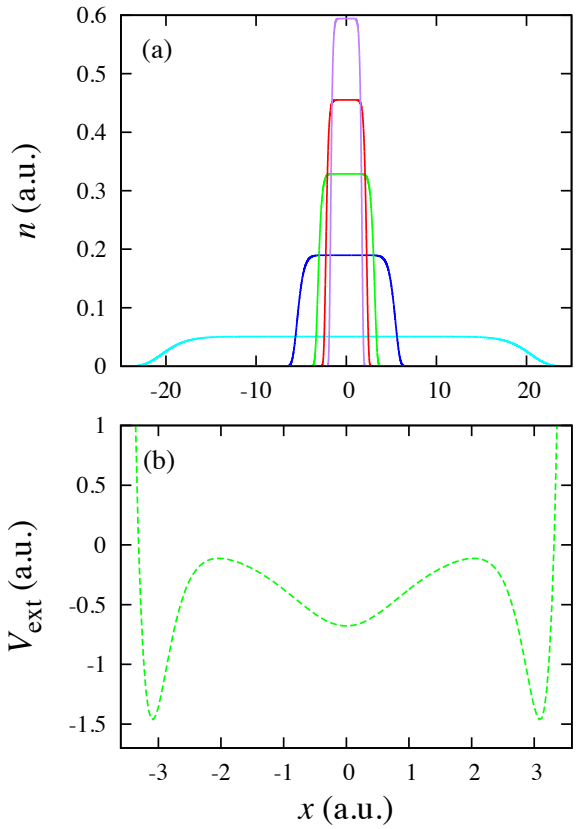


Figure 5.1: (a) The exact many-electron electron density (solid lines) for a selection of the slab systems. The density is of the form $n(x) = n_0 e^{-10^{-11}(mx)^{12}}$, to generate a uniform plateau region that decays exponentially at the edges. (b) The optimised external potential (dashed green line) for a typical two-electron slab system [middle density in (a), $n_0 \approx 0.33$].

### 5.2.2 Generating the LDAs

Having characterised the many-electron slab systems we then find the corresponding Kohn-Sham systems through our reverse-engineering code. By calculating the exact xc energy $E_{xc}$ for each slab system we obtain a set of data points for the exact xc energy per electron $\varepsilon_{xc} = E_{xc}/N$ in terms of the electron density of the plateau regions, *i.e.*, at this stage neglecting the inhomogeneous regions of the slab systems. We then apply a fit to determine a functional form of $\varepsilon_{xc}(n)$ for the two-electron ($2e$) (shown in Fig. 5.2) and three-electron ($3e$) slab systems. These initial LDAs are refined below.

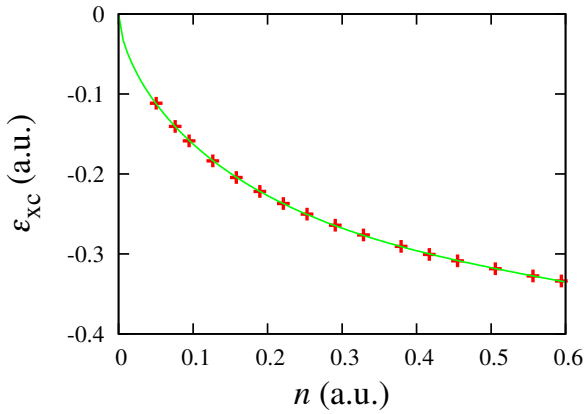


Figure 5.2: The exact $\varepsilon_{xc}$ (red crosses) for the $2e$ slab systems with the assigned values for the electron density being that of the plateau region $n_0$. The fit applied (solid green line) is of the form $\varepsilon_{xc} = (A + Bn + Cn^2)n^D$, where $A, B, C$ and $D$ are constants. This initial LDA is subsequently refined by applying it to the slabs themselves (see text).

To approximate the xc energy of an inhomogeneous system the LDA focuses on the local electron density at each point in the system:

$$E_{xc}^{LDA}[n] = \int n(x)\varepsilon_{xc}(n)\mathrm{d}x, \tag{5.1}$$

where $\varepsilon_{xc}(n)$ is the xc energy per electron of a HEG of density $n$ in a traditional LDA; see Section 2.2.3.2 on page 23. This approximation becomes exact in the limit of the HEG, *i.e.*, the systems from which an LDA is constructed. In the same spirit, we require our LDAs that have been constructed from finite slab systems to yield the exact xc energies when applied to those same slab systems.

We apply the initial LDAs to the $2e$ and $3e$ slab systems. Small errors in the xc energy $\Delta E_{xc}$ are found due to the inhomogeneous regions of the slab systems being ignored when the LDAs were originally constructed. We use the calculated errors to determine refined forms for $\varepsilon_{xc}$ in the LDAs, $\varepsilon_{xc}(n) \to \varepsilon_{xc}(n) - \Delta E_{xc}(n)/N$:

$$2e : \varepsilon_{xc}(n) = (-0.74 + 0.68n - 0.38n^2)n^{0.604} \tag{5.2}$$

$$3e : \varepsilon_{xc}(n) = (-0.77 + 0.79n - 0.48n^2)n^{0.61}. \tag{5.3}$$

These refined forms for $\varepsilon_{xc}$ reduce $\Delta E_{xc}$ from $2\% - 3\%$ to below $0.5\%$ when applied to the slab systems. This refinement process is thus determined to be sufficient.

When the LDAs are applied to inhomogeneous systems it is the xc potential that is the crucial quantity used to determine the electron density. $v_{\mathrm{xc}}$ is the functional derivative of the xc energy which in the LDA becomes:

$$v_{\mathrm{xc}}^{\mathrm{LDA}}(x) = \frac{\delta E_{\mathrm{xc}}^{\mathrm{LDA}}[n]}{\delta n(x)} = \varepsilon_{\mathrm{xc}}(n(x)) + n(x)\frac{\mathrm{d}\varepsilon_{\mathrm{xc}}}{\mathrm{d}n}\bigg|_{n(x)}. \tag{5.4}$$

The following expressions are therefore obtained from Eq. (5.2) and Eq. (5.3) respectively:

$$2e : v_{\mathrm{xc}}(n) = (-1.19 + 1.77n - 1.37n^2)n^{0.604} \tag{5.5}$$

$$3e : v_{\mathrm{xc}}(n) = (-1.24 + 2.1n - 1.7n^2)n^{0.61}. \tag{5.6}$$

### 5.2.3 An LDA from *one-electron* slabs

So far we have constructed LDAs from systems of two and three interacting electrons. Owing to the absence of the Coulomb interaction it is simple to construct *one-electron* (1$e$) slab systems. In a 1$e$ system the Hartree energy is entirely self interaction and so the xc energy is entirely self-interaction correction:

$$\varepsilon_{\mathrm{xc}} = E_{\mathrm{xc}} = -E_{\mathrm{H}} = -\frac{1}{2}\int\int \frac{n(x)n(x')}{|x-x'|+1}\mathrm{d}x\mathrm{d}x', \tag{5.7}$$

where the electron density is of the same form as the 2$e$ and 3$e$ slab systems, $n(x) = n_0 e^{-10^{-11}(mx)^{12}}$; see Subsection 2.5.3.1 on page 26.

A selection of slab systems is chosen and $\varepsilon_{\mathrm{xc}}$ is calculated to build up a set of data points. An initial fit is found and the same refinement process used in the 2$e$ and 3$e$ slab systems is applied. From this an expression for $\varepsilon_{\mathrm{xc}}$ and $v_{\mathrm{xc}}$ follows:

$$\varepsilon_{\mathrm{xc}}(n) = (-0.803 + 0.82n - 0.47n^2)n^{0.638} \tag{5.8}$$

$$v_{\mathrm{xc}}(n) = (-1.315 + 2.16n - 1.71n^2)n^{0.638}. \tag{5.9}$$

### 5.2.4 Comparison of 1e, 2e and 3e LDAs

We now compare the 1$e$, 2$e$ and 3$e$ LDAs that have been developed. The strong similarity between the three LDAs can be seen in the refined curves for $\varepsilon_{\mathrm{xc}}$ [Fig. 5.3(a)]. This is remarkable considering physical correlation is absent in one-electron systems and $\varepsilon_{\mathrm{xc}}$ consists entirely of self-interaction correction. Whilst the three curves effectively overlap at low densities, they deviate slightly at higher densities [inset of Fig. 5.3(a)] with these deviations being numerically significant. There is a clear progression from 1$e$ to 2$e$ to 3$e$.

This is also seen in the refined curves for $v_{\mathrm{xc}}$ [Fig. 5.3(b)]. The 1$e$ and 2$e$ overlap at high densities with the 3$e$ curve deviating slightly.

### 5.2.5 The one-dimensional homogeneous electron gas

Various parameterisations [3, 26, 131] of QMC calculations show that in the case of a 3D HEG, the exchange energy per electron $\varepsilon_{\mathrm{x}}$ is dominant over the correlation energy per elec-

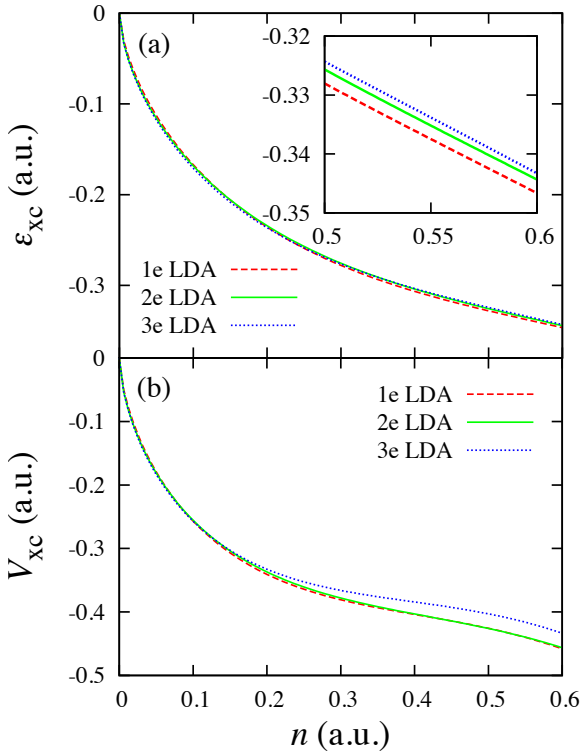


Figure 5.3: (a) The refined curves for $\varepsilon_{xc}$ in the 1$e$ (dashed red line in both plots), 2$e$ (solid green line in both plots) and 3$e$ (dotted blue line in both plots) LDAs. Inset: close-up of the three curves at higher densities. The slight deviations at higher densities are numerically significant. There is a clear progression from 1$e$ to 2$e$ to 3$e$. (b) The refined curves for $v_{xc}$ in the 1$e$, 2$e$ and 3$e$ LDAs. The closeness of the three curves, in each case, is striking.

tron $\varepsilon_c$, particularly for higher densities. We solve the Hartree-Fock (HF) equations to determine the exact $\varepsilon_x$ for a 1D HEG consisting of an infinite number of electrons interacting via the softened Coulomb repulsion $u(x-x')$:

$$\varepsilon_x = -\frac{1}{8\pi^2 n}\int_{-\pi n}^{\pi n} \mathrm{d}k \int_{-\pi n}^{\pi n} \mathrm{d}k' u(k-k'), \tag{5.10}$$

where the Fourier transform of $u(x-x')$ is integrated over the plane defined by the Fermi wave vector $k_F = \pi n$, for a HEG of density $n$.

Using Eq. (5.10) we calculate $\varepsilon_x$ for a set of HEGs covering the range of densities used in the LDAs. We then apply a fit to determine a functional form of $\varepsilon_x$ for the 1D HEG. From this we find that the $\varepsilon_x$ curve in the 1D HEG is surprisingly close to the $\varepsilon_{xc}$ curves in the 1$e$, 2$e$ and 3$e$ LDAs (Fig. 5.4). This suggests that $\varepsilon_x$ is the dominant term in $\varepsilon_{xc}$ in the case of a 1D HEG, even more so than in the 3D case.

In Ref. [126], QMC calculations of a 1D HEG of electrons interacting through a slightly different softened Coulomb interaction are used to determine a functional form for $\varepsilon_c$. We evaluate $\varepsilon_x$ using the method of Eq. (5.10) for this HEG, and find $\varepsilon_c$ to be of the order of a few percent of $\varepsilon_{xc}$, except in the low-density limit. Assuming this result to be applicable to our own (very similar) 1D HEG, we conclude that the $\varepsilon_{xc}$ curve constructed from a HEG for our softened interaction would be close to the three $\varepsilon_{xc}$ curves for our LDAs constructed from finite systems (Fig. 5.4). That is, in 1D, an LDA constructed from small finite systems is very similar to one constructed from the infinite HEG.

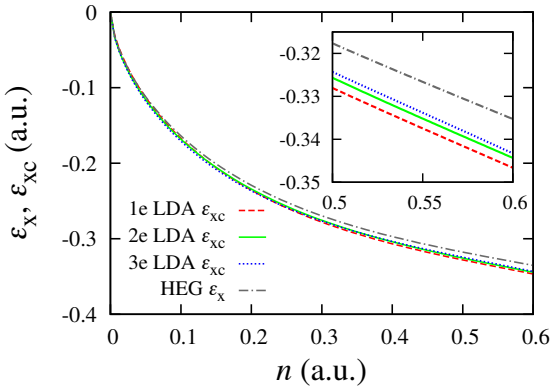


Figure 5.4: The exact exchange energy $\varepsilon_x$ (dotted-dashed dark-grey line) of a 1D HEG of density $n$. The $\varepsilon_{xc}$ curves in the 1$e$ (dashed red line), 2$e$ (solid green line) and 3$e$ (dotted blue line) LDAs are repeated from Fig. 5.3 for comparison. Inset: close-up of the four curves at higher densities. All four curves are remarkably similar, indicating the importance of exchange in 1D, and showing the similarity of the different LDA approaches in 1D systems.

The concept of constructing LDAs from finite systems may be readily extended to higher dimensions, and test calculations show this to be feasible. We find that an LDA constructed from one-electron systems in 3D, for example, exhibits a form for $\varepsilon_{xc}$ that is qualitatively similar to that of a traditional LDA constructed through QMC calculations.

### 5.2.6 Physics of the slab systems

To determine what fraction of $\varepsilon_{xc}$ for the (many-electron) slab systems is due to $\varepsilon_x$ and what fraction is due to $\varepsilon_c$, we apply the HF method self-consistently to the 2$e$ and 3$e$ slab systems (as defined by the external potentials). We find the HF method reproduces accurate densities for high-density slab systems but breaks down for low-density slab systems. This suggests that correlation (which the HF method neglects) increases as we progress to lower densities, which is consistent with the 3D HEG. This agrees with earlier QMC studies of silicon that show the xc hole in lower density regions can have non-local features and hence is impossible to reproduce accurately with a semi-local functional, which implies that lower density regions are generally more correlated [132].

In both the 2$e$ and 3$e$ slab systems, we calculate $\varepsilon_x$ to be the dominant component in $\varepsilon_{xc}$, with $\varepsilon_c$ increasing as we move to lower density slab systems. However, we see that the correlation energy remains small ($<$ few%) in all the slab systems, a feature which is common to all our 1D test systems. The breakdown of the HF method suggests the slab systems are extremely sensitive to this small amount of electron correlation. In this sense, the low-density slabs are in fact systems of relatively strong correlation.

Traditional LDAs become exact in the limit of the HEG, *i.e.*, when applied to the systems from which they were constructed. Our finite LDAs are, by definition, exact for the total energy when applied non-self-consistently to the slab systems, but it is of interest to examine the *self-consistent* application of our LDAs to the slabs; explored below.

We find that in high-density slab systems the electron density is well matched due to the external potential being the dominant component in $v_s$. This becomes less so as we move to lower densities in which the 'base' of the external potential becomes wider [see Fig. 5.1(b)

for a 2$e$ slab case]. Consequently, erroneous dips and bumps form in the plateau regions of the LDA electron density.

To examine the errors in the density we analyse $v_{xc}$. As well as missing out the long-range $v_{xc}$ fields that are present in the exact system, we find the LDAs break down in the critical central region where the vast majority of the electron density is. We can attribute this to the exact $v_{xc}$ being highly nonlocal in these systems whereas the LDAs only depend on the local density.

The self-consistent energies of our slab systems are accurate with errors below 1%, despite the self-consistent density being far from exact. Hence, as shown in Ref. [133], errors in the density can be cancelled by errors inherent in the approximate energy functional. However, the derivative of the energy functional is less forgiving of these errors, leading to an inaccurate xc potential and density.

Electron localisation [113, 134] is the tendency of an electron in a many-body system to exclude other electrons from its vicinity (see Chapter 7). The electron localisation function (ELF) [135, 134, 136], provides a useful indicator of localisation: $ELF = 1$ is complete localisation, *i.e.*, the chance of finding one electron in the vicinity of another is zero. ELF ranges from 0 to 1, and a HEG has $ELF = 0.5$. For comparison we apply the exact ELF developed by Dobson [135] (using our knowledge of the many-body wavefunction) to the 2$e$ slab systems. We find that the electrons are extremely localised towards the edges of the systems but as we approach the interface between the electrons strong delocalisation occurs (Fig. 5.5). The plot shows that as we move to a high-density slab system, this dip in localisation increases in depth and occupies a greater proportion of the overall system. (This is also observed in the 3$e$ slab systems, however there is an extra localisation peak and dip due to the third electron.)

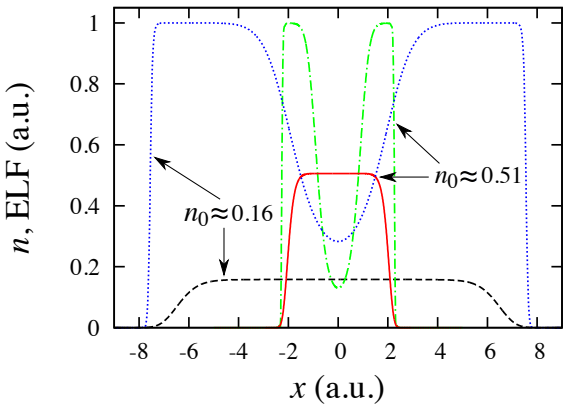


Figure 5.5: The exact many-body electron density (dashed black line) and ELF (dotted blue line) for a low-density two-electron slab system ($n_0 \approx 0.16$). Also plotted are the exact many-body electron density (solid red line) and ELF (dotted-dashed green line) for a high-density two-electron slab system ($n_0 \approx 0.51$). In both systems, we find that the electrons are extremely localised towards the edges but as we approach the interface between the electrons (where they are more likely to be found near one and other) strong delocalisation occurs. In the high-density slab system, this dip in localisation is deeper and occupies a greater proportion of the overall system.

Our results show two major differences in electron localisation between the slab systems and the HEG. First, the ELF is constant across a HEG and is independent of the density. It varies

between (many-electron) slab systems of different densities and is position-dependent. Second, the slab systems have regions of very high localisation. In the HEG, the ELF is defined to be 0.5 in this case, but our results (*e.g.*, Fig. 5.4) indicate that the physical nature of the correlation (in the broad sense) in a HEG is, in fact, much more akin to that in relatively strongly localised systems – such as our finite slab systems – than is often supposed. That is, in a HEG, at densities much greater than those required to obtain strict localisation through Wigner crystallisation, a degree of localisation exists which might be termed incipient Wigner crystallisation.

## 5.3 Application to exchange-dominated systems

In the previous section we observed the dominance of the exchange energy in the slab systems. In this section we investigate the capacity of our LDAs to describe systems dominated either by the exchange energy or by the self-interaction correction.

### 5.3.1 Two-electron triple well

We begin the testing of the LDAs by studying a ground-state system where the electrons are *highly localised*: two electrons subject to an external potential consisting of a deep, central well and two identical, shallow, side wells (two-electron triple well). The exact many-body electron density, which we calculate using iDEA, is compared to the density that is obtained when we apply the 2*e* LDA self-consistently and the density obtained when we use the noninteracting approximation [Fig. 5.6(a)]. The LDA does a remarkable job of matching the exact electron density. The Hartree potential acts to drive the electrons apart, with the xc potential then making the density accurate. However, the noninteracting approximation wrongly predicts both electrons occupying the central well, due to the first two single-particle energy states being lower than the potential barrier between the central well and the side wells. The HF method performs very well in this system due to strong exchange.

To understand these results we analyse the xc potential[2]. The large dips in the exact $v_{\text{xc}}$ [Fig. 5.6(b)] corresponding to the peaks in the electron density are primarily due to the *self-interaction correction*, *i.e.*, occurring in regions of high electron localisation. The LDA does quite an extraordinary job of replicating this which explains the success in approximating the electron density. This is a particularly striking feature as traditional LDAs do not perform well in highly localised systems, as they are unable to accurately describe the self-interaction correction. The discrepancy in $v_{\text{xc}}$ in the low density regions, at the interfaces of the wells in $v_{\text{ext}}$, is due to the LDA being dependent on the local density and hence not accounting for nonlocal effects. These nonlocal features in the exact $v_{\text{xc}}$ lead to, amongst other things, lower peaks in the density in the side wells [inset of Fig. 5.6(a)]. As expected, the LDA incorrectly predicts $v_{\text{xc}}$ decaying exponentially rather than following a Coulomb-like $-1/x$ decay.

We now look at how well each of the LDAs describe the self-interaction correction in this system. To do this we compare the electron density as predicted by each LDA to the exact

[2]The exact $v_{\text{xc}}$ is obtained up to an additive constant, which we choose so that $v_{\text{xc}}$ asymptotically approaches zero as $|x| \to \infty$.

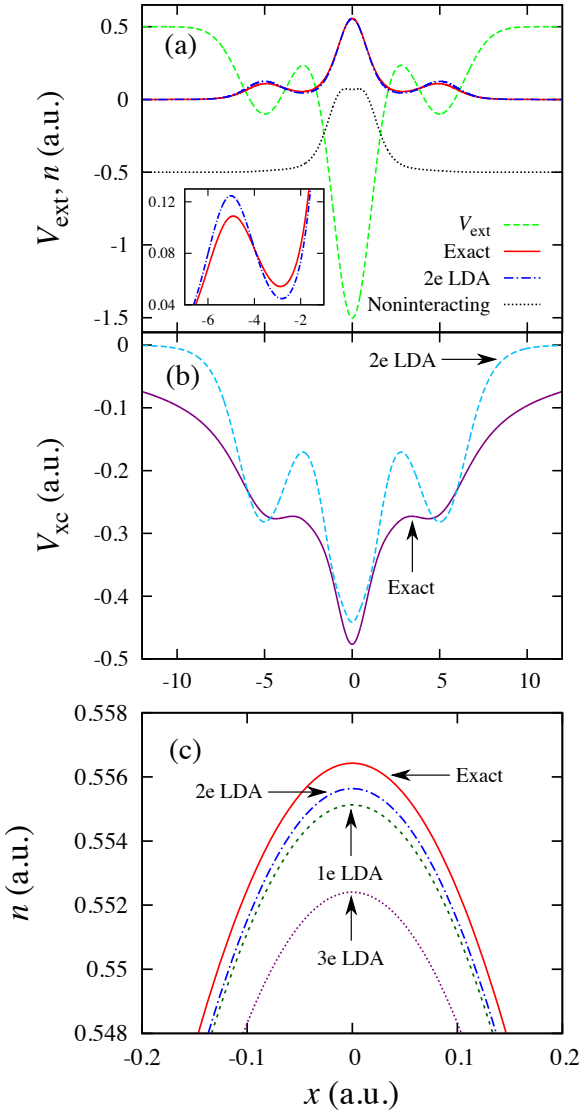


Figure 5.6: A triple well containing two electrons. (a) A comparison of the exact many-body electron density (solid red line), the density obtained from applying the 2*e* LDA (dotted-dashed blue line) and the density obtained when we use the noninteracting approximation (dotted black line, shifted down by 0.5 to more easily distinguish between the different densities), along with the external potential (dashed green line). The LDA approximates the density remarkably well, whilst the noninteracting approximation incorrectly predicts both electrons occupying the central well. Inset: close-up of the exact density and the 2*e* LDA density at the interface between the left-hand side well and the central well. (b) The exact $v_{xc}$ (solid purple line), along with the $v_{xc}$ obtained from applying the 2*e* LDA (dashed light-blue line). The LDA replicates the self-interaction correction remarkably well, seen in the large dips in $v_{xc}$. However, it misses out nonlocal features present in the exact $v_{xc}$. (c) Detail of the peak of the exact many-body electron density (solid red line) in the central well along with the densities obtained by applying the 1*e* (short-dashed dark-green line), 2*e* (dotted-dashed blue line) and 3*e* (dotted purple line) LDAs. All three LDAs accurately describe the self-interaction correction.

Table 5.1: The total energies and xc energies calculated self-consistently using the LDAs and their associated errors for the two-electron triple well. All three LDAs perform very well in both cases.

| LDA | $E^{\mathrm{LDA}}$ (a.u.) | $\Delta E$ (a.u.) | % Error | $E_{\mathrm{xc}}^{\mathrm{LDA}}$ (a.u.) | $\Delta E_{\mathrm{xc}}$ (a.u.) | % Error |
|---|---|---|---|---|---|---|
| 1$e$ | -0.698 | -0.008 | -1 | -0.474 | -0.007 | -1 |
| 2$e$ | -0.697 | -0.007 | -1 | -0.472 | -0.005 | -1 |
| 3$e$ | -0.698 | -0.008 | -1 | -0.472 | -0.005 | -1 |

many-body electron density in the highly-localised central well [Fig. 5.6(c)]. The 2$e$ LDA is the most accurate, closely followed by the 1$e$ LDA and then the 3$e$ LDA. However, in general, we find that the $N$-electron LDA ($N = 1, 2$ or 3) does not necessarily perform best when applied to an $N$-electron system. In the majority of systems we study, the 1$e$ LDA most accurately describes the self-interaction correction, followed by the 2$e$ LDA and then the 3$e$ LDA.

The final quantities we use to compare the merits of the LDAs are the approximations to $E$ and $E_{\mathrm{xc}}$, due to the fundamental importance of energy calculations in DFT. To do this we first calculate the exact $E$ for the two-electron triple well system through iDEA and from this we calculate the exact $E_{\mathrm{xc}}$. We obtain $E = -0.690$ a.u. and $E_{\mathrm{xc}} = -0.467$ a.u.

For each LDA we take the self-consistently calculated electron density to determine the self-consistently calculated energies. The set of self-consistently calculated $E$, $E^{\mathrm{LDA}}$, along with the error relative to the exact $E$, $\Delta E$ and the corresponding percentage error, % error are given in Table 5.1. Also given are the set of self-consistently calculated $E_{\mathrm{xc}}$, $E_{\mathrm{xc}}^{\mathrm{LDA}}$, along with the error relative to the exact $E_{\mathrm{xc}}$, $\Delta E_{\mathrm{xc}}$ and the corresponding percentage error, % error. The results show that all three LDAs do an impressive job of approximating $E$ and $E_{\mathrm{xc}}$.

### 5.3.2 One-electron harmonic well

We now study a ground-state system in which exchange and correlation consist exclusively of the self-interaction correction: *one* electron subject to a harmonic external potential (one-electron harmonic well). The electron behaves as a quantum harmonic oscillator with the density forming a single peak in the centre of the well. This exact electron density is compared to the density that is obtained when we apply the 1$e$ LDA self-consistently and the density obtained when we set $v_{\mathrm{xc}} = 0$, *i.e.*, Hartree theory (HT)[3] [Fig. 5.7(a)]. Much like in the two-electron triple well, the LDA gives a result which closely matches the exact electron density. It captures the central peak in the density and correctly predicts its rate of decay towards the edges of the system. It is worth noting that all three LDAs give very similar results with the 1$e$ LDA performing the best by a small margin. We choose to only illustrate the 1$e$ LDA here. Again, using HT gives a poor performance which misses out both of these features. Both the HF method and the noninteracting approximation are exact in a one-electron system.

In a one-electron system the exact $v_{\mathrm{xc}}$ is just the negative of the Hartree potential $v_{\mathrm{H}}$. Much like the LDAs' remarkable success in the two-electron triple well, in which $v_{\mathrm{xc}}$ is mostly self-

[3]The $v_{\mathrm{xc}} = 0$ approximation (Hartree theory) provides a benchmark against which we test the LDAs' ability to describe the self-interaction correction; see Section 2.3 on page 24.

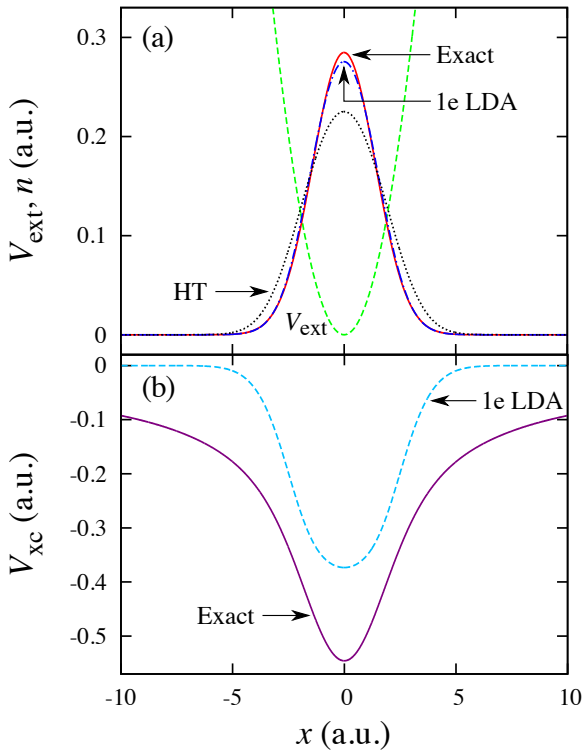


Figure 5.7: A harmonic well containing one electron. (a) A comparison of the exact many-body electron density (solid red line), the density obtained from applying the 1$e$ LDA (dotted-dashed blue line) and the density obtained when we use HT (dotted black line), along with the external potential (dashed green line). Again, the LDA approximates the density remarkably well. It captures the central peak in the density and correctly predicts its rate of decay towards the edges of the system. This is a significant improvement on HT. (b) The exact $v_{xc}$ (solid purple line) for the one-electron harmonic well, along with the $v_{xc}$ obtained from applying the 1$e$ LDA (dashed light-blue line). $v_{xc}$ in this system is entirely self-interaction correction and the LDA performs well, much like it did in the two-electron triple well in which $v_{xc}$ was mostly self-interaction correction. The LDA accurately describes the dip in $v_{xc}$ in the centre of the system, however, there is an error relative to the exact $v_{xc}$. Again, the LDA incorrectly predicts $v_{xc}$ decaying exponentially rather than following a Coulomb like $-1/x$ decay.

Table 5.2: The total energies and xc energies calculated self-consistently using the LDAs and their associated errors for the one-electron harmonic well. Whilst the % errors in the total energy and the xc energy are larger than in the two-electron triple well, the relative errors are of the same order. Again, all three LDAs give similar results.

| LDA | $E^{\mathrm{LDA}}$ (a.u.) | $\Delta E$ (a.u.) | % Error | $E_{\mathrm{xc}}^{\mathrm{LDA}}$ (a.u.) | $\Delta E_{\mathrm{xc}}$ (a.u.) | % Error |
|---|---|---|---|---|---|---|
| 1$e$ | 0.138 | 0.011 | 9 | -0.225 | 0.012 | 5 |
| 2$e$ | 0.139 | 0.012 | 9 | -0.223 | 0.014 | 6 |
| 3$e$ | 0.137 | 0.010 | 8 | -0.224 | 0.013 | 5 |

interaction correction, it also performs well at approximating $v_{\mathrm{xc}}$ in this system [Fig. 5.7(b)]. The LDA accurately describes the dip in $v_{\mathrm{xc}}$ in the centre of the system, however, there is an error relative to the exact $v_{\mathrm{xc}}$. Again, the LDA incorrectly predicts $v_{\mathrm{xc}}$ decaying exponentially rather than following a Coulomb like $-1/x$ decay. (We have tested the LDA in a variety of harmonic wells as we vary the angular frequency $\omega$ and we obtain similar results.)

As for the two-electron triple well, we perform energy calculations to obtain $E = 0.127$ a.u. and $E_{\mathrm{xc}} = -0.237$ a.u. We calculate $E^{\mathrm{LDA}}$ for each LDA along with $\Delta E$ and the % error. This is displayed in Table 5.2. Also given is the calculated $E_{\mathrm{xc}}^{\mathrm{LDA}}$ for each LDA along with $\Delta E_{\mathrm{xc}}$ and the % error. Whilst the % errors are noticeably larger in this system than in the two-electron triple well (see Table 5.1), it is the relative errors $\Delta E$ that are important. (Adding a constant to $v_{\mathrm{ext}}$ will change the % errors but not $\Delta E$.) These are of the same order as those in the two-electron triple well, with all three LDAs performing similarly.

### 5.3.3 Summary

We observe our LDA calculations to yield accurate electron densities for a variety of exchange-dominated systems, even when the LDA is constructed from one-electron systems. The most striking aspect of our LDAs are their ability to accurately describe the self-interaction correction. This is remarkable as local approximations are traditionally known to be incapable of accurately describing this feature. However, we note that some systems exhibit highly nonlocal features in the exact exchange-correlation potential, such as potential steps and other features in low density regions [137, 138]; see Chapters 7 and 8. These absent nonlocal features in $v_{\mathrm{xc}}^{\mathrm{LDA}}$ can lead to inaccurate electron densities for ground-state systems, as well as for time-dependent systems; see Section 5.4.2 and Section 5.5.

## 5.4 Application to more strongly correlated systems

In the previous section we observed the capacity of our LDAs to describe exchange and the self-interaction correction. We now study systems in which correlation is stronger, a feature which should challenge local approximations.

### 5.4.1 Two-electron harmonic wells

We now consider a pair of systems which demonstrate the effect on the LDAs when electron correlation increases: *two* electrons confined to a harmonic external potential. First,

for purposes of comparison, we consider a strongly-confining harmonic external potential ($\omega = 0.4$ a.u.) so that the system is dominated by exchange, and correlation is very low (strongly-confined harmonic well). We contrast this with a weakly-confining harmonic external potential ($\omega = 0.01$ a.u.) in which correlation increases *significantly*, as kinetic energy diminishes (weakly-confined harmonic well).

In the strongly-confined harmonic well, the HF method is almost exact due to the near absence of electron correlation. The exact electron density is compared to the density that is obtained when we apply the $2e$ LDA self-consistently and the density obtained when we use the noninteracting approximation [Fig. 5.8(a)]. We find that our LDA performs very well in this system, which is consistent with the other two exchange-dominated systems in the previous section. (All three LDAs perform similarly.) Again, we analyse $v_{\text{xc}}$ and find that the LDA misses out key nonlocal features, *e.g.*, a central bump in the exact $v_{\text{xc}}$, formed from the superposition of two steps (yielded by a single interaction term), which acts to drive the electrons further apart, leading to a discrepancy in the electron density; see Chapters 7 and 8. Even though $v_{\text{ext}}$ is the dominant component in $v_{\text{s}}$, the Coulomb interaction is key to push the electrons apart, which is evident by comparing the exact density and the LDA density to the noninteracting approximation.

As we move to the weakly-confined harmonic well, we find that correlation increases. This is evident in the electron density produced by the HF method becoming worse, which we compare with the exact density, the density obtained when we apply the $2e$ LDA self-consistently and the density obtained when we use the noninteracting approximation [Figure 5.8(b)]. Despite the LDA being constructed from slab systems in which correlation is significant, we find that it completely breaks down in this system. It incorrectly predicts three peaks in the electron density and appears to closely approximate a slab-like system. The noninteracting approximation performs much worse than in the strongly-confined harmonic well.

We analyse $v_{\text{xc}}$ and find that, unlike in the strongly-confined harmonic well in which the LDA underestimated the central bump present in the exact $v_{\text{xc}}$, it does worse in this system by incorrectly predicting a central dip in $v_{\text{xc}}$ [Fig. 5.8(c)]. This, along with the LDA vastly underestimating the two other dips in $v_{\text{xc}}$, leads to the three peaks that are seen in its approximation to the electron density. Again, the LDA incorrectly predicts an exponential decay of $v_{\text{xc}}$ towards the system's edges.

Finally, we perform energy calculations to obtain $E = 0.068$ a.u. and $E_{\text{xc}} = -0.215$ a.u. for the weakly-confined harmonic well. We calculate $E^{\text{LDA}}$ for each LDA along with $\Delta E$ and the % error. This is displayed in Table 5.3. The LDAs give good approximations to $E$ despite poor electron densities [133].

We calculate $E_{\text{xc}}^{\text{LDA}}$ for each LDA along with $\Delta E_{\text{xc}}$ and the % error for the weakly-confined harmonic well. This is also displayed in Table 5.3. Clearly the LDAs perform much worse at approximating $E_{\text{xc}}$ than they do at approximating $E$. Whilst we find the errors are substantially larger than in the strongly-confined harmonic well (error $\sim 2\%$ for all three LDAs), one might expect a larger error on the basis of the inaccuracy of the density given by the LDAs [see Fig. 5.8(b) for the $2e$ LDA].

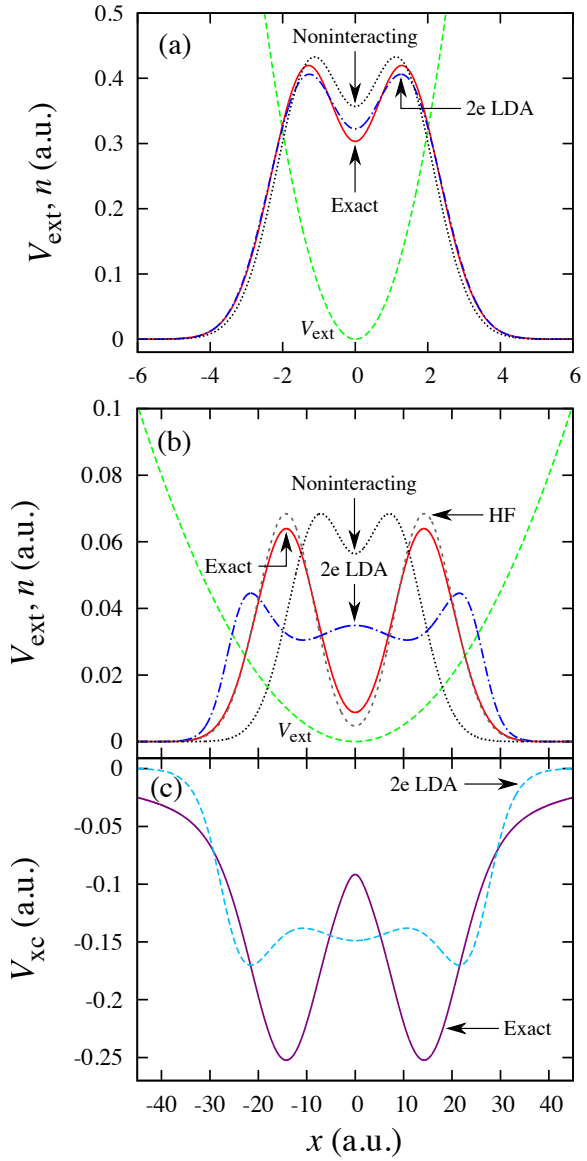


Figure 5.8: Two-electron harmonic wells with weak and stronger correlation. (a) A comparison of the exact many-body electron density (solid red line), the density obtained from applying the 2$e$ LDA (dotted-dashed blue line) and the density obtained when we use the noninteracting approximation (dotted black line), along with the external potential (dashed green line) for the strongly-confined harmonic well. The LDA performs very well in this exchange-dominated system. (b) A comparison of the exact many-body electron density (solid red line), the density obtained from applying the 2$e$ LDA (dotted-dashed blue line), the density obtained when we use the noninteracting approximation (dotted black line) and the density obtained when we use the HF method (short-dashed dark-grey line), along with the external potential (dashed green line) for the weakly-confined harmonic well. The LDA completely breaks down in this strongly-correlated system. (c) The exact $v_{xc}$ (solid purple line) for the weakly-confined harmonic well along with the $v_{xc}$ obtained from applying the 2$e$ LDA (dashed light-blue line). The LDA incorrectly predicts a central dip in $v_{xc}$. This, along with the LDA vastly underestimating the two other dips in $v_{xc}$, leads to the three peaks that are seen in the electron density.

Table 5.3: The total energies and xc energies calculated self-consistently using the LDAs and their associated errors for the weakly-confined harmonic well. The LDAs give good approximations to $E$ despite poor electron densities, which we attribute to a cancellation of errors. They perform much worse at approximating $E_{\rm xc}$.

| LDA | $E^{\rm LDA}$ (a.u.) | $\Delta E$ (a.u.) | % Error | $E_{\rm xc}^{\rm LDA}$ (a.u.) | $\Delta E_{\rm xc}$ (a.u.) | % Error |
|---|---|---|---|---|---|---|
| 1$e$ | 0.072 | 0.004 | 6 | -0.182 | 0.033 | 15 |
| 2$e$ | 0.066 | -0.002 | -3 | -0.186 | 0.029 | 13 |
| 3$e$ | 0.063 | -0.005 | -7 | -0.191 | 0.024 | 11 |

### 5.4.2 Tunnelling system

We now extend our study to a *highly correlated* time-dependent system in which there is *strong current flow*: two electrons confined to an external potential consisting of two wells separated by a long flat barrier, $v_{\rm ext} = \alpha x^{10} - \beta x^4$, where $\alpha = 5 \times 10^{-11}$ a.u. and $\beta = 5 \times 10^{-5}$ a.u. For $t > 0$ a perturbing electric field $v_{\rm pert} = -\varepsilon x$, where $\varepsilon = 0.01$, is applied [Fig. 5.9(a)] to induce quantum tunnelling (tunnelling system) [14].

The Pauli exclusion principle, combined with the Coulomb repulsion, forces the electrons to localise in opposite wells resulting in a small-density barrier (central) region. This is well matched, both when we apply the 2$e$ LDA and when we use the noninteracting approximation [Fig. 5.9(b)]. We apply the HF method and find this to be an exchange-dominated system. Again, the LDA accurately describes the large self-interaction correction present in the highly-localised wells. As in the strongly-confined harmonic well, there is a central bump present in the exact $v_{\rm xc}$, which is due to the superposition of two steps; see Chapter 8, Section 8.7.1 on page 110. The LDA misses out this key feature, which acts to drive the electrons apart, leading to higher peaks in the exact electron density.

The application of the electric field initially causes the electrons to oscillate within their respective wells. Eventually the electron in the left hand well begins to tunnel through the potential barrier towards the right hand well. Correlation increases as the electrons begin to explore different orbitals. We apply the LDA adiabatically, $v_{\rm xc}^{\rm ALDA}[n](x,t) = v_{\rm xc}^{\rm LDA}[n(t)](x)$, to examine how well it approximates the dynamic electron density once there has been sufficient tunnelling ($t = 40$ a.u.), along with the result that is obtained when we use the noninteracting approximation [Fig. 5.9(c)]. Whilst the LDA still manages to replicate the exact density well, it fails in the critical central region which indicates that the tunnelling rate is too high. However, it is an improvement on the density that is obtained when we neglect the Coulomb interaction.

To explore this we first define the tunnelling rate as the rate at which the total electron density in the left hand side (LHS, $x < 0$) of the system decreases with time. (This is deemed to be a sufficient approximation as the electrons start in a highly localised ground state.) We now plot the exact total electron density in the LHS as a function of time, the approximation produced from applying the LDA and the result obtained when we use the noninteracting approximation (Fig. 5.10). The exact and ALDA tunnelling rates increase as the LHS electron gains kinetic energy, before decreasing in response to an increase in the Coulomb repulsion; whereas the noninteracting tunnelling rate continues to increase. It is clear that the LDA over-predicts the rate of tunnelling. By taking the gradients of the three curves, we measure the magnitude of the LDA tunnelling rate to be, on average, nearly twice that of the exact

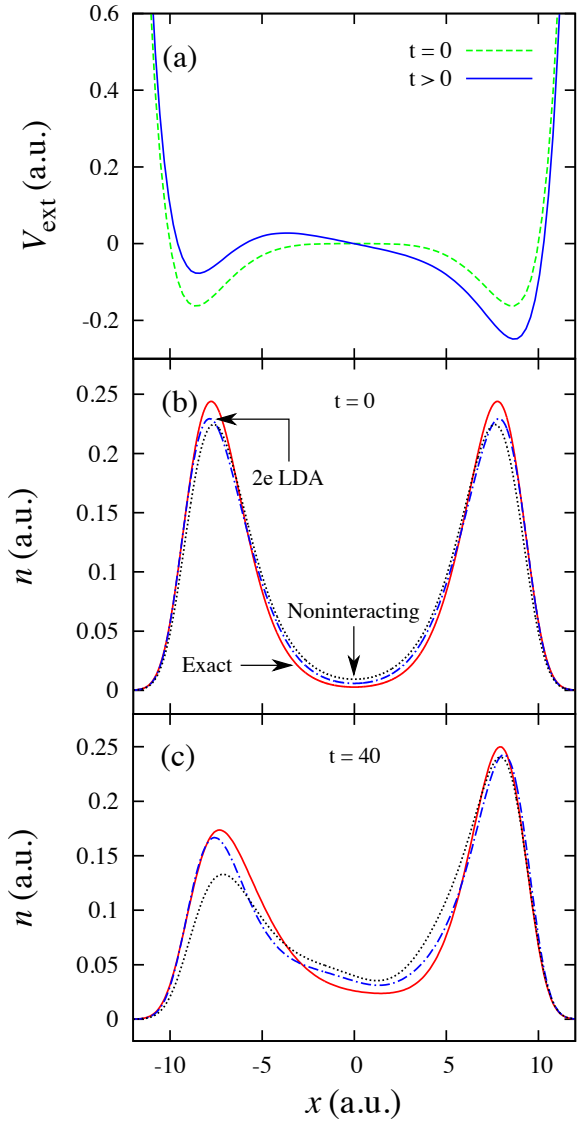


Figure 5.9: A tunnelling system containing two electrons. (a) The unperturbed external potential $v_{ext} = \alpha x^{10} - \beta x^4$, $t = 0$ (dashed green line), and the perturbed external potential with the electric field $-\varepsilon x$, applied for $t > 0$ (solid blue line). (b) A comparison of the exact many-body electron density (solid red line), the density obtained from applying the $2e$ LDA (dotted-dashed blue line) and the density obtained when we use the noninteracting approximation (dotted black line) for the system's ground-state, $t = 0$. The Pauli exclusion principle, combined with the Coulomb repulsion, forces the electrons to localize in opposite wells resulting in a small-density barrier (central) region. The LDA and the noninteracting approximation both match this well. (c) A comparison of the exact many-body electron density (solid red line), the density obtained from applying the $2e$ LDA (dotted-dashed blue line) and the density obtained when we use the noninteracting approximation (dotted black line) at a later time, $t = 40$ a.u., once there has been sufficient tunnelling. Whilst the LDA still manages to replicate the exact density well, it fails in the critical central region which indicates that the tunnelling rate is too high.

tunnelling. Although this is a large reduction in the erroneous tunnelling rate obtained when we use the noninteracting approximation.

Dynamic potential steps have previously been shown to be important nonlocal features which give rise to accurate electron densities [6, 138, 139]; we explore the exact Kohn-Sham system in Chapter 6. We observe a dynamic step to grow in the exact $v_{\mathrm{xc}}$ (and hence $v_{\mathrm{s}}$) in the central density minimum, which in turn controls the tunnelling rate. Unsurprisingly, this characteristic is missing from the LDA $v_{\mathrm{xc}}$. In order to slow the tunnelling rate to an appropriate amount, a better approximate functional will be needed; one that takes into account the current density, which is particularly sensitive to interaction in this system; see Chapter 7. We observe this through the LDA current density quickly deviating from the exact current density, which is reflected in the time-dependent density.

We find that at early times, errors in the time-dependent density depend heavily on how well the ground state is approximated. Therefore, we find that accurately describing ground-state features is crucial. At later times, the error in the LDA density grows primarily due to increasing correlation.

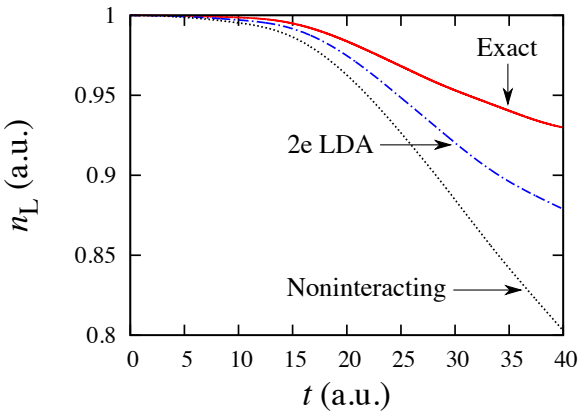


Figure 5.10: The exact total electron number in the LHS ($x < 0$) of the system $n_{\mathrm{L}}$ (solid red line), the approximation produced from applying the $2e$ LDA adiabatically (dotted-dashed blue line) and the one obtained when we use the noninteracting approximation (dotted black line). The tunnelling rates are therefore given by the gradients of the curves. It is clear that the LDA overestimates the rate of tunnelling. By taking the gradients of the three curves, we measure the magnitude of the LDA tunnelling rate to be, on average, nearly twice that of the exact tunnelling rate. At early times, this error is due to the LDA missing out key ground-state features. At later times, it is primarily due to increasing correlation as the electrons explore different orbitals. The noninteracting approximation further overestimates the tunnelling rate.

### 5.4.3 Summary

Similar to traditional local approximations, we have found that our LDAs are unable to accurately describe systems in which correlation is significant. The transition from the strongly-confined harmonic well to the weakly-confined harmonic well demonstrates that whilst the LDAs can successfully be applied to exchange-dominated systems, an increase in the correlation energy causes them to become severely inaccurate. This is also observed in the tunnelling system, in which starting from a highly localised ground state, the approximation to the electron density becomes worse as correlation increases with time. Therefore, despite

the low-density slab systems being strongly correlated, correlation effects in test systems do not appear to be captured by the LDAs.

## 5.5 Landauer-style formulation

Next we explore the tunnelling system (above) more fully, and how various approximations perform for this challenging situation.

We discussed in Chapter 3 a basic, noninteracting model for current carrying, many-electron systems – the Landauer formulation. We also considered the slightly more sophisticated approach of using the ground-state Kohn-Sham potential at $t = 0$, then allowing the system to evolve with an applied, *external* field (added to the ground-state Kohn-Sham potential), *i.e.*, excluding all changes to the Kohn-Sham potential once the system becomes dynamic – an approximation more primitive than the adiabatic approximation. Both of these approaches are simple, and, as shown in Chapter 3, break down for systems where the interaction between the electrons plays a large role in the dynamics.

We asses the accuracy of the Landauer approach for our tunnelling system, and we simulate the system for a much longer time, 160 a.u. However, we note that we do not simulate the system for long enough for a steady state to be reached, and hence we refer to this as a 'Landauer-style formulation'.

When the left electron is allowed to tunnel for $\sim$ 160 a.u., we find that the interacting, localised electron experiences the Coulomb repulsion, which reduces the tunnelling rate (as seen above), and eventually reverses it. Figure 5.11 shows the exact tunnelling as a function of electron number (same as above), as well as the ALDA, the noninteracting[4] and the Landauer-style tunnelling rates for the same system. (The reverse in tunnelling does not occur for noninteracting electrons for $t < 160$ a.u.)

The Landauer-style formulation we use takes the *exact* ground-state Kohn-Sham potential (above we describe the exact ground-state Kohn-Sham potential), then we apply the perturbing electric field ($-0.01x$), and we *do not* update the potential; we term this the 'exact Landauer'. Therefore, we are giving the Landauer-style formulation the best possible chance. Even so, the formulation fails to predict the long term effects of the interaction between the electrons (not a surprising result), *i.e.*, it fails to predict the reverse in tunnelling at the correct time.[5] The approximation performs well for early times, showing that the ground-state potential is important early on, however, eventually time-dependent effects start to dominate the system; see Section 6.3 on page 71.

[4] By noninteracting, we mean that interaction is neglected entirely in the simulation.

[5] We find that by modelling this system with the Landauer-style approximation for a much longer time, the reverse in tunnelling does eventually occur, however, far later than for the exact simulation.

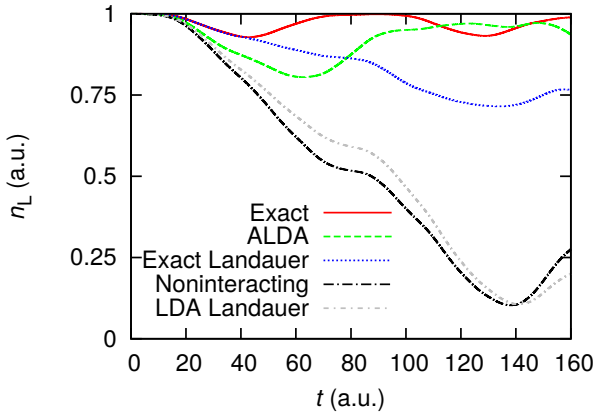


Figure 5.11: The integrated density of the left-hand subsystem for two electrons in a tunnelling system, for the exact (solid red), ALDA (dashed green), Landauer-style (dotted blue), and noninteracting (dotted-dashed black). The Coulomb repulsion causes the left, tunnelling electron to be forced back into the left well after $\sim$ 60 a.u. This total reversal of the tunnelling does not occur for the noninteracting electrons, nor does it occur for the Landauer-style approximation. The ALDA does reverse the tunnelling, but substantially later than it should, $\sim$ 80 a.u.

A Landauer formulation that is more representative of calculations commonly found in the literature is to use the LDA ground-state Kohn-Sham potential instead of the exact. In this case the approximation, unsurprisingly, performs much worse – giving similar results to simply neglecting interaction all together. For early times, using the exact ground-state xc potential in the Landauer-style formulation performs well compared to using the LDA xc potential. This shows that the *nonlocal* features of the exact *ground-state* xc potential are very important in describing the *dynamics* of the interacting system as tunnelling begins. Hence, for an approximation to work well in the time-dependent case, it not only has to replicate the nonlocal features in the exact time-dependent Kohn-Sham potential, which give rise to the correct dynamics (here reversed tunnelling), but also the nonlocal ground-state features; see Er. 1 in Section 3.3 on page 34.

The use of the adiabatic approximation (ALDA) improves the accuracy of the simulation, however, the density is still far from exact; the reverse in tunnelling occurs much later and the initial tunnelling rate is too large (see above). In order to improve the accuracy of this simulation, we must first identify what the ALDA is missing from the xc potential compared to the exact. Hence in the next chapter we model this tunnelling system *exactly*.

## 5.6 Summary

The 'usual' local density approximation (LDA), originally proposed by Kohn and Sham, is the most basic approximation to the exchange-correlation (xc) functional, but one that has performed surprisingly well for solid state physics in the past. However, problems arise from using such a simple approximation to the xc potential. Our 1D LDA is constructed from finite systems, unlike the usual LDA. This novel method of constructing the LDA yields a reasonable description of exchange [specifically the self-interaction correction (SIC)], even when the LDA is constructed from a *single* electron. We showed that while our LDA does well for strongly localised systems, due to a good description of SIC, when correlation is strong our LDA performs poorly, *e.g.*, when applied adiabatically to a time-dependent sys-

tem (in this case dynamic electron tunnelling). Furthermore, we show that nonlocal features of the exact Kohn-Sham potential are not correctly accounted for by local approximations.

Finally, we used our LDA adiabatically, along with an 'exact Landauer' approach[6], to demonstrate that important features of the exact xc potential, needed for accurate electron and current densities, are missing from these approaches when modelling many-electron tunnelling. Hence, a functional that can reproduce these features is required for a more accurate simulation. However, one must first identity these features. Hence, the tunnelling system studied in this chapter is modelled using exact time-dependent density functional theory next.

[6]By 'exact Landauer' we refer to using the *exact* ground-state Kohn-Sham potential at $t = 0$, then we apply a perturbing field and allow the system to evolve, without updating the time-dependent potential.

# Chapter 6

# Many-electron tunnelling[1]

In this chapter we study a tunnelling system using exact time-dependent density functional theory (TDDFT) because of the poor performance of local approximations at modelling such systems; see Chapter 5, Sections 5.4.2 and 5.5 on pages 62 and 65. Hence, we use our iDEA code to find the *exact*, time-dependent Kohn-Sham potential for this highly correlated system, in order to determine what features of the exact potential are absent from the local approximations.

## 6.1 Introduction

Electron tunnelling and reflection are features of all molecular devices, but many-electron aspects of these processes are generally not included in transport calculations. Fundamental studies of tunnelling in strongly correlated systems, such as Coulomb blockade [140], have shown the importance of a time-dependent description of electronic correlation. Strong correlation and tunnelling both pose particular challenges [141] for the usual approximations in TDDFT which remain to be addressed. To accurately model electron transport there is a need for studies of the xc potential for systems of multiple electrons with strong correlation and quantum tunnelling. We calculate the exact xc potential of a one-dimensional interacting model system, intended to inform the development of improved approximate functionals suitable for realistic three-dimensional systems.

## 6.2 Our tunnelling system

To determine the Kohn-Sham potential we adjust the potential experienced by noninteracting electrons such that they reproduce, at all times, the charge and current densities of the interacting system, calculated by exact numerical propagation of the time-dependent many-electron Schrödinger equation; see Chapter 4. Our iDEA code describes two electrons in one dimension, where our spatial and temporal grid spacings are $\delta x = 0.05$ a.u. and $\delta t = 0.002$ a.u. We treat our electrons as spinless, in order to maximise the richness of the exchange

[1] This chapter describes collaborative work that has been published: M. J. P. Hodgson, J. D. Ramsden, J. B. J. Chapman, P. Lillystone and R. W. Godby, 'Exact time-dependent density-functional potentials for strongly correlated tunneling electrons', *Physical Review B (Rapid Communications)* **88**, 241102(R) (2013). Sections 6.1-6.3 are adapted from that paper. Matt Hodgson participated fully in the formulation and analysis of the research, and executed the calculations shown in the paper, and prepared the first draft of the paper.

and correlation for a given computational effort; our two electrons occupy different Kohn-Sham orbitals. The form of the interaction used is $(|x - x'| + 0.1)^{-1}$, which represents a 3D nano-wire with a diameter of 1 a.u.; see Appendix A.2, on page 121, for detail.

We first describe our system through many-body quantum mechanics. Our confining potential consists of two wells separated by a long flat barrier, $v_{\text{ext}} = \alpha x^{10} - \beta x^4$, where $\alpha = 5 \times 10^{-11}$ a.u. and $\beta = 1.3 \times 10^{-4}$ a.u. For $t > 0$ a polarising uniform electric field $-\varepsilon x$, where $\varepsilon = 0.1$, is applied (Fig. 6.1), driving the electrons to the right. This is the same as the tunnelling system in Chapter 5 except we have chosen to use a much stronger electric perturbing field and hence increased the tunnelling barrier; the reason for this is explained below.

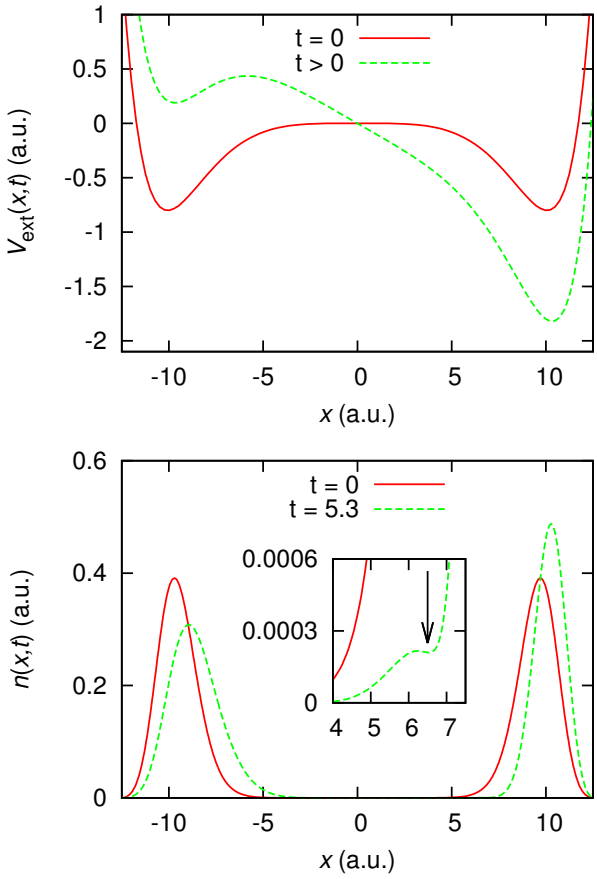


Figure 6.1: The unperturbed external potential ($v_{\text{ext}} = \alpha x^{10} - \beta x^4$, $t \leq 0$, solid red) and its perturbed counterpart (the uniform field $-\varepsilon x$ added, $t > 0$, dashed green) (top figure). The interacting charge density (bottom figure) at $t = 0$ and at a later time $t = 5.3$ a.u. The inset shows a close-up of the density in the tunnelling region; at the later time a minimum appears in the density (arrow) as a result of an interference effect (see text).

As suggested by the form of the ground-state charge density, the Pauli exclusion principle, for two spinless electrons, tends to localise the electrons in opposite wells, and this effect is enhanced by the Coulomb repulsion. Thus, the barrier region of the system has vanishingly small density (Fig. 6.1).

Accuracy in our simulations is limited by the build-up of noise over time in the reverse engineering algorithm. Figure 5.11 in Section 5.5 on page 65 clearly shows that the time-dependent features of the $v_{\text{xc}}[n](x,t)$ become crucial for an accurate description of the density in the tunnelling system at $t \sim 40$ a.u. for a field strength of $\varepsilon = 0.01$. However, our reverse engineering algorithm struggles to produce highly accurate results for such a long

simulation. Therefore, we find the exact time-dependent Kohn-Sham potential for the tunnelling system of this section, *i.e.*, with a much stronger field, $\varepsilon = 0.1$, where important features manifest *earlier* in the simulation – before noise becomes noticeable. Then we reverse engineer the system of Section 5.5 (with $\varepsilon = 0.01$) up to $t = 40$ a.u., with the understanding that, while the potential may be less accurate, feature(s) responsible for the reverse in tunnelling (see Section 5.5) will still be discernible and may correspond to the accurate features of the system described here. (Note the differences between this system and the one studied in the previous chapter; the perturbing field strength has been increased, hence the potential barrier between the electrons is larger to ensure the electron tunnels from the well.)

The initial application of the electric field begins to establish oscillatory motion of the electrons within their respective wells. Prolonged exposure to the E-field causes the left electron to tunnel through the potential barrier towards the right well, experiencing the Coulomb repulsion. This then allows a current to build in the low-density barrier region. The strength of the E-field relative to the confining potential means that both electrons acquire considerable kinetic energy within their respective wells. In the right-hand well this results in standing-wave-like 'ripples' in the density, due to interference between the waves incident on, and reflected from, the right-hand wall. (This phenomenon does not itself rely on the interaction; we have checked that similar interference ripples occur for a single electron in a single perturbed well.) When tunnelling begins, the time-evolution of the density is affected by the Coulomb repulsion, as the two electrons try to distance themselves from one another within the right-hand well.

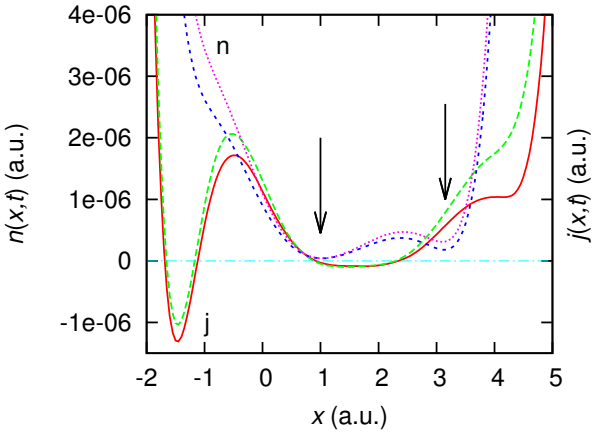


Figure 6.2: A zoomed view of the interacting charge density ($n$) in the central region (short dashed blue) and the noninteracting charge density (dotted purple), together with the interacting current density ($j$) (solid red) and the noninteracting current density (dashed green), at $t = 5.3$ a.u. The regions of particularly high current-to-charge ratio are indicated by arrows; the modification of this ratio by the Coulomb interaction is evident.

Figure 6.2, which is a further close-up, shows the charge and current density in the central part of the tunnelling region, for $t = 5.3$ a.u. (see below for details on why this time was chosen), together with the corresponding quantities in the absence of Coulomb interaction. Two effects are evident. First, as the left electron tunnels into the right well, the effect of the Coulomb repulsion is to suppress the current density on the right-hand side of the region shown. Second, the arrows in both Fig. 6.1 and Fig. 6.2 indicate locations where the ratio of current density to charge density is particularly high.

## 6.3 Steps in the exact Kohn-Sham potential

Time-dependent density functional theory (TDDFT) describes the evolution of the interacting electron density using an auxiliary noninteracting system, with an effective potential $v_s$ which we now calculate.

The nonlocal density-dependence of the xc potential is already apparent in the ground state. Owing to the double-well external potential and the Coulomb repulsion, our electrons begin in a highly localised state, which means that the dominant effect in the ground-state xc potential is the full cancellation of the spurious self-interaction described by the Hartree potential, $v_H$. Accurate self-interaction corrections of this sort are, generally, thought to be beyond the capability of the usual LDA [142]. Our LDA – constructed from finite systems – provides a surprisingly good SIC; see Chapter 5. However, it still fails to give a proper description of electron tunnelling, showing that SIC is not the only important feature of the exact $v_{xc}$ missing from local functionals.

The ground-state Hartree-xc (Hxc) potential, $v_{Hxc} = v_s - v_{ext}$, because it includes both the self-interaction and its exact cancellation, most clearly displays the *remaining* important features of the Kohn-Sham potential. The Hxc potential (Fig. 6.3) shows a highly-non-LDA 'bump' (arrow in Fig. 6.3) between the wells in the region of low charge density; as well as oppositely-signed xc electric fields within each well[2], which together push the Kohn-Sham charge density peaks apart to account for the inter-well Coulomb repulsion. Neither of these features is present in local approximations, showing the failure of the LDA in this system. These ground-state nonlocal features are also important for the *dynamics* early in the simulation; see Section 5.5 on page 65.

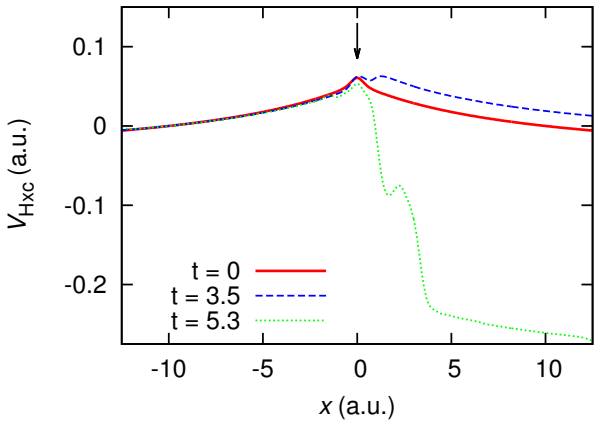


Figure 6.3: The Hxc potential in the ground state ($t = 0$) and at later times $t = 3.5$ a.u. and 5.3 a.u. Steps form and grow as a result of minima in the charge density in the regions of finite current density. The distinctive 'bump' in the ground-state Hxc potential remains to serve its initial purpose (arrow).

In the time-dependent regime, the self-interaction continues to be exactly cancelled within the Hxc potential. The locally varying corrections to $v_{Hxc}$ in the region of highest density remain minimal. Figure 6.4, the time-dependent xc potential alone, shows clearly how $v_{xc}(= v_{Hxc} - v_H)$ in the left and right wells provides the necessary self-interaction corrections, changing its form in accordance with the moving and tunnelling charge density.

[2]By removing the self-interaction correction from the xc potential we have calculated the strength of the linear xc electric field in the regions of highest charge density $|\varepsilon_{xc}| \approx 0.016$ a.u.

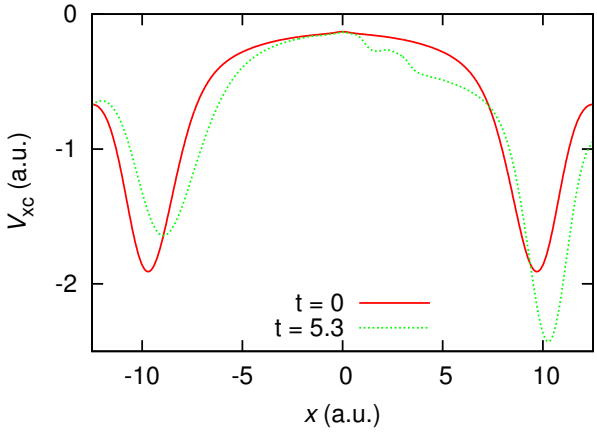


Figure 6.4: The xc potential at $t = 0$ and 5.3 a.u. In addition to the features noted in $v_{\mathrm{Hxc}}$, the changing strength of the self-interaction correction as the left electron tunnels into the right well is evident.

For the time-dependent Hxc potential (Fig. 6.3) the first feature occurs at the position of the central density minimum, $x_{min}$ (initially 0). As the left electron tunnels through the barrier, current builds in the central region, and so $x_{min}$ moves to the right, as already observed in Fig. 6.2. The build-up of current in the vicinity of the density minimum means that the current-to-charge ratio is large. In the Kohn-Sham regime this high ratio is replicated by a prominent time-dependent step in the level of the xc potential by a positive constant, that later becomes negative due to the change in sign of the current density (Fig. 6.3).

After enough time has elapsed, further steps form in the right-hand region, as a direct result of the standing-wave effect, associated with the points of high current-to-charge ratio identified above. This ratio, $u\left(x,t\right) = j\left(x,t\right)/n\left(x,t\right)$, the velocity field, can account for the steps observed in the time-dependent Kohn-Sham potential, since it is clear from Eq. (4.5) that the velocity field and the time-dependent Kohn-Sham potential are closely linked: in particular, a feature in the velocity field will in general be associated with a feature in the time-dependent Kohn-Sham potential. From $u$ it is apparent that when the current-to-charge ratio is very high, *i.e.*, for density minima, there is a peak in the velocity field, which will translate into a time-dependent peak in the Kohn-Sham vector potential. When subsequently transforming each of these peaks to the gauge in which $A_{\mathrm{s}} = 0$ in order to obtain the Kohn-Sham scalar potential (see Section 4.1.1 on page 39), we integrate its time derivative spatially, giving rise to a step, particularly if the peak is narrow, as will generally be the case at density minima. However, the mere presence of a density minimum is not a sufficient condition for a step: without the effect of the Coulomb repulsion, $j$ and $j_0$ in Eq. (4.5) can be equal without the need for a correction in the potential. To achieve any feature, the density in the neighbourhood of its minimum must be modified by the interaction; in this case this arises primarily from direct inter-well Coulomb repulsion. The arrows in Fig. 6.2 indicate those density minima that are significantly reduced in value by the Coulomb interaction. In Chapter 8 we explain the formation of steps at *some* density minima from DFT fundamentals.

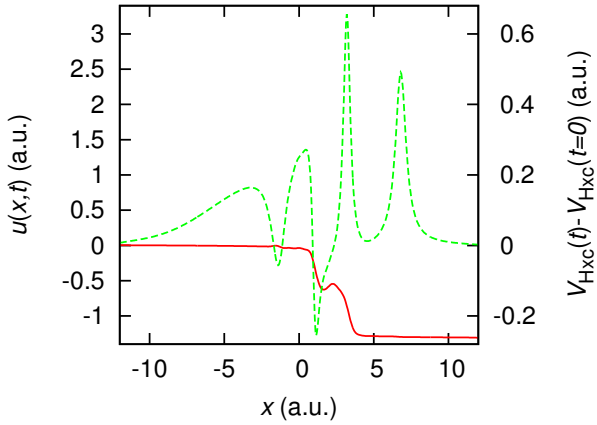


Figure 6.5: For $t = 5.3$ a.u. the velocity field (dashed green, many-body and Kohn-Sham coincide), together with the difference between the Hxc potential at $t = 5.3$ a.u. and the ground-state Hxc potential (solid red). The peaks in the velocity field align with the steps in the potential. The largest features correspond to the density most affected by the Coulomb interaction.

Figure 6.5 demonstrates the correlation between peaks in the velocity field and the step functions in the potential. The largest steps are in the central region where the density has been significantly altered by the Coulomb repulsion. Peaks further from the centre correspond to smaller steps because the strong initial localisation of the electrons reduces the effect of the Coulomb interaction on the velocity field. Our analysis of the origin of steps in the Kohn-Sham potential is quite general; in particular, we have checked that it also explains the time-dependent steps observed in Ref. [10]. Since the two ingredients of the velocity field, the current and charge densities, are always available in a TDDFT calculation, accounting for prominent features of the velocity field should be given strong consideration in the development of improved approximate functionals for use in general time-dependent systems.

Finally, we reverse engineer the system for a field strength of $\varepsilon = 0.01$ and $\beta = 5 \times 10^{-5}$ – the same system of Section 5.5. As stated above, the xc potential for later times is less accurate due to noise in the reverse engineering algorithm with an integrated absolute error in the current density $\sim 10^{-2}$ and an error in the density $\sim 10^{-1}$. However, this level of accuracy is enough for us to observe that steps continue to play a key role in determining the dynamics of the system; see Fig. 6.6. This shows that the features missing from the ALDA in Section 5.5 are nonlocal steps. The dynamic step occurs at $t \sim 40$ a.u. and develops over about 10 a.u., it acts to reduce the energy of the left well relative to the right, allowing the electron to tunnel back into the left-hand well – for the many-body system, this is done by the Coulomb repulsion. (Note, for consistency, we use the interaction term of Chapter 5 here, *i.e.*, $\gamma = 1$.)[3]

[3]Here, and the rest of this chapter, is the sole work of Matt Hodgson.

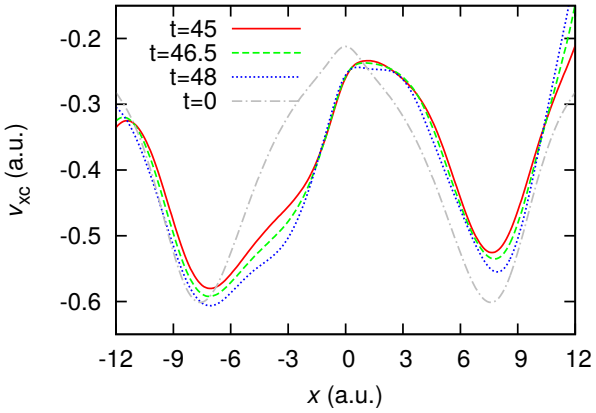


Figure 6.6: The exchange-correlation (xc) potential for the tunnelling system for $t = 45$ a.u. (solid red), $t = 46.5$ a.u. (dashed green), $t = 48$ a.u. (dotted blue) and the ground state (dotted-dashed grey). A dynamic step forms at $t \sim 40$ a.u. over about 10 a.u.; this step acts to reverse the tunnelling of the left electron. Note that the accuracy of the xc potential here is less than for the potential above, because we have reserve engineered this system for much longer. The integrated absolute error in the current density is $\sim 10^{-2}$ and $\sim 10^{-1}$ for the electron density.

## 6.4 Summary

We found the *exact* time-dependent Kohn-Sham potential for strongly correlated tunnelling electrons. The exact Kohn-Sham potential exhibits pronounced, time-dependent spatial steps that are important for a proper description of tunnelling. These steps are highly non-local in space and time, and are far beyond the scope of local and semi-local functionals, like the local density approximation and the generalised gradient approximation. We found that the steps occur at minima in the density, corresponding to peaks in the velocity field (current density divided by electron density). We noted that not all minima in the electron density correspond to steps; further insight into why steps form at some density minima is given in Chapter 8. The SIC is also a prominent feature of the exact time-dependent xc potential, due to the strong localisation of the electrons.

We then calculated the exact Kohn-Sham potential for the tunnelling system of Section 5.5 within numerical accuracy. We found that a dynamic spatial step grows over a relatively long time in order to force the the tunnelling Kohn-Sham electron back, like the electron in the exact system. Hence, showing that the nonlocal feature absent from the adiabatic local density approximation is a spatial step.

The localisation of the electrons relative to each other (one electron per well) is an important concept for features like the self-interaction correction. The act of the left localised electron tunnelling towards the right localised electron is also key in giving rise to steps in $v_{xc}$, suggesting that localisation is an important concept for our studies. Hence in the next chapter we explore the degree of localisation in our systems and the role it plays in approximating density functionals.

# Chapter 7

# The role of electron localisation in density functionals[1]

## 7.1 Introduction

Steps in the xc potential observed in the previous chapter, occur, in part, due to strong electron localisation; this is explained more fully in Chapter 8. The localisation of the electrons also gives rise to the need for a strong self-interaction correction. Electron localisation is an important concept, for example, when considering chemical bonds, however the notion of a 'localised electron' is not always well defined when one is working with quantum mechanics. Hence first we explore the concept in detail. In the rest of the chapter we demonstrate how electron localisation, driven by the Coulomb interaction and the Pauli principle, can form a powerful ingredient in approximations for the Kohn-Sham potential.

## 7.2 Localisation[2]

Electron localisation describes the tendency of an electron to exclude other same-spin electrons from its vicinity (*i.e.*, the position entanglement of like-spin electrons) [136, 143]. We choose to start from the idea that localised electrons tend to avoid one another, whereas delocalised electrons will share the same region of space. Localisation is driven by Pauli exclusion, a repulsion which acts to localise like-spin electrons in separate regions. The Coulomb interaction further enhances the tendency to localise [135]. The electrons' attempts to avoid each other increases the kinetic energy, which, however, is minimised by spreading electrons over as large a volume as possible. It is the balance between these factors that makes electron localisation challenging to quantify.

[1] This chapter describes collaborative work that has been published: M. J. P. Hodgson, J. D. Ramsden, T. R. Durrant and R. W. Godby, 'Role of electron localization in density functionals', *Physical Review B (Rapid Communications)* **90**, 241107(R) (2014). Sections 7.4-7.7.1, 7.7.3, 7.7.4 and 7.7.6 are adapted from that paper. Matt Hodgson participated fully in the formulation and analysis of the research, and executed the calculations shown in the paper, and prepared the first draft of the paper. We also give thank to Daniele Torelli for his assistance with some of the calculations in this chapter.

[2] This section and Section 7.3 are adapted from collaborative work that has been submitted for publication: T. R. Durrant, M. J. P. Hodgson, J. D. Ramsden, and R. W. Godby, 'Electron localization in static and time-dependent systems' arXiv preprint arXiv:1505.07687, (2015). Matt Hodgson participated fully in the formulation and analysis of the research, and in the collaborative writing of the paper. Tom Durrant executed most of the calculations shown in the paper, and prepared the first draft of the paper.

An understanding of electron localisation is useful chemically, placing the ubiquitous concepts of chemical bonds and localised electron pairs on a formal footing [144]. Although measures of localisation provide an understanding of bonds and electron pairs made up of electrons of *opposite spin*, these details are revealed by looking at the localisation of *like-spin* electrons, which provides the regions in which localised opposite-spin electron pairs can be found. Localisation also describes a fundamental aspect of electron correlation that approximate DFT functionals should take into account [59, 113, 145, 146, 147].

We stress that localisation is a true *many-body* property of electrons, dependent on the positions of all electrons, and not accessible through the spatial character of any one Kohn-Sham orbital. Although many early efforts focused on the extent of molecular or Kohn-Sham orbitals, it was soon realised that these orbitals are not unique and that quite different choices could be selected [143].

## 7.3 Measures of localisation

The traditional method of approximating the localisation in a system is the ELF of Becke and Edgecombe [136]. Reference [143] provides a comprehensive review of the ELF. Originally developed for Hartree-Fock calculations, the method can also be applied to Kohn-Sham orbitals.

To produce the ELF, Becke and Edgecombe scaled their measure of local localisation with that of a homogeneous electron gas (HEG) of the same local density. Hence, ELF ranges from 0 to 1, where 1 represents total localisation and 0.5 represents the degree of localisation in a HEG of the same density. Later work by Dobson [135] provides an alternative way of calculating the ELF directly from the wavefunction. And as we have access to the many-electron wavefunction for our system, we choose to use the more accurate Dobson ELF [148] below.

ELF calculations have been widely used, but less is known about their accuracy. By construction, ELF is exact in Hartree-Fock theory. Previous work on molecules has suggested that ELF can perform poorly for density functional calculations where correlation is strong [149], by comparison with the accurate configuration interaction (CI) method. It remains unclear if this is caused by approximate ELF's reliance on a single Slater determinant, or is instead due to approximate exchange-correlation (xc) potentials leading to an incorrect degree of localisation.

Durrant *et al.* evaluate the performance of the above mentioned ELFs for finite, ground-state and time-dependent systems in Ref. [148]. We find that the Dobson and Becke and Edgecombe ELF perform well for the ground state. However, once the system is strongly perturbed, the approximate form of the ELF – based on exact Kohn-Sham orbitals – reports a less accurate representation of localisation.

In the rest of this chapter we use the concept of localisation, and to a lesser extent the ELF itself, to construct an approximate density functional. We note that for a practical density functional calculation, an approximate ELF could be used to describe localisation in the system. However, in order for an approximate functional, that relies on a good description of localisation, to yield accurate electron densities, the measure of localisation would need

to be secure in the presence of strong correlation. Hence, efforts to include more accurate measures of localisation, secure for correlated systems, are desirable [150].

## 7.4 Application to density functionals

Previously we established that density functional theory (DFT) is the most widely used tool for the simulation of many-electron systems in numerous fields of physics, chemistry and materials science. Its success hinges on approximations to the xc part of the Kohn-Sham functional. Particular attention has been given to improving the time-dependent xc potential, used within time-dependent DFT (TDDFT), where the use of adiabatic functionals of the electron density ignores the role of currents and memory effects; see Chapters 3 and 5.

In this chapter we use the concept of localisation (see Sections 7.2 and 7.3), to introduce a new functional that utilises localisation as an ingredient – the mixed localisation potential (MLP) – for simulating ground-state and time-dependent electronic systems within DFT. The functional combines an expression for the exact Kohn-Sham potential in the limit of complete electron localisation with a measure of the actual localisation. We find accurate self-consistent charge densities, even for systems where the exact xc potential exhibits nonlocal dependence on the density, such as potential steps. We compare our results to the exact Kohn-Sham potential for each system. The self-interaction correction is accurately described, avoiding the need for orbital-dependent potentials.

## 7.5 The single orbital approximation

Our starting point is the Kohn-Sham potential of Refs. [82] and [112], originally derived for a system of two spin-half electrons in their spin-zero ground state; see also Appendix B.1 on page 126. We observe that the logic applies exactly to any one-electron system, and, indeed, in a general system, to all regions of space where the electron density is dominated by any one Kohn-Sham orbital[3]. For such a region the Kohn-Sham equations may be approximated as $\left(-\frac{1}{2}\nabla^2 + v_\mathrm{s}\right)\sqrt{n} = \varepsilon_k\sqrt{n}$ for the dominant orbital $\phi_k$, where $n \approx |\phi_k|^2$ in the region, yielding the ground-state Kohn-Sham potential, which we term the *single orbital approximation* (SOA),

$$v_\mathrm{SOA} = \frac{\nabla^2 n}{4n} - \frac{(\nabla n)^2}{8n^2}. \tag{7.1}$$

(Here the zero of energy in the Kohn-Sham system is at $\varepsilon_k$.)

We begin by considering Eq. (7.1) as an approximation to the universal Kohn-Sham functional. We find that the SOA not only works well for the strongly localised orbital regions, but also accounts for nonlocal features and corrects self interaction in the Kohn-Sham potential in regions of low localisation. We compare the SOA to the exact Kohn-Sham potential for a variety of ground-state and time-dependent systems that exhibit nonlocal behaviour in the xc potential. We then extend our approach by combining the SOA with a potential suited to delocalised systems, in proportions depending on the strength of localisation: the

[3] In such situations, symmetry may cause the exact Kohn-Sham orbitals to extend throughout the system. As the localised limit is approached these orbitals become degenerate and can be rotated within the Hilbert space onto effectively localised orbitals while remaining eigenfunctions of the Hamiltonian.

mixed localisation potential (MLP), introduced in Eq. (7.2) below, which is amenable to self-consistent use in DFT calculations.

## 7.6 The mixed localisation potential

A useful approximate functional must give accurate densities when applied self-consistently without prior knowledge of the exact density. The SOA is not suited to self-consistency, as it is 'unanchored' to the external potential, *i.e.*, the SOA approximates the Kohn-Sham potential and not just the xc part, hence the external potential is not fixed throughout the self-consistent iterative procedure. However, by mixing the SOA with a suitable reference potential we can better approximate the Kohn-Sham potential:

$$v_{\mathrm{MLP}} = f v_{\mathrm{SOA}} + g v_{\mathrm{ref}}, \tag{7.2}$$

where $f(x)$ and $g(x)$ depend on the localisation. We term this the *mixed localisation potential* (MLP).

For complete localisation ($ELF = 1$), $f = 1$ and $g = 0$. Similarly for the HEG ($ELF = 0.5$) $v_{\mathrm{ref}} = v_{\mathrm{LDA}}$, and hence $f = 0$ and $g = 1$ (assuming the LDA performs well for delocalised regions of density). The precise mapping between the ELF and $f$ must be that appropriate to the reference potential used. We can also infer, from the sum rule of the xc hole [20], that $f + g \approx 1$. (Note, we use this relationship to replace $g$ with $1 - f$.)

## 7.7 Calculations

Our seven test systems consist of either two or three spinless electrons in one dimension of varying degrees of electron localisation. As before, spinless electrons maximise the richness of exchange-correlation for a given computational effort, with each electron occupying a distinct Kohn-Sham orbital. The electrons interact through the appropriately softened Coulomb repulsion $(|x - x'| + 1)^{-1}$; this form of the interaction represents a nanowire of diameter 6 a.u.; see Appendix A.2, on page 121, for detail. The calculations are performed using our iDEA code [14], which determines the exact Kohn-Sham potential from the fully correlated ground-state or time-dependent many-electron wavefunction.

### 7.7.1 Double well (System 1)

We begin by studying a ground-state system where the electrons are highly localised: two spinless electrons subject to an external potential consisting of two identical spatially-separated wells together with a potential step – *in the external potential* – between them that shifts the level of the right well relative to the left [Fig. 7.1(a)]. In the absence of interaction, the electrons would simply occupy the two lowest single-particle states, which are both located in the left-hand well. The Coulomb repulsion, however, localises the electrons, with one electron per well. To reflect this (as originally noted by Almbladh and von Barth [151]), the xc part of the Kohn-Sham potential must incorporate a second spatial step between the wells, ensuring one electron per well through the ordered filling of the Kohn-Sham orbitals.

(We explore the mechanism that gives rise to steps in the xc potential fully in Chapter 8.)

We calculate the exact Kohn-Sham potential for this system and compare to that given by the SOA [Eq. (7.1)], evaluated for the exact density [Fig. 7.1(b)]. The anticipated new step in the exact Kohn-Sham potential [arrow in Fig. 7.1(b)] appears, located at the density minimum: the 'interface' between the two electrons where the localisation is lowest. The SOA replicates this xc step quite well[4], despite being at its least secure in this region of low localisation. The SOA's ability to form this potential step is particularly impressive in this region of very low electron density, showing the proper sensitivity of Eq. (7.1) to tiny variations in the density [inset in Fig. 7.1(b)]. The self-interaction correction, which is the dominant new feature in the exact $v_{xc}$ within the wells, is very well reproduced by the SOA, owing to its exactness in the limit of complete localisation.

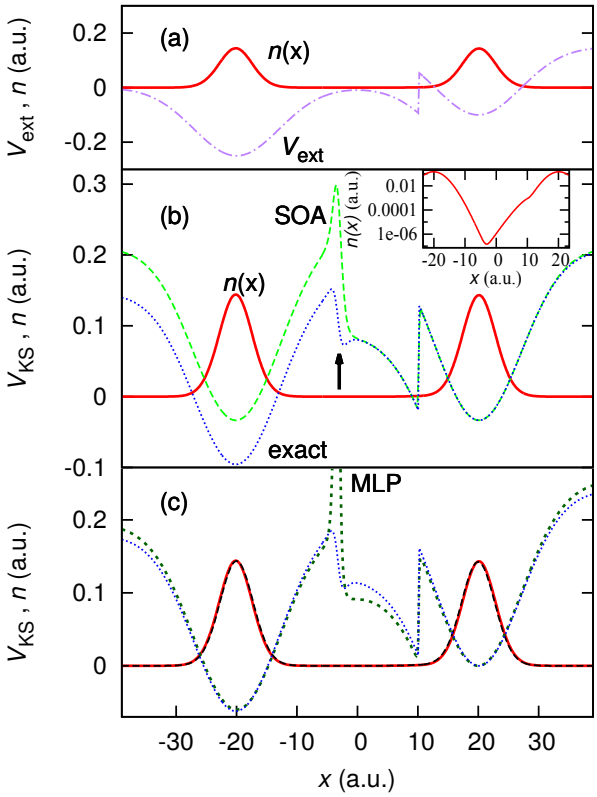


Figure 7.1: *Double well (System 1)* — (a) The exact many-body electron density (red solid line for all three plots) with the external potential (dotted-dashed purple). A potential step gives the right-hand well a lower ionisation energy, while the Coulomb repulsion ensures one electron per well. (b) The exact Kohn-Sham potential [blue dotted, also in (c)]; an xc potential step (arrow) forms at the minimum in the electron density. The SOA potential (green dashed) replicates the position and magnitude of the step well. Inset: detail of the density in the neighbourhood of the two steps. The delicate features that give rise to the steps in $v_s$ are visible at $x = -3$ a.u. and $x = 10$ a.u. (c) The *self-consistent* MLP potential, for $f = 0.6$, (short-dashed dark green) with the corresponding electron density (dashed black), which matches the exact density very well.

For a highly localised system, such as System 1, any failure of the LDA to correct the self-interaction (see Section 7.8 later) would make its use as a reference potential damaging in the regions of high density, and in the regions of low density any LDA-like potential will have small Hartree and exchange-correlation (Hxc) terms. Thus $v_{ext}$ is a superior choice of

[4]Tests indicate that the step in the exact and SOA potentials always forms at the density minimum; more detail given in Chapter. 8.

reference potential[5].

We use the MLP to solve, *self-consistently*, for two electrons in the double well system, using the standard potential-mixing iterative procedure of DFT. We choose the simplest approximation for $f(x)$ – a constant throughout space. For multiple spinless electrons we must have some delocalisation, especially at the 'interface' between the electrons, implying that $f < 1$. We have investigated a range of values of $f$, and find the density to be accurate when $f$ is in the range $0.6 - 0.99$ [Figure 7.1(c)]. (Note that for our spinless electrons in this double-well system the Kohn-Sham potential is approximately the external potential plus a new step. Therefore, $v_{\mathrm{MLP}}$ is unaffected by assuming $f$ to be lower than 1 for the regions of strong localisation, as it is simply mixed with the external potential.)

Here, $f(x) = 0.6$ (consistent with the partial delocalisation in the interface region) reproduces the features of the exact $v_{\mathrm{s}}$ with remarkable accuracy, including the alignment of the wells and the magnitude and position of both steps, correctly allowing one electron to occupy each well[6]. (In addition to the step, $v_{\mathrm{MLP}}$ also exhibits a high, narrow peak, arising from $f$ being approximated as a constant, but this has little effect on the electron density, owing to the density being very small in this region.)

### 7.7.2 Dissociated molecule (System 2)

Next we consider a system with an external potential that represents a dissociated molecule (System 2): two separated atoms where $v_{\mathrm{ext}} = -\frac{1.0}{|x-5|+1} - \frac{4.0}{|x+5|+2}$. Our dissociated molecule behaves similar to System 1; the external potential is such that two *noninteracting* electrons both localise on the left-hand atom, whereas electrons that interact via the Coulomb repulsion localise on different atoms – one electron in the left well, one in the right well; see Fig. 7.2(a). Hence, as for System 1, a step must form in the exact Kohn-Sham potential in order for the Kohn-Sham electron density to match the many-body density; see Fig. 7.2(c).

In Chapter 3 we detail why local approximations are notorious for localising the incorrect amount of charge density on each atom of a dissociated molecule. A solution to this problem is to develop an approximate functional that can reproduce steps in the xc potential, as a step is the most effective way of localising the correct amount of charge on each atom without introducing new errors into the density [151], such as the delocalisation error discussed in Chapter 3. As seen for System 1, the MLP is capable of producing accurate steps in the xc potential. Thus we now apply the MLP to our model molecule. We also apply our LDA to the same system.

Figure 7.2(b) shows the self-consistent LDA and MLP densities compared against the exact. As expected, the LDA incorrectly localises non-integer amounts of charge density on each atom, *i.e.*, the total amount of electron density on the left atom is 1.25, and hence 0.75 for the right atom, according to the LDA density; see, also, Fig. 7.3. Despite the challenging behaviour of the exact Kohn-Sham potential for this system, the MLP density agrees extremely well with the exact, localising one electron on each atomic site; see Fig. 7.3. For this system we have used $f = 0.35$ and $v_{\mathrm{ref}} = v_{\mathrm{ext}}$. Note that this system has stronger delocalisation

[5] In this case, we can approximate Eq. (7.2) as $v_{\mathrm{MLP}} = f v_{\mathrm{SOA}} + (1-f)v_{\mathrm{ext}} = v_{\mathrm{ext}} + f v_{\mathrm{SOA}}^{\mathrm{Hxc}}$, showing that the role of $f$ is to adjust the SOA Hxc potential.

[6] For potentials with sufficiently high steps, the SOA correctly places *both* electrons in the lower well, even if each Kohn-Sham electron begins in a different well at the start of self-consistency.

than System 1 because the potential wells are closer together, hence $f$ is lower. However, one should note that, once again, the MLP is accurate for a range of $f - 0.35 - 0.99$, with $f = 0.35$ yielding the most accurate form for the Kohn-Sham potential; see Fig. 7.2(c).

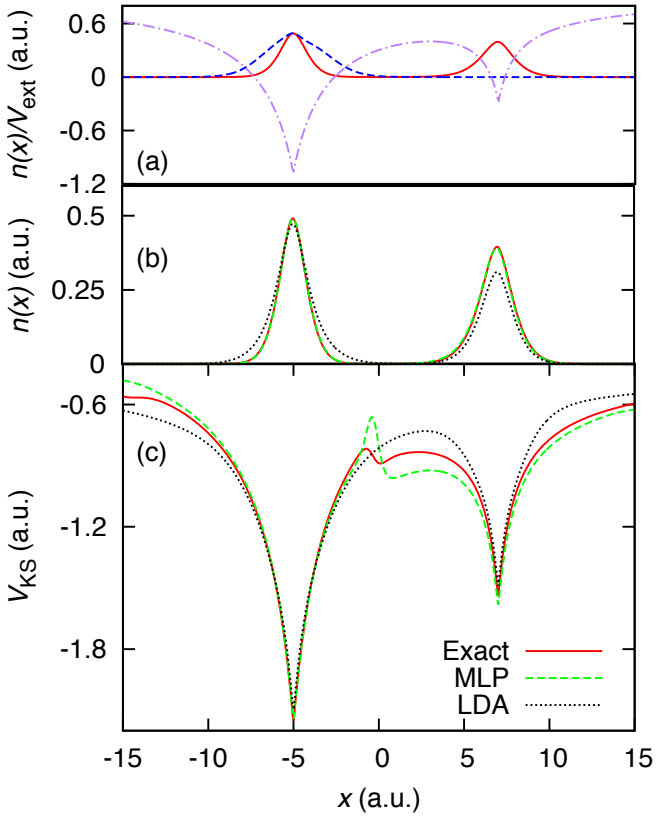


Figure 7.2: *Dissociated molecule* — (a) the external potential (dotted-dashed purple) with the ground-state density (solid red) and the noninteracting density (dashed blue). Two interacting electrons dissociate such that there is one electron's worth of charge on each atom. (b) The self-consistent LDA density (dashed-dotted black), with the exact density (solid red) and MLP density (green dashed). The LDA predicts non-integer amounts of charge in the region of each atom, whereas the exact localises exactly one electron's worth of charge on each site. The MLP density overlaps exactly with the exact. (c) The exact, LDA and MLP Kohn-Sham potential. The success of the is due to the nonlocal step in the potential. The LDA fails due to its inability to reproduce nonlocal features of the xc potential.

Figure 7.2(c) shows the exact Kohn-Sham potential for this system together with the MLP and LDA Kohn-Sham potentials. As for System 1, a step forms at the density minimum to allow for correct filling of the Kohn-Sham orbitals. Once again the MLP success in yielding an accurate electron density is due to its ability to reproduce steps in the xc potential. The failure of the LDA here is due its inability to capture the nonlocal features of the potential.

By taking the cumulative integral, from the left-hand side of the system, of the exact, MLP, LDA and noninteracting electron densities [$N(x) = \int_{-\infty}^{x} n(x')\,\mathrm{d}x'$], shown in Fig. 7.3, we can see how the exact density has precisely one electron's worth of charge on each site.

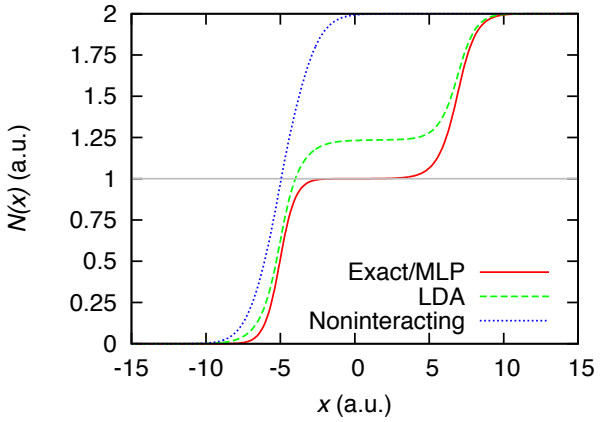


Figure 7.3: *Dissociated molecule* — the cumulative integral of the electron density, $N(x)$, for the exact/MLP (solid red) and LDA (dashed green). The self-consistent MLP density lies exactly over the exact. The LDA overestimates the amount of charge on the first site considerably, and the error persists. The blue dotted line shows $N(x)$ for the noninteracting density – the LDA performs better then this, but is still far from exact.

As predicted (see Chapter 3) the LDA does not yield one electron's worth of charge on each atom. By design, the noninteracting cumulative integrated density shows two electrons in the first potential well. The MLP, however, matches the exact strikingly well, demonstrating the improvement in the electron density when a nonlocal functional is used over the local approximation.

### 7.7.3 Single well (System 3)

Next we consider a system where the localisation of the electrons drops *significantly* below 1: two spinless electrons confined to a single well. This will establish the performance of the MLP functional well outside the limit in which the underlying SOA is exact. Figure 7.4(a) shows the Dobson ELF for this system together with the exact electron density and the MLP density, showing that the electrons are significantly delocalised in the central region. In this region the exact potential has a 'bump' which acts to push the density peaks apart, together with long-range Hxc fields on either side; the raw SOA contains both features, though their magnitude is overestimated in the delocalised region.

In forming the MLP, we are guided by the ELF in the region of low localisation and have explored a range of values for $f$ of $0.2 - 0.3$. For simplicity, we continue to use the external potential as our reference. The MLP yields high accuracy for the Hxc potential in this central region. The central bump in the potential is accurate across our range of $f$, and the corresponding densities are in good agreement with the exact. We find that $f = 0.25$ reflects the delocalisation in the central region (approximately the average of the ELF in this section), and hence yields a highly accurate $v_{\mathrm{MLP}}^{\mathrm{Hxc}}$ in the central region [see Fig. 7.4(b)].

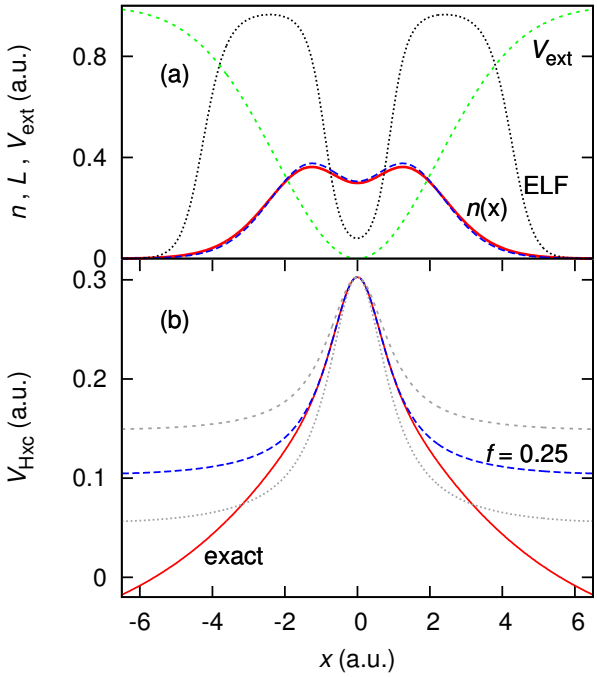


Figure 7.4: *Single well (System 3)* — (a) The many-body electron density (solid red), self-consistent MLP density (dashed blue), external potential (short-dashed green) and ELF [$L(x)$ – dotted black]. Note the large dip in the localisation of the electrons in the centre of the well. (b) The exact Hxc potential (solid red) together with the Hxc potential from the self-consistent MLP, for $f = 0.25$ (dashed blue; also $f = 0.2$ and 0.3 in grey). The MLP Hxc potential is in very good agreement with the exact in the centre; the two potentials differ at the edges as a result of approximating $f$ as a constant.

For the edges of the system the approximate and exact potentials differ; this is attributable to the approximation of $f(x)$ as a constant tailored to the central delocalised region, causing $v_{\text{MLP}}^{\text{Hxc}}$ to subdue the long-range Hxc fields. To improve this result one would need to have a spatially varying $f$, dependent on localisation, which introduces more of the SOA into these outer regions. Nevertheless, even with a constant $f$ and a simple $v_{\text{s}}^{\text{ref}}$ the MLP performs remarkably well, far from its exact limit.

### 7.7.4 Polarised three-atom chain (System 4)

We study a chain of three atoms (one electron per well), with an applied electric field in the ground state; see Fig. 7.5(a). We chose this system to test the MLP primarily due to the charge imbalance predicted by the LDA, which fails to screen the field sufficiently [152, 153], since it lacks ultra-nonlocal density-dependence of the exact $v_{\text{xc}}$ [154, 155].

We find that the exact xc potential partly counteracts the applied external electric field, principally through two potential steps [Fig. 7.5(b)]. The SOA predicts complete screening of the applied bias via similar steps, aligning the lowest Kohn-Sham eigenvalue within each potential well.

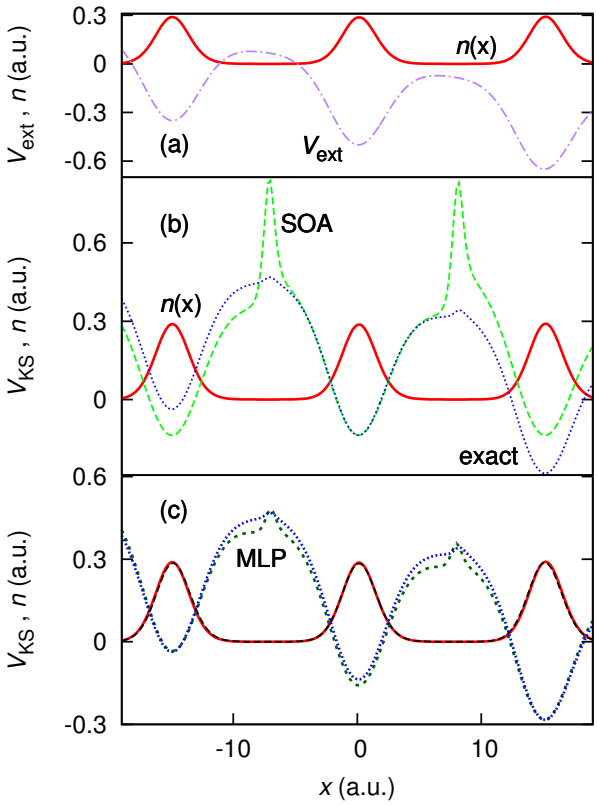


Figure 7.5: *Polarised three-atom chain (System 4)* — (a) The electron density for a chain of three atoms (one electron per well) in the many-body picture (solid red for each plot), with the external potential (dotted-dashed purple). (b) The exact Kohn-Sham potential [dotted blue, also in (c)]; xc steps act to screen the external electric field. The SOA Kohn-Sham potential (dashed green) is also shown; this predicts complete screening of the electric field. (c) The self-consistent MLP density (dashed black) and Kohn-Sham potential (short-dashed dark green), mixing in the external potential with $f = 0.17$.

For this system, we would expect strong localisation, except in the two crucial 'interface' regions where the Kohn-Sham potential exhibits a step, and therefore use the external potential as reference as discussed for System 1. A range of values of $f(x)$ from 0.17 to 0.99, applied self-consistently in the MLP, yield accurate densities, with $f(x) = 0.17$ yielding the most accurate screening in the MLP potential. [We note in passing that a position-dependent $f(x)$ that increases to 0.99 at the edges produces more accurate Hxc fields in the two outer wells, causing the density in these wells to become more accurately polarised.]

The MLP solution correctly finds one electron's worth of charge on each site. Next we apply our one-dimensional LDA of Chapter 5 to this system, and find that the LDA incorrectly localises non-integer amounts of total electron density on each site; see Fig. 7.7. Figure 7.6 shows the external potential with the exact ground-state density, the density given by the LDA, and for reference, the noninteracting density[7].

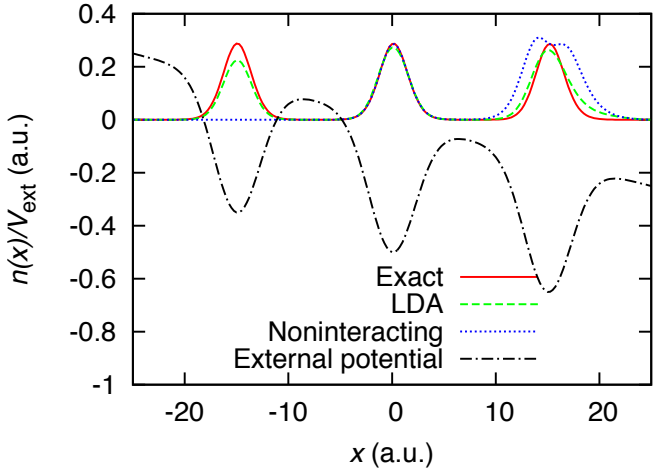


Figure 7.6: *Polarised three-atom chain* — the external potential (dotted-dashed black) with the ground-state density (solid red). Three interacting electrons dissociate such that there is one electrons worth of charge on each atom, despite the polarising electric field. Due to this field, noninteracting electrons (density shown – dotted blue) occupy the lowest two wells, and the LDA (density shown – dashed green) predicts non-integer amounts of charge in the region of each atom. The MLP density overlaps exactly with the exact; see Fig. 7.5(c).

As for the dissociated molecule, we take the cumulative integral of the electron density for this system. It is apparent from Fig. 7.7 that the exact electron density integrates to an integer amount on each atom in the chain. However, this is not the case for the LDA density. Although it is an improvement over the noninteracting electron density, just as for the dissociated molecule, the LDA is far from exact. Note that for this system the MLP density almost perfectly localises the electron density, and hence the MLP cumulative integrated density overlaps with the exact for Fig. 7.7.

[7]Here, and the rest of this section, is the sole work of Matt Hodgson.

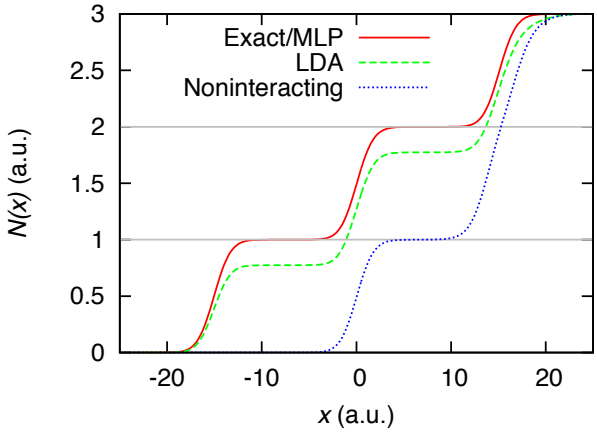


Figure 7.7: *Polarised three-atom chain* — the cumulative integral of the electron density, $N(x)$, for the exact/MLP (solid red) and LDA (dashed green). The self-consistent MLP density lies exactly over the exact. The LDA underestimates the amount of charge on the first site considerably, and the error persists. The blue dotted line shows $N(x)$ for the noninteracting density – the LDA performs better then this, but is still far from exact.

Our results here imply that local approximations, that are missing the steps we observe here, are incapable of producing accurate electron densities owing to their inherent lack of nonlocal density dependence. Hence, the need for nonlocal functionals, such as the MLP, is clear.

### 7.7.5 Correlated atoms (Systems 5 and 5′)

In this section we study how secure the SOA is in the presence of strong correlation. Generally, we find that 1D atoms, defined by their external potential $v_{\text{ext}} = -\frac{Z}{|x|+\alpha}$, have strong correlation. (The degree of correlation in the system is deduced by comparing the exact electron density to the Hartree-Fock density; as in Chapter 5, Section 5.2.5 on page 51.) In this section we study two atoms that each confine two spinless electrons to varying degrees. The first system [see Fig. 7.8(a)], where $Z = -1.5$ and $\alpha = 1$ (System 5), has little correlation, with the Hartree-Fock approximation yielding an accurate electron density.

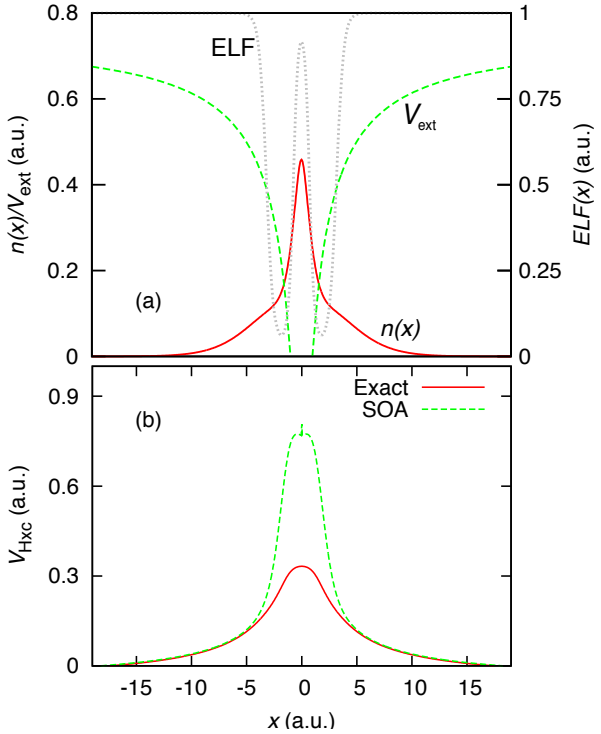


Figure 7.8: *Weakly-correlated two-electron atom (System 5)* — (a) The external potential (dashed green) with the exact electron density (solid red). The Hartree-Fock density coincides with the exact. The ELF (dotted grey) shows that an electron is localised in the centre with significant delocalisation either side of it (the SOA is least secure in these regions). (b) The exact Hartree-exchange-correlation potential (Hxc) (solid red) and the Hxc potential given by the SOA (dashed green). Note the quantitive similarities between the two potentials.

Figure 7.8(b) shows the Hartree-xc (Hxc) potential for this system with the Hxc potential predicted by the SOA given the exact electron density. Despite overestimating the central peak in the potential due to strong delocalisation in this central region, the form of the SOA Hxc potential is correct.

For comparison, we now change how confined the electrons are in the atom by using $Z = -0.02$ and $\alpha = 20$ in the external potential; see Fig. 7.9(a). For this less confining system the correlation is much stronger as the excited energy levels of the Kohn-Sham potential are closer together, as in Chapter 5, Section 5.4 on page 59. Hence, the Hartree-Fock approximation does not reproduce the electron density.

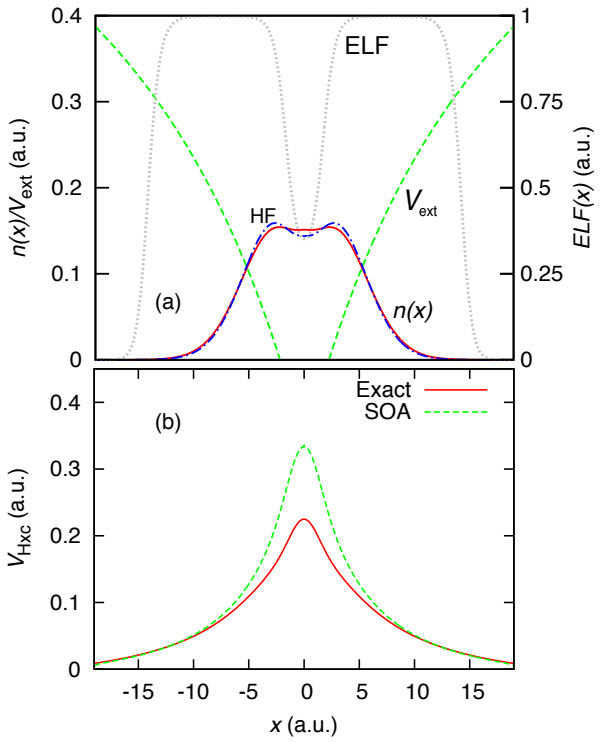


Figure 7.9: *Strongly-correlated atom (System 5')* — (a) The external potential (dashed green) with the exact electron density (solid red). The Hartree-Fock density (dotted-dashed blue) gives a poor account of the density in the central region. The ELF (dotted grey) shows electron delocalisation in the centre of the density. However, the system is more localised than System 5; see Fig. 7.8(a). (b) The exact Hartree-exchange-correlation potential (Hxc) (solid red) and the Hxc potential given by the SOA (dashed green). Note the quantitive similarities between the two potential, and how they are more accurate than for System 5, despite the system having stronger correlation.

Figure 7.9(a) shows the exact electron density, note that the form of the density is quite different to that of Fig. 7.8(a). The SOA Hxc potential is once again compared to the exact. Despite the electron density being distinctly different to that shown in Fig. 7.8(a), the exact Hxc potential is notably similar, hence the dependence of the xc potential on the density is challenging for approximations. Despite this, the SOA correctly yields, once again, a peak in the Hxc potential. However, as there is a large degree of delocalisation for this region, the peak is overestimated. Incidentally, the more confining atom (above) causes the electrons to delocalise more, but to be correlated less, than for this atom. Yet, as the SOA Hxc potential is more accurate for this atom, this implies that the accuracy of the SOA depends not on correlation, but on electron localisation.

The ELF for both these systems shows the need for a spatially varying $f$ – the SOA is exact for the regions where $ELF(x) = 1$ and needs to be suppressed in the delocalised regions.

### 7.7.6 Time-dependent molecule (System 6)

We now consider the extension of our functional to the time-dependent regime. Consider two electrons confined to a symmetric double well (inset of Fig. 7.10). For $t \geq 0$ an applied $E$-field $(-0.1x)$ forces the left electron towards the right electron. After sufficient time has elapsed (5 a.u.), an appreciable dynamic spatial step has formed in the corresponding Kohn-Sham potential between the electrons – at the electron density minimum – in order to replicate the effect of the Coulomb repulsion, as we showed in Chapter 6. We demonstrated, in Chapter 6, that there is a local dependence between the dynamic spatial steps and peaks in the velocity field ($\mathbf{u} = \mathbf{j}/n$), making $\mathbf{u}$ the natural focus when considering appropriate functional development. We therefore extend Eq. (7.1) to include the extra terms that come about from solving the time-dependent Kohn-Sham equations for a single orbital, following Ref. [82], giving

$$v_{\mathrm{SOA}}(\mathbf{r},t) = \frac{\nabla^2 n}{4n} - \frac{(\nabla n)^2}{8n^2} - \int_{-\infty}^{\mathbf{r}} \frac{\partial \mathbf{u}}{\partial t} \cdot \mathrm{d}\mathbf{r}' - \tfrac{1}{2}u^2. \tag{7.3}$$

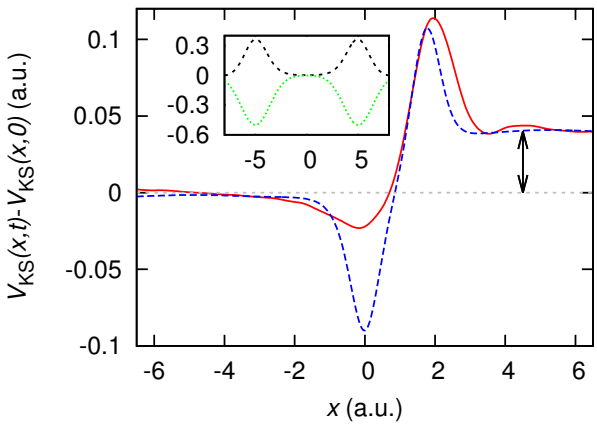


Figure 7.10: *Time-dependent molecule (System 6)* — Inset: ground-state external potential (dotted green) and ground-state density (dashed black). Main panel: exact $v_{\mathrm{s}}(x,t) - v_{\mathrm{s}}(x,0)$, at $t = 5$ a.u. (solid red), together with the corresponding quantity for the MLP (dashed blue): both replicate the potential step introduced by the time-evolution (arrow). Here $f(x,t) = 0.2$.

In the MLP, $f$ in principle becomes time-dependent, but for simplicity we choose it to be constant in space and time. In order to focus on the purely time-dependent part of the MLP,

we add the difference between the MLP potential at time $t$ and the MLP potential just after application of the external field at $t = 0$ to the exact ground-state Kohn-Sham potential, and allow the Kohn-Sham orbitals to propagate through time, recalculating the MLP densities on each time step.

Once again we find that a range of values for $f$, $0.1 - 0.3$, give accurate current and charge densities, even in the barrier region, with $f(x,t) = 0.2$ most accurately replicating the potential. Figure 7.10 shows $v_s(x,t) - v_s(x,0)$, at $t = 5$ a.u. (the latest time studied due to noise build-up in the time-dependent reverse engineering algorithm), together with the same potential given by the time-dependent MLP for $f = 0.2$. Several features are replicated by the MLP, most importantly the time-dependent xc potential step that is clearly far outside the ability of the adiabatic LDA; see Chapter 5. The details of the time-evolution of this step differ between the exact and MLP potentials, especially at earlier times. Nonetheless, the general features of the exact Kohn-Sham potential, as well as the time-dependent charge and current densities, are reproduced by the MLP. The ability of the time-dependent MLP to produce time-dependent steps is important for reproducing the dynamics of non-adiabatic systems, such as that demonstrated in Section 5.5 on page 65 and in Section 6.3 on page 71.

### 7.7.7 Return to the tunnelling system

Finally we apply the time-dependent MLP, *fully self-consistently* (including the ground-state), to the tunnelling system of Chapter 5. Note that for our previous time-dependent MLP calculation we used the exact ground-state (in order to focus on the MLP's ability to replicate time-dependent features of the exact Kohn-Sham potential), however, here we are initially calculate the MLP ground-state and then evolve the Kohn-Sham equations using the time-dependent MLP.

Because of the relatively good performance of our ALDA for this system (see Section 5.5), we use it as the reference potential (previously we have used the external potential). As is appropriate for the MLP, we mix the LDA with the SOA using $f$. First, we calculate the ground-state MLP density and potential. We find that $f(x) = 0.5$ gives an accurate density for the ground-state of this system and an accurate potential in the tunnelling region; this value of $f$ is consistent with the degree of delocalisation at the 'interface' between the two localised electrons in the double well. However, as before, a large range of values of $f$ yield an accurate density ($0 - 0.99$ – only in the ground state).

The time-dependent MLP uses the velocity field ($\mathbf{u} = \frac{\mathbf{j}}{n}$); the inclusion of this term can pose a difficult numerical challenge because of the small value of $n(x,t)$ at the edges of the system. Therefore, we switch electromagnetic gauge in order to increase numerical stability in our MLP code. By adding $\chi = -\int_{-\infty}^{r} \frac{\partial \mathbf{u}}{\partial t} \cdot \mathrm{d}r'$ to Eq. (7.3) one can remove the numerically troublesome integral term from the expression. Hence, in this gauge, $\mathbf{A}_{\mathrm{SOA}} = -\mathbf{u} = -\frac{\mathbf{j}}{n}$; see Appendix B.2 on page 126.[8] Because of the simplicity, and physical interpretation of this term (displacement current = vector potential $\times$ electron density), one should consider its form when developing approximate time-dependent density functionals; see, again, Appendix B.2.

Figure 7.11 shows the total amount of electron density in the left-hand side of the tunnelling

[8] Note that the MLP code is one-dimensional, so we use the 1D versions of these expressions.

system (same as Figs. 5.10 and 5.11 on pages 64 and 66). As seen in Chapter 5, the left electron initially tunnels towards the right electron, however, the Coulomb repulsion causes a reverse in the direction of tunnelling, beginning at $t \sim 40$ a.u. We modelled this same tunnelling system using our Landauer-style approximation, our ALDA and noninteracting electrons in Section 5.5. We found that the noninteracting, and Landauer electrons experienced no reverse in tunnelling. Whereas the ALDA predicted a reverse in tunnelling that was too late. The time-dependent MLP – with $v_{\text{ref}} = v_{\text{LDA}}$, and $f(x,t) = 0.5$ – yields good tunnelling behaviour. Here, we continue to use the ground-state value of $f$ for all times. This is justified by the fact that in the many-electron system the localisation does not vary a large amount due to the electrons remaining well separated because of the Coulomb interaction. However, we note that in a general system, $f$ should vary in time in accordance with the localisation of the electrons.

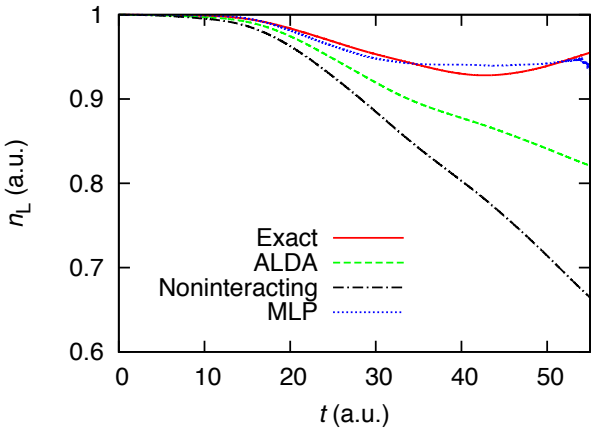


Figure 7.11: *Time-dependent two-electron tunnelling system* — The integrated density of the left-hand subsystem for two electrons in a tunnelling system, for the exact (solid red), ALDA (dashed green), noninteracting (dotted-dashed black), and the time-dependent MLP (dotted blue). The Coulomb repulsion causes the tunnelling to reverse at $t \sim 40$ a.u. (This reversal of the tunnelling does not occur for the noninteracting electrons.) The ALDA does reverse the tunnelling, but substantially later than it should ($\sim 80$ a.u.; see Fig. 5.11 on page 66). However, the MLP reproduces the behaviour well, 'forcing' the electron backwards, partially via a dynamic spatial step. Numerical noise begins to dominate the system at $t \sim 55$ a.u.

The MLP achieves the reverse in tunnelling, in part, due to the SOA's ability to form a dynamic potential step, like the exact; see Fig. 6.6 on page 74. However, it is this nonlocal behaviour of the MLP which makes modelling this system for times greater than $\sim 50$ a.u. very difficult because of the increase in numerical noise.

## 7.8 SOA exact properties

We briefly discussed the importance of approximate functionals satisfying exact properties in Chapter 2. We noted that the need for one's approximate functional to be exact in certain limits should not come at the cost of non-exact properties that lead to improved electron densities. After all, producing accurate electron densities and energies is the goal of DFT. However, we take the opportunity here to examine which exact limits the SOA satisfies, as this is important for how applicable of the SOA is to certain physical systems.

Of course the SOA satisfies *all* exact properties for a single occupied Kohn-Sham orbital, as

the SOA is exact in this limit. However, the question remains; in systems with more than one occupied Kohn-Sham orbital, which exact properties are still satisfied reasonably well? (This is also explored in Chapter 8.)

We have already discussed the success of the SOA at cancelling the self interaction of the electrons when they are localised. However, as they delocalise the SOA becomes less valid. Figure 7.12 shows the xc potential of the SOA, our LDA and the exact. The LDA is calculated self-consistently for our system but the SOA is given the exact density as an input (as the SOA cannot be solved self-consistently).

The system is similar to that of Subsection 5.3.1 on page 55, it is comprised of two spinless electrons in a triple well; one electron localises in the central, deep well, and the second electron spatially delocalises and splits the electron density – 50% in the left-most well, and 50% in the right-most well. Despite spatially delocalising, the electron is localised relative to the other central electron. Hence, the SOA applies well in the regions of high electron density and thus has a self-interaction correction in very close agreement with the exact. The LDA is not so successful at reproducing the self-interaction correction; see Fig. 7.12.

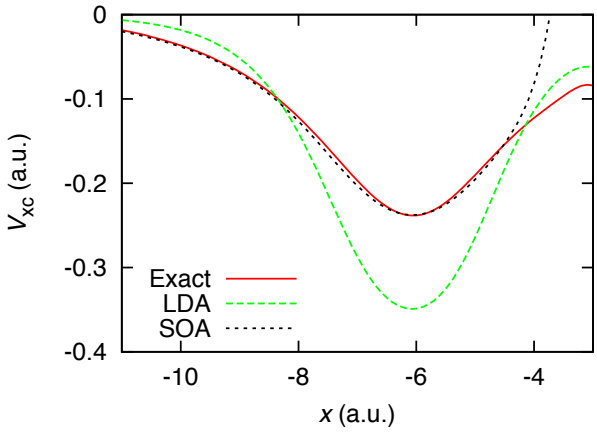


Figure 7.12: The exchange-correlation potential (exact – solid red, LDA – dashed green and the SOA – short-dashed black), in the region of the left outer well of the triple well external potential (see Fig. 5.6). The Self-interaction correction is the dominant feature, here the SOA performs extremely well, whereas the LDA overestimates it.

The exact xc potential is known to decay as $-1/x$ from any atom [22, 23]. Figure 7.13 shows the xc potential for a single-well external potential containing two spinless electrons. Once again the SOA, LDA (calculated using the exact density and self-consistently respectively) and the exact are shown, as well as a plot of $-1/x$. As expected the SOA has the correct form and matches the exact very well away from the central density, due to the tendency of electrons to localise at the edge of a finite system. The LDA decays far too rapidly to zero due to the local form of the functional, and thus will predict densities that are too confined within the well.

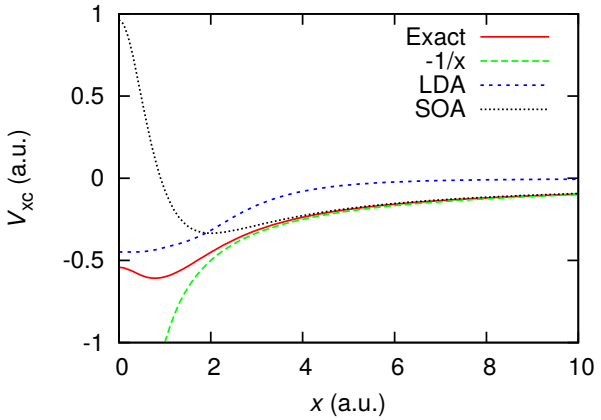


Figure 7.13: The exchange-correlation potential far from an atom. The exact (solid red) decays as $-1/x$ (long-dashed green), the SOA (dotted black) also decays with the correct form, owing to the increase in localisation far from any atom. The LDA xc potential is also shown (dashed blue), the local dependence of the functional means that the potential decays far too rapidly.

## 7.9 Furthering the mixed localisation potential

In Section 7.7.5 we showed that the SOA can reproduce the quantitative features of the exact potential well, even for challenging electron densities. However, in order for the MLP to yield a qualitatively accurate potential using the SOA, a spatial varying $f$ is required.

When considering an $f$ that varies in space, one must account for the possible constant shift in the potential of each term in the MLP. It is known that the Kohn-Sham potential tends to zero as $|x| \to \infty$, therefore $v_{\text{MLP}}$ should also. However, by considering the asymptotic form of the electron density far from any molecule [$n(x) \propto e^{-2\sqrt{2I}x}$ [21, 29], where $I$ is the ionisation energy of the molecule] it is simple to show that $v_{\text{SOA}}(|x| \to \infty) = I$. Assuming that our $v_{\text{ref}}(|x| \to \infty) = 0$, which it will for choices such as the external potential or the LDA, it must follow that in order for the constant shift of $v_{\text{SOA}}$ not to effect the spatial form of the MLP when $f = f(x)$, *i.e.* if $v'_{\text{SOA}} = v_{\text{SOA}} + c$, then $v'_{\text{MLP}} = g(x)v_{\text{ref}} + f(x)(v_{\text{SOA}} + c) = v_{\text{MLP}} + cf(x) \neq v_{\text{MLP}}$ unless $c = 0$. Hence we must ensure that the SOA goes to zero for large $x$, insuring that the MLP potential does also, thus we rewrite Eq. (7.2) as

$$v_{\text{MLP}} = f(x)(v_{\text{SOA}} - I) + (1 - f(x))v_{\text{ref}}. \tag{7.4}$$

As further investigations are required to determine a good approximate form for $f(x)$ and $f(x,t)$, the above form of the MLP should be taken into account.

## 7.10 Summary

The importance of localisation in our finite systems is evident from the above, hence we constructed an approximate density functional with localisation as an ingredient. Our starting point was the Kohn-Sham potential for a spin-singlet (a completely localised pair of opposite spin electrons), which is analytically known. We first use this form of the Kohn-Sham potential as an approximation to the universal Kohn-Sham potential, we termed this the single orbital approximation (SOA). For reasonably localised electrons, the SOA reproduces

important features of the exact Kohn-Sham potential well, such as spatial steps – unlike any other functional – and the self-interaction correction. However, for regions of medium to low localisation we mixed the SOA, at each point in space and time, with a reference potential (such as the LDA) in proportions based on the degree of localisation at that point – we termed this the mixed localisation potential (MLP). The MLP gives accurate, self-consistent electron densities and currents for some of the systems that the usual approximations find challenging, such as the disassociated molecule or a polarised chain of atoms, as well as systems with considerable delocalisation (a single atom). The time-dependent MLP, used fully self-consistently, can yield the nonlocal features necessary for an accurate electron density and current for strongly correlated systems like our simple tunnelling system.

The MLP calculations we present are accurate despite the use of the most simple choices for the reference potential and mixing of the SOA with the reference potential, even for the time-dependent regime. Hence future development of the MLP should focus, initially, on these simplifications, and the most effective ways of including a measure of localisation as a way of mixing the SOA with the reference potential. The MLP has shown promising results here. However, for the MLP to be used for practical density-functional calculations of molecules and solids, further investigations into $f$ are required. This has been undertaken recently by Torelli and others [156], yielding promising results.

So far we have found that step structures are very important features in the exact (time-dependent) exchange-correlation potential. We have shown them crucial for some common static and dynamic systems, and proposed an approximate density functional which can reproduce them. However, little about the origin of these steps is known. In the next, and final, results chapter, we derive a fundamental understanding of these subtle features.

# Chapter 8

# The origin of steps in the Kohn-Sham potential[1]

The mixed localisation potential (MLP) promises accurate densities for systems where the common approximations struggle, such as a disassociated molecule, a chain of hydrogen atoms and strongly perturbed systems, via its ability to reproduce steps, and other important features of the xc potential. However, a more fundamental understanding of the way that the MLP uses localisation as an ingredient is desirable.

In general, as well as for the improvement of the MLP, understanding the position, height and shape of steps in the exact Kohn-Sham potential is important for developing approximate functionals. Therefore, in this chapter we look at the origin of steps structures (ground-state and time-dependent) from fundamental principles.

We then develop, from fundamental principles, practical arguments for determining the position of steps, and give a range for the magnitude of the step in order for the potential to yield accurate densities.

Finally, we investigate other features of the exact Kohn-Sham potential that manifest as a result of superimposing steps, for static and dynamic systems.

## 8.1 Introduction

Density functional theory (DFT) and time-dependent DFT (TDDFT) have been applied widely to calculate the properties of ground-state and time-dependent systems of interacting electrons. In some cases the approximations made in practice perform extremely well; in others they become less valid, and hence the accuracy of the approach suffers.

Steps in the exchange-correlation (xc) potential (a jump in the level of the xc potential over a relatively short distance) have been shown to be crucial for an accurate description of the electron density for a variety of ground-state and time-dependent systems [10, 11, 14, 113, 151, 157, 158, 159, 137, 160, 161], such as tunnelling electrons and charge transfer/excitations.

[1] This chapter describes collaborative work that has been published: M. J. P. Hodgson, J. D. Ramsden and R. W. Godby, 'Origin of static and dynamic steps in exact Kohn-Sham potentials', *Physical Review B* **93**, 155146 (2016). Sections 8.1-8.7 are adapted from that paper. Matt Hodgson participated fully in the formulation and analysis of the research and executed the calculations shown in the paper, and prepared the first draft of the paper.

Atomic structure calculations by van Leeuwen *et al.* [157] demonstrated that steps arise at the boundaries between atomic shells. Yang *et al.* [161], using ensemble DFT, showed how, as more atomic Kohn-Sham orbitals are occupied, steps form in the exact xc potential. However, much remains to be understood regarding their position, shape and magnitude.

Common approximate functionals struggle to model systems such as those above, as well as molecular dissociation, Van der Waals interaction and open-shell molecules [162]; see Chapter 3. Therefore improved functionals must be developed, thus understanding features, such as steps in the xc potential, is of great importance; see Chapter 7.

We study the nature of steps that form in the Kohn-Sham potential for asymmetric ground-state and time-dependent, 'molecule-like' systems (where the external potential tends to zero far from any atom), and expand the concept to symmetric systems. We examine the precise shape, height and position of steps, and show how steps combine to make other features in $v_{\text{xc}}$, even in the time-dependent regime.

In Section 8.2 we begin our analysis by considering the thought experiment of Almbladh and von Barth [151], where a step in the xc potential forms for a finite system of two spin-half electrons. By analysing the effect of the step on the electron density, we deduce the principles underlying the position, height and shape of steps, applying even when multiple Kohn-Sham orbitals are occupied. We then extend these ideas to the time-dependent regime. We derive, from these principles, arguments for the position and magnitude of steps, to aid the development of approximate functionals which have the ability to produce steps in $v_{\text{xc}}$, such as the MLP of Chapter 7.

In Sections 8.3-8.6 we model finite systems in one dimension using our iDEA code [14] in which we find the exact xc potential by first solving the time-dependent many-electron Schrödinger equation to obtain the fully correlated wavefunction. From this we calculate the *exact electron density* for ground-state, and subsequently time-dependent, systems. We then reverse-engineer the Kohn-Sham potential via an optimisation algorithm which matches the noninteracting density to the interacting density. Our main calculations use *spinless* electrons in order to explore systems with more exchange-correlation for a given computational cost, *i.e.*, with each electron occupying a different Kohn-Sham orbital (same as before). Our focus will be on nano-wires and devices for which one-dimensional descriptions are appropriate, and hence we use the appropriately softened Coulomb repulsion $(|x' - x| + 1)^{-1}$, as before (Appendix A.2 on page 121).

## 8.2 The Almbladh-von Barth thought experiment

When using DFT to simulate neutral molecules, such as that described below, the use of local and semilocal density functionals to approximate the xc potential gives rise to errors that affect observables such as binding energy curves and energy surfaces. These errors arise in part due to the inability of such approximations to correctly predict the amount of charge on each atomic site [21, 49, 63], therefore it is essential for the development of improved functionals to understand the role of the xc step in accurately localising the Kohn-Sham electrons within the molecule.

We consider a one-dimensional double-well external potential, representing two separated

open-shell atoms, where the right well has single-particle energy states that are lower than those of the left well. Owing to their Coulomb repulsion, two *spin-half, interacting* electrons occupy different wells; however two *noninteracting* electrons would both occupy the right-hand well; see Fig. 8.1(a). Hence, a step must form in the Kohn-Sham potential to allow the Kohn-Sham electron density to match the many-body density. This system has been studied for many years, originally by Almbladh and von Barth [151] and Perdew [49].

If we consider each individual well separately, as a subsystem, then the ground-state energies are equal to minus the ionisation energies of the respective atoms [163] (wells) since $v_{\text{ext}}(|x| \to \infty) = 0$. ($I_R$ represents the ionisation energy of the right well and $I_L$ is that of the left well. Considering the left and right atoms as individual systems, or subsystems, is valid for well separated atoms, and in the disassociation limit the concept is exact.)

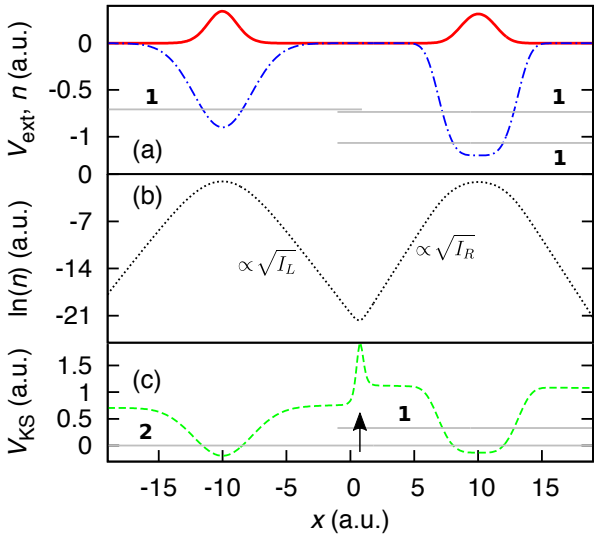


Figure 8.1: *Two spin-half electrons in two separated wells* — (a) The external potential (dotted-dashed blue), together with the electron density for two *interacting, spin-half* electrons (solid red). The horizontal grey lines show the bound single-particle energy states of the potential and the number adjoining each energy level indicates the degeneracy of that state. (b) The natural logarithm of the density, allowing the density minimum to be clearly identified. The decay of $\ln(n)$ on either side of the density minimum is proportional to the square root of the ionisation energy of the well the electron occupies. (c) The exact Kohn-Sham potential (dashed green): the step of height $I_R - I_L$ (arrow) ensures that one electron is in each well. Note that the step aligns the ground-state energies of the two wells, as anticipated by Almbladh and von Barth [151].

Treated individually, both subsystem's Kohn-Sham potential decays to different, but approximately spatially constant, values, therefore at their region of intersection in the complete system a step exists whose height is the difference between those constants. We define the step height as $S_{\text{xc}} \equiv v_R^{\text{xc}} - v_L^{\text{xc}} = v_R^{\text{s}} - v_L^{\text{s}}$, where $v_R^{\text{s}}$ and $v_L^{\text{s}}$ are the constants of the Kohn-Sham potentials in the right and left subsystems respectively, and likewise for the xc potentials $v_R^{\text{xc}}$ and $v_L^{\text{xc}}$. This definition is exact in the limit that the wells are infinitely separated, as the xc potential tends to a constant value far from the subsystem, hence the step acts to shift $v_{\text{xc}}$ by $S_{\text{xc}}$ between the subsystems. We find, however, that the formula holds well for electrons with only a few ångströms of separation; see Fig. 8.1(c).

We reverse-engineer the exact Kohn-Sham potential[2] for this system and, as predicted [49,

[2]Reverse-engineered potentials, such as this one, are determined to within an additive constant.

151], we observe a step in the xc potential between the wells; see Fig. 8.1(c). The argument made by Almbladh and von Barth was that the step must align the Kohn-Sham single-particle energy levels of the two wells in order for the highest occupied molecular orbital (HOMO) to have sufficient weight in each well, *i.e.*, one electron's worth of charge per atom (well). Hence, the step must have a magnitude which equals the difference between the HOMO energies of the two wells.

While the above argument is robust for this system, we may come to the same conclusion via a different point of view. Consider now the form of the electron density far from any atom. Even for the many-body case, the density will decay asymptotically like that of a single particle occupying the well [21, 29] $n(x) \propto e^{-2\sqrt{2I}x}$. As only one Kohn-Sham orbital is occupied for this system, the single orbital approximation (SOA) [112, 113], of Chapter 7, is exact (up to an additive constant). Applying the SOA to the density of Fig. 8.1(a), we find that *at the density minimum* the xc potential jumps by $I_R - I_L$; see Fig. 8.1(b) and (c). (In Chapters 6 and 7 we found that the step always forms at a density minimum.) The SOA is correctly sensitive to the decay of the electron density either side of the step when the density is of the form $e^{-2\sqrt{2I}x}$, a result also observed by Helbig *et al.* [158]. Thus, at the interface between the electrons, where the density decaying from the left meets the density decaying from the right (the density minimum), the potential jumps from $I_L$ to $I_R$; see Fig. 8.1(b). As this happens over a short range, a sharp step forms. Therefore the step can be considered to arise from this change in the decay of the electron density, which we will henceforth refer to as a change in the *'local effective ionisation energy'*.

Below we study systems where more than one Kohn-Sham orbital is occupied. We find that a change in the local effective ionisation energy remains responsible for steps. However, owing to the analogue of this effect in the Kohn-Sham picture (see Section 8.5), the magnitude and shape of steps can change.

## 8.3 The origin of steps

To begin this section, we detail why, in general, the magnitude of the step may change for systems with more than one occupied Kohn-Sham orbital. In the following section we explore the effect the magnitude of the step has on the electron density, and whether the step height $I_R - I_L$ (given by the SOA in all cases) is a good approximation for the step height in a general system.

We consider the form of the decay of the density either side of the step for both the many-body picture and the Kohn-Sham picture, in order to more fully understand what determines the step's magnitude in general. In the many-body picture, the density decaying from the left-hand subsystem (more generally, simply decaying from the left), as the wells are separated far from one another, is given by $n'_L(x) \propto e^{-2\sqrt{2I_L}x}$. Likewise, the right-hand subsystem contributes $n'_R(x) \propto e^{+2\sqrt{2I_R}x}$. The decay of the density coming from the left-hand subsystem in the Kohn-Sham picture is $n_L(x) \propto e^{-2\sqrt{2\left(v_L^{\mathrm{s}}-\varepsilon_L\right)}x}$, where $\varepsilon_L$ is the energy of the highest occupied Kohn-Sham orbital that dominates the asymptotic density of the left-hand subsystem. And for the right-hand subsystem $n_R(x) \propto e^{+2\sqrt{2\left(v_R^{\mathrm{s}}-\varepsilon_R\right)}x}$, where $\varepsilon_R$ is defined correspondingly. As $n' = n$, for the exact Kohn-Sham potential, it must follow that $v_L^{\mathrm{s}} = I_L + \varepsilon_L$ and $v_R^{\mathrm{s}} = I_R + \varepsilon_R$ (within an overall additive constant). Noting that the step

height is $S_{\rm xc} = v_R^{\rm s} - v_L^{\rm s}$, it follows that

$$S_{\rm xc} = (I_R - I_L) + (\varepsilon_R - \varepsilon_L), \tag{8.1}$$

where a negative value indicates a step that drops when going from left to right, and a positive value *vice versa*. Equation (8.1) is exact in the limit that the atoms are infinitely separated, however, we have found the equation to be accurate for separations of a few ångströms. [Equation (8.1) requires knowledge of the exact Kohn-Sham eigenenergies $\varepsilon_R$ and $\varepsilon_L$, determined partially by the step, and hence cannot be used to *predict* the step height, unless the energies can be approximated or neglected, *e.g.*, $\varepsilon_R \approx \varepsilon_L$.]

The energies $\varepsilon_L$ and $\varepsilon_R$ refer to the highest occupied Kohn-Sham orbitals that dominate the density in the outer region of each subsystem. When the system consists of localised, well-separated subsystems, this concept is well defined, and it is in this case that a sharp step may form in $v_{\rm s}$. Where the subsystems are closer and the electrons less localised, we find that the energies remain a useful interpretive concept.

Equation (8.1) shows that the step arises from two effects: the change in the local effective ionisation energy in the many-body picture ($I_R - I_L$), and its counterpart in the Kohn-Sham picture ($\varepsilon_R - \varepsilon_L$); see Section 8.5 later. Thus, the overall step can be considered as the sum of two steps, $S_{\rm xc} = S_{\rm xc}^I + S_{\rm xc}^\varepsilon$, where $S_{\rm xc}^I = I_R - I_L$ and $S_{\rm xc}^\varepsilon = \varepsilon_R - \varepsilon_L$; see Section 8.7.

The above argument applies to spin-half electrons as well as spinless electrons. We note that if we apply the above logic to a system consisting of spin-half electrons, where there is an *odd* number of electrons on each site, the highest occupied Kohn-Sham orbital must be spread over both wells. Hence, in this case $\varepsilon_R = \varepsilon_L$, and therefore the step height is that of the Almbladh-von Barth thought experiment discussed above ($S_{\rm xc} = I_R - I_L$).

When developing approximate xc functionals, there are certain known exact properties that one aims to satisfy, such as the derivative discontinuity of the xc energy with respect to electron number [21]; see Chapter 2. The derivative discontinuity predicts a jump in the xc potential by a constant as the electron number passes through an integer, which may lead one to connect steps in the xc potential with the derivative discontinuity. However, it is apparent from the above analysis that the magnitude of the step in $v_{\rm xc}$ is a result of the precise way in which the electron density decays from each subsystem. The decay of the density, in the many-body picture, and in the Kohn-Sham picture, has no direct association with the electron affinity of the subsystem [$-\varepsilon_{N+1}(N+1)$], nor the affinity of the system as a whole. We therefore conclude that the step which forms in $v_{\rm xc}$ is not attributed to the derivative discontinuity. For example, in the Almbladh-von Barth system this insensitivity to the affinity is complete.

## 8.4 Height of steps

Next we examine the effect that under- or overestimating the step height would have on the electron density. For example, noting that any step given by the SOA is of height $I_R - I_L$, we may ask whether this is an appropriate value for the step height in a general system. To answer this, one must consider the effect that altering the step height has on the electron density.

For spin-half electrons in a separated double-well system where the occupied Kohn-Sham orbitals are atomic orbitals, changing the step height equates to adding a constant to the potential within a given subsystem, and so usually affects the density only in the region of the step (see below). However, if the change in step is too large – enough to alter the occupation of the wells – the electron density will be affected everywhere. In the case where the highest occupied orbital is spread over both sites, the step height must be exactly $I_R - I_L$.

Building on the arguments of Perdew [49] for the range of allowed energies of a system connected to a reservoir, we find a range for our step height for our molecular system consisting of spinless electrons. If we consider a system where, in the Kohn-Sham picture, $M$ states are filled in the left well, and $N$ states are filled in the right well, we can place a range on the magnitude of the step that must exist in $v_{\mathrm{xc}}$ based on correctly filling the eigenstates of the individual wells; see Fig. 8.2. For this case we are assuming that the wells are sufficiently separated so that the single-particle eigenenergies ($\varepsilon$) of each well are unaffected by the electrons in the other well, other than the shift by a constant due to the step – in all cases this degree of well separation would be needed in order for a sharp step to form.

We know that the HOMO of the left well [$\varepsilon^L_M(M)$], plus the shift in energy due to the step ($S_{\mathrm{xc}}$, without loss of generality we set $v^{\mathrm{s}}_R = 0$), must be less than the lowest unoccupied molecular orbital (LUMO) of the right well [$\varepsilon^R_{N+1}(N)$], and *vice versa*, allowing the amount of charge in each well to be correct. Thus, we can infer that

$$\varepsilon^L_M(M) - \varepsilon^R_{N+1}(N) < S_{\mathrm{xc}} < \varepsilon^L_{M+1}(M) - \varepsilon^R_N(N). \tag{8.2}$$

A schematic representation of the range is shown in Fig. 8.2. The external potential has been chosen such that the lowest two single-particle states are located in the right-hand well, thus in the Kohn-Sham picture the step must correct this to allow the lowest two energy states of the overall system to be located in separate wells. The green arrow indicates the minimum the step height can be, whereas the red (long) arrow shows a step that is too large. These limits define the allowed range for the step height, in order for the electron density to be reasonably accurate.

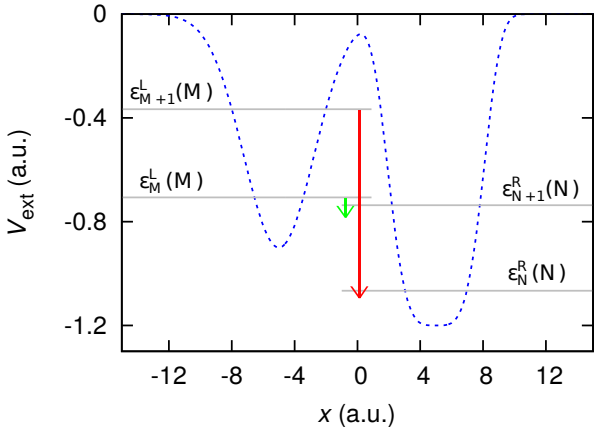


Figure 8.2: The external potential (dashed blue) for the a general double-well molecule, the lines indicate the bound single-particle energy levels of the individual wells, where, in this case, $M = N = 1$. As it is, the external potential in the absence of interaction would give the incorrect filling of each well, *i.e.*, both electrons in the right hand well. The green arrow indicates the minimum step height to achieve one electron per well, and the (longer) red arrow indicates a step height that is too large. Any value of $S_{\text{xc}}$ between the two values would give a fairly accurate electron density.

Equation (8.2) applies also for spin-half electrons (noting that the number of electrons will be different, as two electrons may occupy each energy level), except for the case where there is an odd number of electrons on each site. In this case the above arguments do not apply, however the step height is known exactly ($S_{\text{xc}} = I_R - I_L$; derived above).

Finally, we look at how changes in the step height affect the detailed electron density in the region of the step, and hence show which features of the density determine the exact step height. Consider a finite molecule that is very similar to the Almbladh and von Barth thought experiment (System 1), except two Kohn-Sham states are now occupied as opposed to one; two *spinless* electrons, where the external potential is a double well, designed such that the first excited state of the right-hand well is lower than the ground state of the left-hand well (Fig. 8.2). Hence, in the absence of interaction, both spinless electrons would occupy the lowest *two* states of the right-hand well. As the many-electron density has one electron's worth of charge in each well due to the Coulomb repulsion and Pauli exchange, the exact Kohn-Sham potential must form a step to achieve this in the Kohn-Sham density. The step acts to shift the ionisation energy of the two wells here, as opposed to aligning them, allowing the ground-state of the left-hand well to be lower in energy than the first excited state of the right-hand well, in accordance with our range (Fig. 8.2).

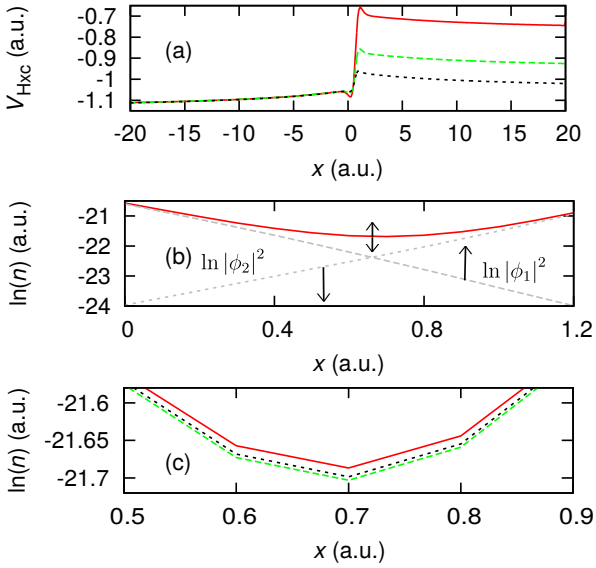


Figure 8.3: *System 1 (two spinless electrons in an asymmetric double well)* — (a) The exact $v_{\text{Hxc}}$ potential (solid red) and two artificial stepped $v_{\text{Hxc}}$ potentials (long-dashed green and dashed blue). (b) Natural log of the density at the density minimum. The natural log of the Kohn-Sham densities for the ground-state ($|\ \phi_1\ |^2$) and the first excited state ($|\phi_2|^2$) are shown. As the step height is decreased these densities change (indicated by the arrows), and thus affect the overall density by increasing or decreasing the magnitude at the density minimum (determined by the precise way the Kohn-Sham densities superimpose). (c) The densities corresponding to the step heights of (a), where the colours and line styles correspond.

Figure 8.3 shows how an artificially imposed change in step height affects the electron density. We observe that the change to the electron density is small, provided the step height is in the range given by Eq. (8.2). The change in step height has the effect of reducing or increasing the density minimum very slightly. Precisely how the density minimum is affected is determined by the individual Kohn-Sham densities, *e.g.*, $n_1 = |\phi_1|^2$ and $n_2 = |\phi_2|^2$. As the magnitude of the step is decreased, less of the right-hand Kohn-Sham density tunnels through to the left, and the opposite effect happens for the left-hand Kohn-Sham density. Thus we can conclude that *the step height ultimately determines the degree to which the left-hand electron occupies the right well and vice versa* – this applies to all cases. Thus, local and semilocal approximations to the xc potential must be exceedingly sensitive to changes in the density at the location of the step, or else a fully nonlocal approximation must be employed (such as the MLP).

## 8.5 Position of steps

We consider the xc potential far from a molecule (*e.g.*, one composed of several subsystems), hence the subsystems are no longer distinguishable. And therefore, the density must decay with the ionisation energy of the *whole* molecule, which in the case of a molecule comprised of separated atoms is the *lowest* ionisation energy of all the wells. This means that for any subsystem's density which does not decay with the ionisation energy of the whole system, there must be a *second* change in the local effective ionisation energy far from the system, and therefore another step must form. This second step was first observed by Perdew [49] and also by Makmal *et al.* [164] in the exact exchange potential for LiF, where they attribute

the steps to shifts in the Kohn-Sham eigenvalues. They discuss the 'domain' of each atom being dominated by the HOMO of that atom, resulting in a plateau to correct for the non-zero asymptotic limit caused by the HOMO eigenvalue being non-zero. This is the analogue of the change in the local effective ionisation energy in the Kohn-Sham picture. Hence, generally, this causes a step in the exact Kohn-Sham potential in accordance with our derivation of Eq. (8.1). Thus, the 'overall' step in the exact xc potential is a combination of the steps caused by the change in local effective ionisation energy and the crossover of the single-particle Kohn-Sham densities (see below). When correlation effects are taken into account *both* these effects must also be considered.

We define, as a function of space, $\tilde{I}(x) = \frac{1}{8n^2}\left(\frac{\partial n}{\partial x}\right)^2$ [which is also the second term in the SOA expression for the Kohn-Sham potential – Eq. (7.1) in Chapter 7 – hence showing the correct sensitivity of the SOA to the ionisation energy], which represents the local effective ionisation energy when the density decays asymptotically, which is true for regions of the density near the edge of a subsystem[3]. Hence, in such a region $\tilde{I}(x) = I$, and between subsystems $\tilde{I}(x)$ may have a step demonstrating the change in the local effective ionisation energy. (While in this chapter we apply this formula to spinless electrons, the concept applies to spin-half electrons also.)

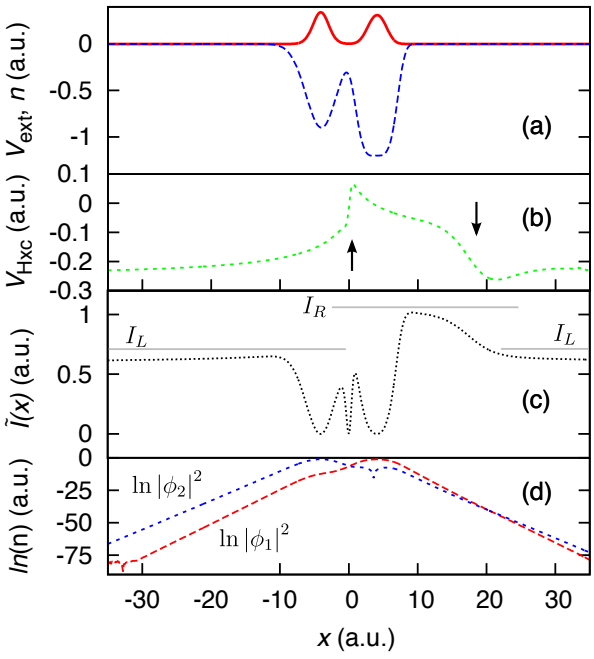


Figure 8.4: *System 2 (two spinless electrons in a molecule)* — (a) The electron density (solid red) and external potential (dashed blue). (b) The Hxc potential (dashed green), the arrows indicate where the steps are. One step forms at the density minimum, where the Kohn-Sham single-particle densities cross. The second step forms far from the molecule, again where the Kohn-Sham densities cross. (c) There are two changes in the local effective ionisation energy (black dotted) in the many-body density, each corresponding to a step in $v_{xc}$, the grey lines indicate the ionisation energies of the subsystems ($I_L$ and $I_R$). (d) The natural log of the Kohn-Sham densities, blue short-dashed is the first excited Kohn-Sham density and red dashed is the ground-state Kohn-Sham density. As the decay rate of the first excited-state must be less than that of the ground state, far from the molecule the densities must cross.

Figure 8.4(a) shows a molecular system (System 2) where we observe the second, postulated

[3] $\tilde{I}(x)$ is simply found by rearranging the asymptotic density, $n = n_0 e^{-2\sqrt{2I}x}$, where $n_0$ is a normalisation factor, not dependent on $x$, to find $I$.

step far from the molecule; see Fig. 8.4(b). In Ref. [164] the correcting step is observed for the exact exchange potential. Our step is, in part the same as this correcting step, however it superimposes with the a step which forms as a result of a change in local effective ionisation energy at the same point in space. Also in Ref. [158] the second step was deduced to exist, however, was not observed. Our findings show that their thinking was correct, as our argument here applies to the spin-half case (as well as for our spinless electrons). Furthermore, Fig. 8.4(c) and (d) show that the step forms at the point where there is a crossover of the single-particle Kohn-Sham densities, *e.g.*, where the dominant contributing single-particle density switches (applying also to spin-half electrons for systems where more than one Kohn-Sham orbital is occupied). This is consistent with the findings of Ref. [164] (discussed above) and Ref. [157], where the xc potential has 'a clear step structure and is constant within the atomic shell and changes rapidly at the atomic shell boundaries' (also where the local ionisation energy can change). Reference [161] also found that a step structure forms when more than one orbital begins to be occupied.

Here we observe that the change in the local effective ionisation energy and the crossover in the Kohn-Sham single-particle densities manifest at the same point, hence the two steps superimpose ($S_{\mathrm{xc}} = S^I_{\mathrm{xc}} + S^\varepsilon_{\mathrm{xc}}$). In general, a change in the dominant single-particle Kohn-Sham density corresponds to a change in the local effective ionisation energy, but not necessarily *vice versa*. For example, in the Almbladh-von Barth system there is a change in the local effective ionisation energy without a crossover of the localised Kohn-Sham densities, since only one orbital is occupied ($\varepsilon_R = \varepsilon_L \Rightarrow S_{\mathrm{xc}} = I_R - I_L$).

Della Sala and Görling showed that for a three dimensional system, along a direction $\mathbf{r}$ which corresponds to a nodal surface of the HOMO, the exact xc potential will approach a non-zero constant [165]. Our analysis can be generalised to 3D, and agrees with this result; if the HOMO is zero in the direction $\mathbf{r}$, then, as $r \to \infty$, the dominant contribution to the overall density from the single-particle Kohn-Sham densities must come from the highest occupied Kohn-Sham orbital that does not correspond to a nodal surface. Hence, the non-zero Kohn-Sham density and the 'true' HOMO Kohn-Sham density cannot cross. Thus the counteracting step we observe in Fig. 8.4 will not manifest and the xc potential may tend to a non-zero constant.

The role of the Kohn-Sham orbitals in this argument is reminiscent of the appearance of Kohn-Sham orbitals in meta-GGA [30, 166] functionals and the Becke-Edgecombe electron localisation function (ELF) [136], and draws attention to the power of the Kohn-Sham orbitals in improving density functionals. Our MLP approximation, likewise, makes use of the Kohn-Sham orbitals in defining the degree of localisation.

### 8.5.1 Time-dependence

We look at the single-particle time-dependent Kohn-Sham densities for two electrons in an asymmetric double-well external potential, where for $t \geq 0$ a perturbing field ($0.1\,|x|$) pushes the electrons together (System 3), and find that the dynamic steps also occur at the points where the individual Kohn-Sham densities cross, showing that, to some degree, the dynamic steps occur as a result of this phenomenon; Fig. 8.5. However, this concept is less well defined for the time-dependent case, as the idea of a well defined ionisation energy is no longer applicable.

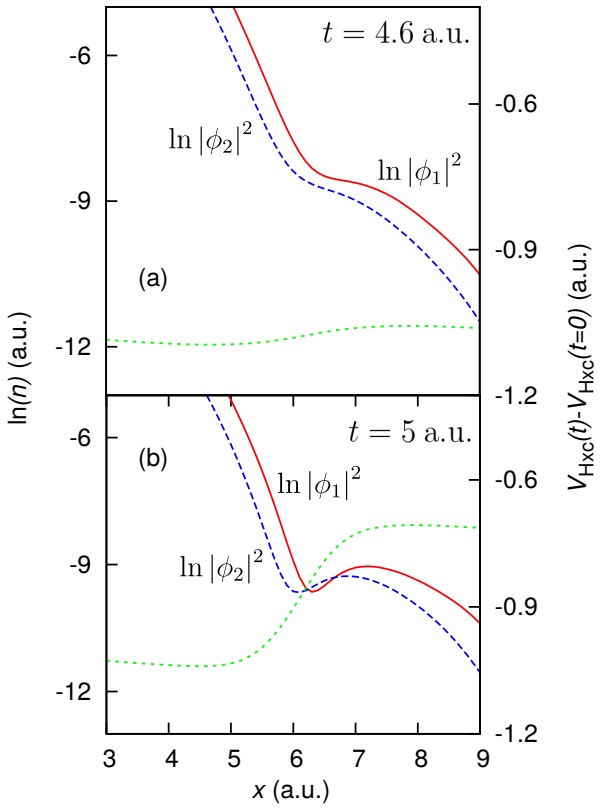


Figure 8.5: *System 3 (dynamic double-well)* — Two electrons in an asymmetric double-well external potential, where a perturbing field ($0.1\,|x|$) pushes the electrons together for $t \geq 0$. (a) The natural logarithm of the single-particle Kohn-Sham densities (ground-state – solid red, first excited-state – dashed blue), with the time-dependent part of the Hxc potential (short-dashed green) at $t = 4.6$ a.u. (b) The same as (a) but at $t = 5$ a.u. and the single-particle Kohn-Sham densities have crossed, causing a time-dependent step to form in the Hxc potential at the point where the densities cross.

The step here does correspond to a peak in the velocity field (current density divided by electron density), which in turn forms as a result of a minimum in the electron density, as in Chapter 6. We find that in the system studied in Chapter 6 there are density minima, and thus peaks in the velocity field, that do *not* correspond to steps in the time-dependent xc potential. We have confirmed that this is because these density minima do not correspond to Kohn-Sham single-particle densities crossing.

Thus, the question remains; why do the Kohn-Sham single-particle densities seem to always cross at density minima? For dynamic finite systems interference 'ripples' in the density are likely to occur (as seen in Chapter 6), hence if an orbital density develops an extremum, there is an enhanced likelihood of it crossing an adjacent orbital density. Thus, minima in the dynamic electron density may also serve to indicate where steps will form. However, as the energy levels are not well defined in the dynamic regime the magnitude of the step may vary from that given by Eq. (8.1). But, if the system is in the adiabatic limit then our arguments for the ground-state steps would approximately apply for the time-dependent system.

### 8.5.2 The role of density minima for ground-state systems

A turning point often occurs when the dominant contribution shifts from one electron to another. Thus a density minimum is likely to correspond to a change in the local effective ionisation energy and/or a crossover of the single-particle Kohn-Sham densities. Hence, in our calculations we observe that density minima are usually good indicators of where steps will form; seen in Chapters 6 and 7. Next we will show that steps do *not* form at *all* density minima, as some density minima cannot correspond to a change in the local effective ionisation energy or this concept is not well defined. However, we demonstrate below how certain density minima, which also represent the interface between localised electrons, are indicators for where in the electron density steps will form for ground-state systems.

Consider a subsystem where the majority of the electron density corresponds to one strongly localised electron. If there is a minimum in the density within the subsystem it cannot correspond to a change in the local effective ionisation energy, because there is only one occupied energy state. Thus, there can never be an overall step in $v_{\mathrm{xc}}$ for a minimum within a subsystem consisting of one electron. This then shows that not all density minima correspond to steps in the xc potential. Yet, the question remains; which density minima will give rise to steps?

In systems containing well-separated subsystems, the local effective ionisation energy is well defined near the boundary of each subsystem, but can change from one value to another as the boundary is crossed. If the number of electrons in this subsystem integrates to an integer (which is usual for localised systems), we can define the *integer electron point* (IEP) as an indicator of this boundary, and hence of where a step may form. (We note that as a given subsystem may contain several, localised electrons, features in $v_{\mathrm{xc}}$ within the subsystem may correspond to IEPs due to changes in the local effective ionisation energy and/or crossing single-particle Kohn-Sham densities. However the possible delocalisation due to the electrons being confined within the subsystem may cause these features to be unrecognisable as steps; see Sections 8.6 and 8.7, and Fig. 8.7.) Therefore, if, in 1D, the density minima ($a$ and $b$) satisfy $\int_a^b n(x)\mathrm{d}x = N$, where $N$ is an integer, those density minima are good indictors of

where steps (or other features) may form, provided that the IEPs and density minima tend to coincide (which we observe them to). We show below how the Coulomb repulsion and the degree of localisation in the system are responsible for density minima and IEPs being at approximately the same point. We note that in the time-dependent regime (as observed above and in Chapter 6), owing to energy levels being less well defined, the IEP is *not* an indicator of a density minimum that may correspond to a step, as orbitals are likely not to cross at the boundaries of localised subsystem, but anywhere in the system.

To explore the relationship between density minima and integer electron points (IEPs) in the ground state, we examine how a system may be split into subsystems. With a sufficient degree of localisation for all electrons in a system, IEPs indicate the crossover from one electron to the next. In the limit of complete electron localisation, the IEPs are definite intersections between the electrons, hence giving a clear boundary between the subsystems. As the electrons delocalise, some of the on-site electron spreads into the neighbouring sites. This delocalisation, and the effect it has on the shape of steps in the xc potential at the IEPs, is studied below.

We observe in calculations of electron densities that an IEP typically occurs approximately at a minimum in the electron density. To show that the Coulomb repulsion is largely responsible for this phenomenon, we introduce a 2-electron system (System 4), where the IEP and density minimum are designed to be significantly different for *noninteracting* electrons; see Fig. 8.6(a). With two *interacting* electrons in the *same external potential* we observe the IEP and the density minimum tending to the same point; see Fig. 8.6(b).

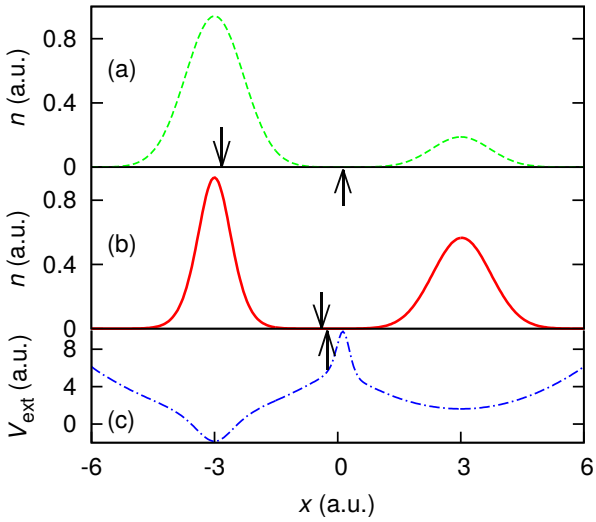


Figure 8.6: *System 4 (crafted external potential)* — (a) The noninteracting electron density (dashed green) for two electrons in the external potential of (c). The IEP (see text) is shown by the downward facing arrow at $x \sim -2.8$ a.u. and the density minimum is by the upward facing arrow at $x \sim 0.13$ a.u. (b) The interacting electron density (solid red) for two electrons in the external potential of (c). Again the IEP is shown by the upward facing arrow at $x \sim -0.39$ a.u. and the density minimum by the downward facing arrow at $x \sim -0.26$ a.u. The interaction acts to draw the IEP and density minimum together. (c) Shows the external potential for this system. This potential has been crafted so that, for noninteracting electrons, the density minimum and IEP are very different.

To understand this, we imagine artificially increasing the interaction strength between the electrons: the likelihood of finding the left electron in the right subsystem, *i.e.*, to the right of the IEP, and *vice versa*, reduces owing to the electron repelling the other from its vicinity.

Thus, the electrons localise and the density at the IEP tends to zero. For a non-negative quantity, such as the electron density, any zero point must correspond to a minimum.

For the physical interaction strength, it is possible for a system (*e.g.*, System 5 below) to have an IEP that does *not* correspond to a minimum in the density of *interacting* electrons. However, achieving this requires a carefully crafted external potential which causes the appropriate degree of delocalisation.

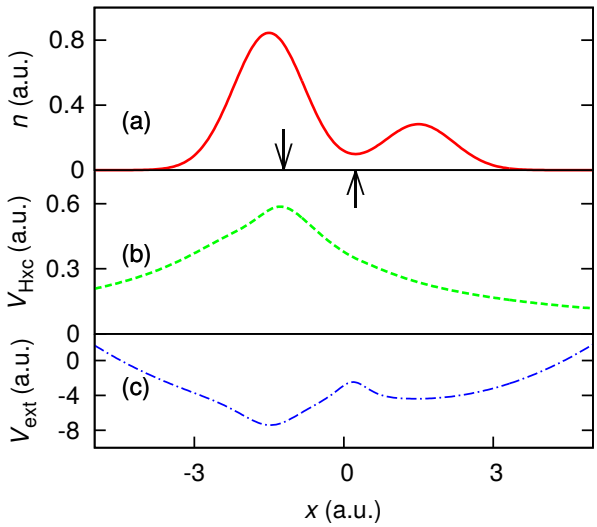


Figure 8.7: *System 5 (crafted external potential)* — (a) The electron density for two interacting electrons (solid red) in a potential crafted such that the IEP (defined by the condition that the electron density to the left of the point integrates to exactly one electron) is distinctly different from the density minimum. The downward facing arrow indicates the IEP at $x \sim -1.2$ a.u., and the upward facing arrow indicates the density minimum at $x \sim 0.24$ a.u. (b) The Hartree exchange-correlation potential (dotted green): the predominant feature of the potential – not a step – is at the IEP. (c) The external potential (dashed-dotted blue).

Figure 8.7 shows that the predominant feature in the Hartree exchange-correlation (Hxc) potential ($v_{\mathrm{H}} + v_{\mathrm{xc}}$) forms at the IEP, however there is no step as the local effective ionisation energy does not have a well defined value on each side of the feature – a characteristic of the exact functional shared by the SOA in more delocalised systems such as this one.

To summarise, a change in the local effective ionisation energy is required for a step to form – usually indicated by a density minimum corresponding to an IEP. The IEP and density minimum will be at approximately the same point in the electron density owing to the degree of localisation in the system coupled with the Coulomb repulsion. Future improved density functionals may exploit this approximate functional relationship to include features of the exact Kohn-Sham potential examined above.

## 8.6 Sharpness of steps: effect of delocalisation

Considering how the step forms, it is apparent that the more abrupt the switch between dominant Kohn-Sham orbitals (correlated with localisation), and between local effective ionisation energies, the sharper the step will be. Therefore, next we test what happens to the shape of a step as the region of delocalisation increases. (We note that the step forms in the

region of highest delocalisation, which corresponds to the interface between the electrons[4].) This type of investigation is aimed to assist with the development of approximate functionals, specifically the MLP which uses localisation as an ingredient. Tempel *et al.* considered a singlet case where two potentials were separated, and the effect on the step was observed [167]. Their findings are in agreement with our concept of the local effective ionisation energy. They find that as the molecule dissociates the step becomes clear as the separation increases, *i.e.*, as the local effective ionisation energy becomes well defined [*i.e.*, $\tilde{I}(x) \to I$].

We introduce another system (System 6), which has the usual form: two spinless electrons in an asymmetric double well. Figure 8.8(b) shows the Hxc potential for System 6 – note the sharp step.

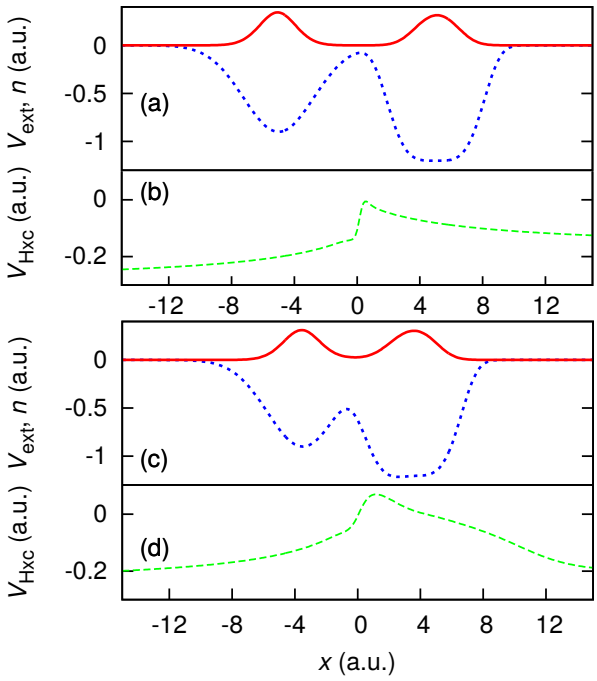


Figure 8.8: *System 6 (increase separation of wells)* — (a) The external potential (dotted blue) and electron density (solid red). (b) The Hartree exchange-correlation (Hxc) potential has a step; this ensures that both Kohn-Sham electrons occupy just one well each. (c) The external potential and electron density for System 6′. The system is that of System 6, except that the wells have been brought closer together. (d) The Hxc potential for System 6′ shows a step, like that of System 6, but because the delocalisation is stronger the step is less sharp.

Figure 8.8 shows that as the localisation decreases the 'sharpness' of the step decreases also. This observation is in agreement with our above analysis – sharp steps cannot form in regions where there is not a well-defined difference in ionisation energy. Note the second, very diffuse step about $x \sim 11$ a.u. where the Kohn-Sham single-particle densities cross once more; see Fig. 8.8(d). Here the effect is to counteract the step between the electrons so that there is no net step. [In Fig. 8.8(b) the system is not large enough for the Kohn-Sham densities to cross twice, hence there is only one step.]

We model these systems using the self-consistent MLP and find that it performs well by reproducing the step. Of course, as seen in Section 7.7.1 on page 78, the choice of $f$ has an effect on how well the step matches the exact, however, we find that the MLP density

[4]We have looked at the electron localisation function (ELF) [135] for this system, and found that the electrons are extremely localised towards the edges. As one approaches the 'interface' between the two electrons strong delocalisation occurs.

accurate for a range of values. For details on the MLP applied to systems like these see Ref. [156].

We apply the Hartree-Fock (HF) approximation to System 6 as a means of determining the role that exchange plays in these systems. We reverse-engineer the HF electron density using iDEA to find the local potential which describes the density (HF-Kohn-Sham potential). In this way we can compare the steps of the HF-Kohn-Sham potential to those of the exact Kohn-Sham potential. For some systems – where the Kohn-Sham HOMO and LUMO are distinctly different – we observe the HF-Kohn-Sham potential to have a step that is almost perfect, as for System 6. Whereas for systems where the Kohn-Sham HOMO and LUMO energies are close, correlation is stronger, and the HF-Kohn-Sham potential's step (and other features) are less accurate. Thus both exchange and correlation may be important in determining the properties of the steps.

## 8.7 Bumps and other superpositions of steps

In the following model systems we demonstrate that the steps in $v_{\text{xc}}$ in symmetric systems in effect coalesce to form 'bumps' in the potential, for systems with some degree of delocalisation.

We demonstrate this by studying two examples – one time-dependent and one ground-state – each comprised of three systems (A, B and C). The external potential for the third system (C), in each case, is given by $v_{\text{ext}}^{C} = \frac{1}{2}\left(v_{\text{ext}}^{A} + v_{\text{ext}}^{B}\right)$. From this we can find the relationship between the Kohn-Sham potentials for the three systems. We write (to first order)

$$v_{\text{s}}^{C}(\mathbf{r}) = v_{\text{s}}^{A}(\mathbf{r}) + \int \mathrm{d}\mathbf{r}' \frac{\delta v_{\text{s}}(\mathbf{r})}{\delta v_{\text{ext}}(\mathbf{r}')}\left(v_{\text{ext}}^{C}(\mathbf{r}') - v_{\text{ext}}^{A}(\mathbf{r}')\right)$$
$$v_{\text{s}}^{C}(\mathbf{r}) = v_{\text{s}}^{B}(\mathbf{r}) + \int \mathrm{d}\mathbf{r}' \frac{\delta v_{\text{s}}(\mathbf{r})}{\delta v_{\text{ext}}(\mathbf{r}')}\left(v_{\text{ext}}^{C}(\mathbf{r}') - v_{\text{ext}}^{B}(\mathbf{r}')\right).$$

If we add the two together and divide by two we get

$$v_{\text{s}}^{C}(\mathbf{r}) = \frac{1}{2}\left[v_{\text{s}}^{A}(\mathbf{r}) + v_{\text{s}}^{B}(\mathbf{r}) + \int \mathrm{d}\mathbf{r}' \frac{\delta v_{\text{s}}(\mathbf{r})}{\delta v_{\text{ext}}(\mathbf{r}')}\left(2v_{\text{ext}}^{C}(\mathbf{r}') - v_{\text{ext}}^{A}(\mathbf{r}') - v_{\text{ext}}^{B}(\mathbf{r}')\right)\right],$$

thus, provided the systems are sufficiently similar in character to have similar response functions

$$\left(\frac{\delta v_{\text{s}}(\mathbf{r})}{\delta v_{\text{ext}}(\mathbf{r}')}\right)_{C} \approx \left(\frac{\delta v_{\text{s}}(\mathbf{r})}{\delta v_{\text{ext}}(\mathbf{r}')}\right)_{A} \approx \left(\frac{\delta v_{\text{s}}(\mathbf{r})}{\delta v_{\text{ext}}(\mathbf{r}')}\right)_{B}, \tag{8.3}$$

we can infer that

$$v_{\text{s}}^{C}(\mathbf{r}) \approx \frac{1}{2}\left[v_{\text{s}}^{A}(\mathbf{r}) + v_{\text{s}}^{B}(\mathbf{r})\right]. \tag{8.4}$$

In the present context the bump potential of System C is the sum of two oppositely-stepped potentials A and B.

### 8.7.1 Ground-state example

We study three systems to demonstrate, using the above linearity, how positive and negative steps may manifest in a symmetric system as a bump. The bump we observe is very similar

in character to that of Ref. [109], where a 'peak' in the xc potential arises between atomic shells. Reference [159] describes peaks/bumps forming with steps for molecular systems like our own. We show below how steps and bumps both manifest through the superposition of steps in the xc potential. Reference [164] also observed a peak in the exact exchange potential at 'the crossover point of orbital domination.'

System 7A [Fig. 8.9(a)] is the usual two spinless electrons in an asymmetric external potential designed to give a step, System 7B [Fig. 8.9(b)] is the same as System 7A but reflected about $x = 0$ (explained below), and the symmetric System 7C [Fig. 8.9(c)] is the superposition of 7A and 7B (as described above).

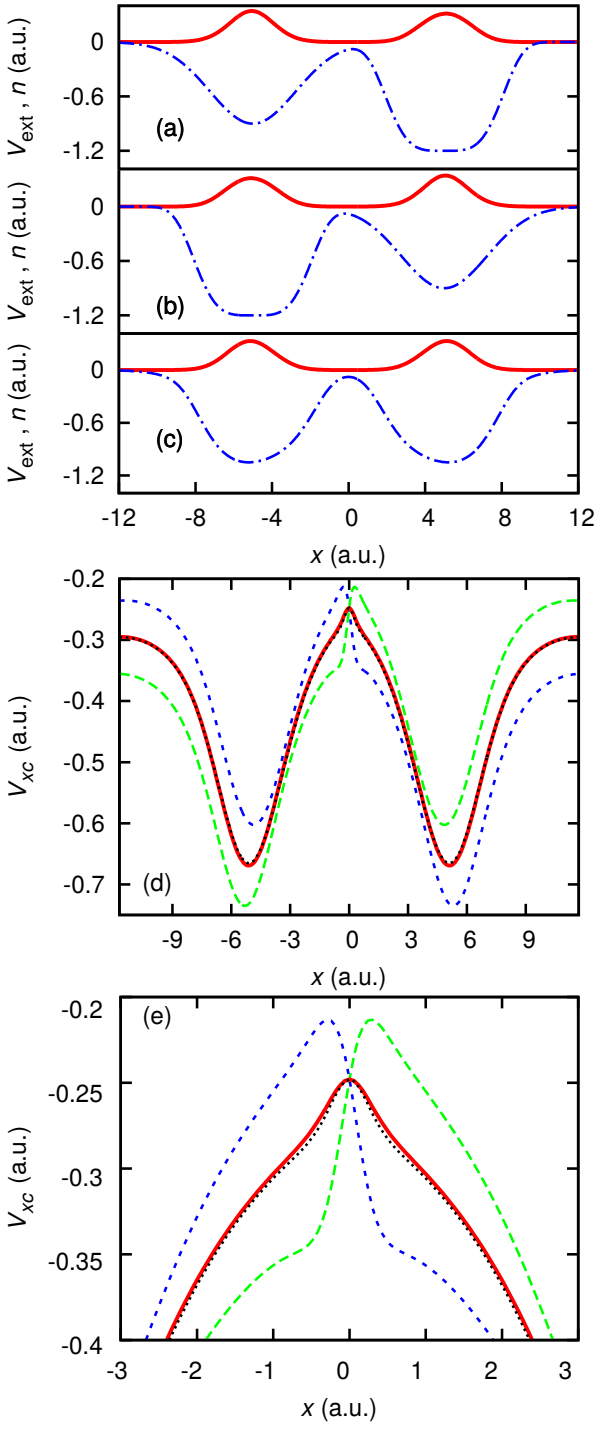


Figure 8.9: *System 7A, 7B and 7C* — (a) The external potential (dotted-dashed blue) and the electron density (solid red) for System 7A. (b) The same for System 7B. (c) The external potential (dotted-dashed blue), defined by averaging the external potentials of 7A and 7B, with the electron density (solid red). (d) The xc potential ($v_{\rm xc}^A$) for System 7A (dotted green), with the xc potential ($v_{\rm xc}^B$) for System 7B (dashed blue). The xc potential for System 7C (solid red) is compared against $\frac{1}{2}(v_{\rm xc}^A + v_{\rm xc}^B)$ (short-dashed black). We note the good agreement between the two, and how well the bump in the potential is reproduced by the superposition of steps. (e) is a close up of the bump and steps in (d).

We choose our second system (System 7B) to be the mirror image of System 7A, so that 7C is symmetric. Finally, we construct System 7C from System 7A and 7B (as stated above). The density minimum is aligned at $x = 0$ in all three systems. As System 7C is symmetric, no overall steps can form in the exact xc potential of C; instead a bump forms at the density minimum; see Fig. 8.9(d) and (e). This bump acts to 'push' the electrons apart, recreating the effect of the Coulomb repulsion. Figure 8.9(d) shows the xc potential given by Eq. (8.4) as well as the exact xc potential for Systems 7C, 7B and 7A. We observe the precision with which the xc potential of System 7C is replicated by the superposition of steps, as well as the self-interaction correction either side of this central feature. This accuracy is due to Eq. (8.4) holding well (in itself a striking result). We have also shown that the symmetric bump feature in the exact xc potential of System 7C can be thought of as the sum of positive and negative steps; see Fig. 8.9(e) for close up.

We stress that Systems 7A and 7B satisfy the requirement that their differences from System 7C may be described within a linear-response framework [Eq. (8.3)]. In this sense, there are several sets of systems which would demonstrate the above superposition of steps to form a bump. We also point out that had System 7A not corresponded to the reflection of 7B about $x = 0$, then 7C could be asymmetric and hence may have an overall step. We have simulated this scenario and found that two differently sized steps superimpose to give a step-and-peak combination for System C, reminiscent of the step and peak of Fig. 8.1(c).

### 8.7.2 Time-dependent example

We extend this concept of superimposing steps to dynamic systems. We once again consider three systems: the first (System 8A), a symmetric double well in its ground state, designed such that, for $t \geq 0$, a dynamic step grows [Fig. 8.10(a)]; the second (System 8B) the mirror image of the first [Fig. 8.10(b)], and the third (System 8C) is symmetric [Fig. 8.10(c)]. Once again we align the origins of the three systems at the density minima.

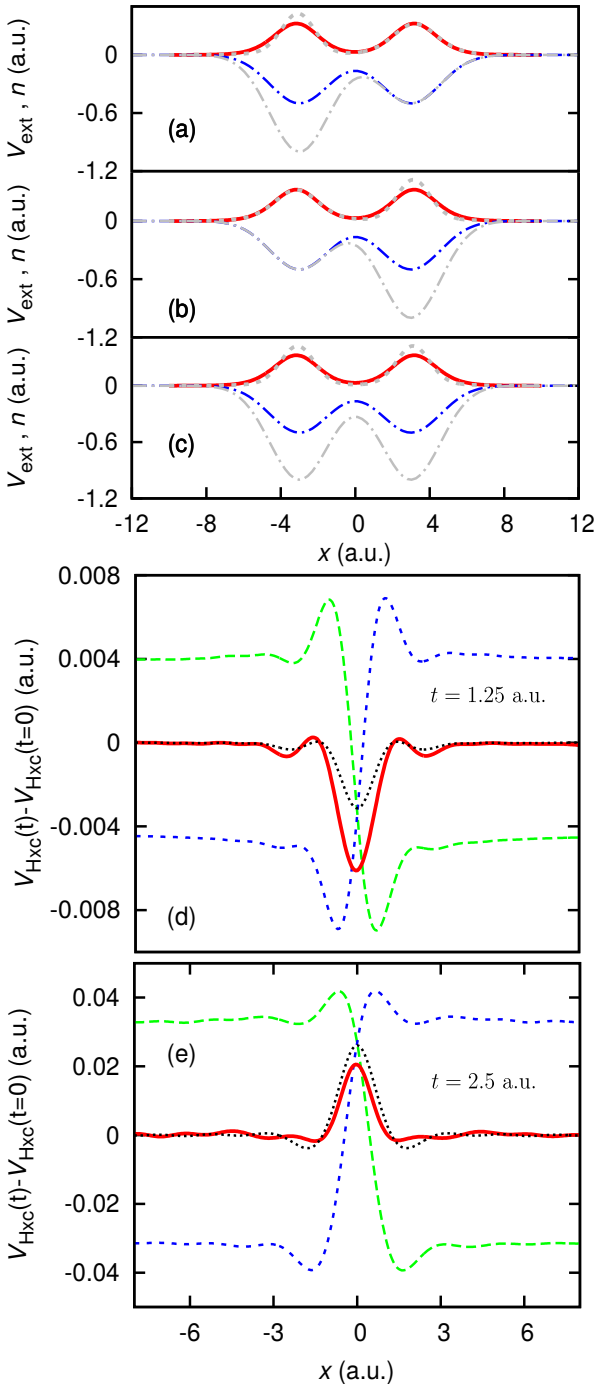


Figure 8.10: *System 8A, 8B and 8C* — (a) The external potential (dotted-dashed blue) and the electron density (solid red) for System 8A at $t = 0$. The grey lines indicate the perturbed potential and the electron density at $t = 2.5$ a.u. (b) The same for System 8B. (c) The external potential (dotted-dashed blue), defined by averaging the external potentials of 8A and 8B (as for the perturbed potential shown in grey), with the electron density (solid red) and at $t = 2.5$ a.u. (grey). (d) The dynamic part of the Hxc potential $[v^A_{\mathrm{Hxc}}(t) - v^A_{\mathrm{Hxc}}(t = 0)]$ for System 8A (dotted green), with the same potential for System 8B (dashed blue). The same potential for System 8C (solid red) is compared against the averaged potential (short-dashed black) at $t = 1.25$ a.u. We note the good agreement between the two, and how well the 'dip' in the potential is reproduced by the superposition of steps. (e) The same graph for $t = 2.5$ a.u., the dip has now become a bump.

System 8A, in the ground-state, is comprised of two electrons in a double well. At $t = 0$ we apply a perturbing field which excites the left electron by increasing the depth of the left well allowing the left electron to explore excited states – a dynamic step grows at the density minimum as a result. System 8B is the same, but reflected about $x = 0$. And System 8C (defined in the same way as the ground-state example) is symmetric, so both electrons explore excited states. As two dynamic steps form, they correctly superimpose at all times to create a feature which oscillates between a bump and a dip; see Fig. 8.10(d) and (e).

## 8.8 Step theory applied to approximate functionals

The above derivation of step structures that form in the xc potential is intended to inform the development of improved density functionals. Hence we now apply some of this 'step theory' to our 1D LDA, a '1D PBE' GGA and the SOA to determine whether these approximate functionals are capable of forming steps in the xc potential.

First we consider the form of the xc potential for the LDA. From Chapter 5 the form of the 1D LDA xc potential is $v_{\text{xc}}^{\text{LDA}} = (\alpha + \beta n + \gamma n^2)n^p$. It is clear, by substituting the analytical form of the density into the function, $v_{\text{xc}}^{\text{LDA}} = (\alpha + \beta e^{-2\sqrt{2I}x} + \gamma e^{-4\sqrt{2I}x})e^{-2p\sqrt{2I}x} \approx 0$ far from the subsystem, that this form of the potential is highly insensitive to the local effective ionisation energy, and hence the LDA xc potential is incapable of reproducing step structures.

While it seems obvious that a local approximation could not give rise to a step, GGAs are semi-nonlocal and hence may have the ability to give step features in the GGA xc potential. If we consider a 1D PBE, where $s_{1D} = \left|\frac{\partial n}{\partial x}\right| \frac{1}{n^2}$ (formulated, as in the 3D case, such that it is dimensionless; see Section 2.2.3.3 on page 23), we can use the form of the density ($n \propto e^{-2\sqrt{2I}x}$) in the region where the local effective ionisation energy is well defined to see whether the additional (relative to the LDA) term in this 1D PBE is sensitive to the ionisation energy, and if so whether the PBE functional form of $F_{\text{xc}}$ (see Section 2.2.3.3) can give rise to a step in $v_{\text{xc}}$.

We calculate $s_{1D}$ using the asymptotically decaying density and hence find $F_{\text{x}}^{\text{PBE}}$, as follows

$$F_{\text{x}}^{\text{PBE}}(x) = 1 + \frac{as^2}{1 + bs^2} = 1 + \frac{8aIe^{4\sqrt{2I}x}}{1 + 8bIe^{4\sqrt{2I}x}} \approx 1 + \frac{a}{b},$$

as $e^{4\sqrt{2I}x}$ is very large far from any subsystem, as $x$ is large. Hence, the 1D PBE $F_{\text{xc}}$ is not sensitive to the ionisation energy in this region ($a$ and $b$ are constants for the system). This means that as the other terms that the PBE functional uses are also not sensitive to the change in local effective ionisation energy, it is very unlikely for the PBE xc potential to form a step. Of course, the only way to prove this absolutely is to model systems which are known to have changes in the local effective ionisation energy, and hence there are steps in the exact xc potential, using PBE and show that no steps form.

Throughout this chapter we commented on the ability of the SOA to produce steps, which can easily be shown to be of magnitude of $I_R - I_L$ and at the correct point using Eq. (7.1): we apply the single orbital approximation (SOA) to the region of density far from a subsystem,

hence the density is of the form $n \sim e^{-2\sqrt{2I}x}$, as follows

$$\begin{aligned} v_{\mathrm{SOA}} &= \frac{1}{4n}\frac{\partial^2 n}{\partial x^2} - \frac{1}{8n^2}\left(\frac{\partial n}{\partial x}\right)^2 \\ &= \tfrac{1}{4}\cdot e^{2\sqrt{2I}x}\cdot 8I\cdot e^{-2\sqrt{2I}x} - \tfrac{1}{8}\cdot e^{4\sqrt{2I}x}\cdot (2\sqrt{2I})^2\cdot e^{-4\sqrt{2I}x} \\ &= 2I - I = I. \end{aligned} \tag{8.5}$$

Clearly $v_{\mathrm{SOA}}$ is correctly sensitive to the ionisation energy. Hence, when there is a change in the local effective ionisation energy, the step height given by the SOA is $S_{\mathrm{SOA}} = v_R^{\mathrm{SOA}} - v_L^{\mathrm{SOA}} = I_R - I_L$. It is this sensitivity to $I$ which is important for approximate functionals. The above demonstration could be used to deduce forms of $F_{\mathrm{xc}}$ that are correctly sensitive to $I$ and hence could produce an approximate functional that gives steps in $v_{\mathrm{xc}}$.

## 8.9 Application to the mixed localisation potential

In Chapter 7 the SOA is applied to electron densities with regions of strong delocalisation. Above we established how a change in the local effective ionisation energy can remain a valid concept even in regions of strong electron delocalisation. We observed features forming in the exact Kohn-Sham potential as a result of these changes – not always a step; see Fig. 8.7. The SOA, in Figs. 7.8 and 7.9 on pages 87 and 88, overestimates the bump features relative to the exact potential. This error occurs because the SOA has no knowledge of crossing single-particle Kohn-Sham densities. Hence, SOA features form due to changes in ionisation alone, and thus when multiple Kohn-Sham orbitals are occupied, the magnitude of bumps/steps is wrong. (This occurs as a result of delocalisation; see Section 8.6.)

A correcting term to the SOA should focus on the change in the dominant Kohn-Sham density from one domain to another – yielding a step of magnitude $\varepsilon_R - \varepsilon_L$. When summed with the SOA's step magnitude $I_R - I_L$, the step height becomes exact: $I_R - I_L - (\varepsilon_R - \varepsilon_L)$; see Section 8.3. This correcting term will also improve non-step features such as bumps for the same reason. However, this term requires prior knowledge of the Kohn-Sham energy ($\varepsilon$) meaning this correcting term is impractical.

## 8.10 Summary

Throughout the thesis we have demonstrated the importance of steps in $v_{\mathrm{xc}}$ (as shown in Chapters 6 and 7), hence, in this chapter we deduced the fundamental origin of step structures in exact Kohn-Sham potentials. Step structures have been shown previously, for many situations (ground-state and time-dependent), to be very important for accurate electron densities and currents, yet much about them remained to be understood. We showed that steps arise when the decay of the electron density coming from a subsystem meets that of a different subsystem. As the density decays asymptotically, proportional to the square root of the ionisation energy of that subsystem, there can be a sudden change in the rate of decay when decaying densities from two different subsystems meet, we termed this a change in the 'local effective ionisation energy'. The analogue of this effect in the Kohn-Sham picture is the changeover of the dominant single-particle density contributing to the

total electron density; this effect also gives rise to a step in the exact xc potential, even in the time-dependent regime. When these two effects occur at the same point in space the two steps superimpose to form one overall step. In the case of a symmetric system we even show, using linear response, that the two steps superimpose to form a 'bump' in $v_{\mathrm{xc}}$. The superposition of steps to form other features of the exact Kohn-Sham potential is even true for time-dependent features. Our insights into the formation of steps and other features of the exact Kohn-Sham potential via the superposition of steps, aims to inform the development of improved approximate functions.

In practical density-functional calculations, the density is readily available. Hence, we also derived a way of approximating where steps form in the electron density, and provide a range of step heights that yield accurate electron densities . We observed the tendency of a step to form at a density minimum due to the likelihood of a minimum to correspond to a change in the local ionisation energy, but note that, owing to this underlining requirement, not all density minima can correspond to steps. However, by integrating the electron density over a region corresponding to a subsystem of localised electrons (relative to the others in the system), we defined our integer electron point which can be used to indicate minima that *do* correspond to steps, *i.e.*, the point in the density where this crossover of the decaying density occurs thus a step can form. We also demonstrated that localisation indicates which systems have a step in the xc potential, and we showed that delocalisation affects the shape of steps.

# Chapter 9

# Conclusions

A cornerstone of materials simulations, theoretical chemistry and solid state physics is density functional theory (DFT). The theory has been hugely successful in many branches of these fields, due to the accuracy and computational efficiency of the theory. However, the sole approximation within the theory – the approximation to the exchange-correlation (xc) potential ($v_{\text{xc}}$) – breaks down in certain situations. The extension of DFT to the time-dependent regime greatly widened the applicability of density functional methods; however with this increased functionality comes the even more difficult task of approximating the *time-dependent* xc potential.

In this thesis we introduced our approach to developing improved xc functionals: our interacting dynamic electrons approach (iDEA) code can simulate one dimensional systems of one, two or three electrons. The electrons are interacting and modelled by solving the time-dependent Schrödinger equation, providing us with the exact electron density and current. We 'reverse engineer' the density to find the exact Kohn-Sham potential ($v_{\text{s}}$). Once the exact Kohn-Sham potential is known it can be compared to the common approximations of $v_{\text{xc}}$, and the origins of their failings can be deduced. Approximate functionals can then be developed, that are more accurate for systems where the usual approximations are less valid.

We used this approach to introduce a new way of constructing approximate density functionals – through the use of mixing approximations based on the degree of electron localisation at a given point. We introduced an approximation to the universal Kohn-Sham potential, that assumes the electrons in the system are sufficiently localised in a region of space such that the density in said region is well described by the modulus squared of a single Kohn-Sham orbital – the single orbital approximation (SOA). The SOA can then be used, self-consistently, to calculate electron densities and currents by mixing it with a reference potential, we termed this the mixed localisation potential (MLP).

We have shown that nonlocal features, such as static and dynamic spatial steps, of the *exact* Kohn-Sham potential are important for accurate electron densities in the Kohn-Sham approach. Furthermore our (time-dependent) MLP can reproduce these steps; a task too difficult for the usual xc approximations. We demonstrated, for simple, finite systems, where the common local approximations fail to model the electron density accurately, that our potential mixing scheme can improve the description of correlation and hence yield more accurate densities.

While more work is required for the MLP, including developing new reference potentials

and more sophisticated ways of mixing the SOA with the reference potential (see Ref. [156]), the initial ground-state and time-dependent results are promising. Approximating our term, $f(x,t)$, which is used to mix the reference potential and the SOA in the MLP, to be constant in both space and time, was shown to be successful for our small systems, simulated for relatively short times. However, the exact nature of the dependence of $f$ on the localisation of the electrons still remains an important concept if the MLP is to be used in practical DFT-based calculations.

Practical MLP calculations require a way of calculating $f$ based on the localisation in the system. Hence, further investigations are required to determine the relationship between $f$ and the degree of localisation in the system. Of course, this approach also relies on the accuracy of the measure of localisation, and practically one must be able to calculate localisation from quantities that one has available when one is performing a DFT calculation.

Continued investigation of the sort presented in this thesis, *i.e.*, understanding features (such as steps) in the exact Kohn-Sham potential, are important for the future development of improved density functionals. Specifically, determining the magnitude of *dynamic* steps from fundamental principles could allow improved, time-dependent functionals to be developed. Our fundamental understanding of the origin of step structures in the exact Kohn-Sham potential, as well as other nonlocal features, presented in this thesis, can also be used to inform the development of improved density functionals and improve our understanding of the highly enigmatic xc functional.

# Appendix A

# iDEA

## A.1 Algorithms

Below we give important details regarding our iDEA code that are peripheral to the main information presented in the thesis, *e.g.*, details on our algorithms.

### A.1.1 The ground-state reverse engineering algorithm

Our ground-state reverse engineering (GSRE) algorithm converges in significantly fewer iterations when we reduce the value of $p$ in Eq. (4.3). To demonstrate this remarkable speed-up we calculate the number of iterations of the GSRE algorithm required to reach full convergence, for $p = 1$ and $p = 0.05$, for two interacting electrons in a harmonic potential, of the form $\frac{1}{2}\omega^2 x^2$. We find, for this system, a speed-up of the order of $10^3$. We also find that this change in $p$ increases the accuracy of the solution by a factor of $10^3$, measured by the absolute integrated difference between the Kohn-Sham electron density and the exact (Eq. 4.4 on page 41).

For systems that are more complicated than the above, the speed-up can be many times that which we observed for the harmonic well. In some cases full convergence may not be possible without changing the value of $p$ and/or $\mu$.

### A.1.2 The time-dependent reverse engineering algorithm

#### A.1.2.1 Gauge transformation

Gauge theory tells us that we are free to make the following change of Gauge

$$\begin{aligned} v' &\to v + \frac{\partial \chi}{\partial t} \\ \mathbf{A}' &\to \mathbf{A} - \nabla \chi, \end{aligned}$$

without affecting the physical characteristics of the system. We can use this in our time-dependent reverse engineering code to 'remove the time-dependence' from the scalar potential $v_\mathrm{s}$ by introducing a non-zero vector potential $A_\mathrm{s}$. This can be done as follows; we

begin in a gauge where

$$v_{\mathrm{s}}(x,t) = v_{\mathrm{ext}}(x,t) + v_{\mathrm{Hxc}}(x,t)$$
$$A_{\mathrm{s}}(x,t) = 0.$$

Currently iDEA is written such that for $t > 0$ the external potential is constant in time. Hence, if we define $\chi(x, t > 0) = -\int_{0^+}^{t} \mathrm{d}t'\, v_{\mathrm{Hxc}}(x, t' > 0)$, we may work in a gauge where, for $t > 0$, there is no time-dependence in the scalar potential, as such

$$v'_{\mathrm{s}}(x, t > 0) = v_{\mathrm{ext}}(x) + v_{\mathrm{Hxc}}(x, 0)$$
$$A'_{\mathrm{s}}(x, t > 0) = \int_{0^+}^{t} \mathrm{d}t'\, \frac{\partial}{\partial x} v_{\mathrm{Hxc}}(x, t' > 0),$$

where the notation $0^+$ denotes a time infinitesimally after 0. Hence, using this gauge, we may avoid the need for a spatial integral and a time derivative for each iteration of the time-dependent reverse engineering algorithm, as we may use Eq. (4.5) on page 42 opposed to the equivalent form for scalar potentials used in Ref. [10].

## A.2 Our interaction term

The separation of variables for the one-particle Schrödinger equation in 3D, assuming that electrons remain in ground state as far as their transverse $(y, z)$ wavefunction is concerned, allows us to consider our electrons in a one-dimensional nano-lead to interact in the same way as two disks, each with charge $e$, in a three-dimensional lead. We model the effects of the transverse wavefunction on the density by assuming that the charge density of the disk is $n(r) = \frac{2\pi}{a^2(\pi^2-4)} \cos^2(\frac{\pi r}{2a})$, where $a$ is the radius of the disk.

Hence we calculate the potential energy between the two disks in order to find what the form of our Coulomb interaction should be. In cylindrical polar co-ordinates the length of the lead has dimension $x$ and radius $a$; see Fig. A.1. The potential energy between any two

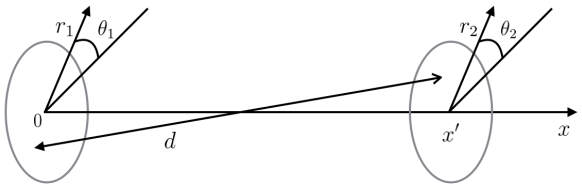


Figure A.1: Diagrammatic representation of our two, 3D, charged disks, nanowire model. This 3D representation is modelled in our 1D iDEA calculations via our interaction term (see text).

points on the disks, where the distance between them is $d$, is

$$\delta v_i = \frac{n_1(r) n_2(r)}{d_i},$$

where $n_1$ and $n_2$ are the charge densities of the disks. We recall that the density of the disks is $n(r) = \frac{2\pi}{a^2(\pi^2-4)} \cos^2(\frac{\pi r}{2a})$. Therefore the total potential energy between the disks is the sum

of all these contributions. Therefore

$$v(x) = \frac{8\pi^3}{(\pi^2-4)^2 a^4} \int_0^{2\pi} \mathrm{d}\theta \int_0^a \mathrm{d}r_1 \int_0^a \mathrm{d}r_2 \frac{r_1 r_2 \cos^2(\frac{\pi r_1}{2a}) \cos^2(\frac{\pi r_2}{2a})}{\sqrt{r_1^2 + r_2^2 - 2r_1 r_2 \cos(\theta) + x^2}}. \tag{A.1}$$

Figure A.2 shows $v(x)$ for a nano-lead with width 6 a.u. (approximately the diameter of a gold nano-lead), together with $\frac{1}{|x|}$, $\frac{1}{|x|+1}$ and $\frac{1}{\sqrt{x^2+1}}$. The form of the curve which most

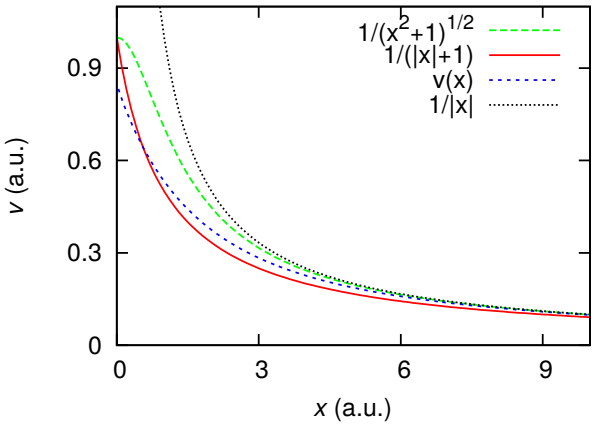


Figure A.2: Potential $v$ against distance $x$ for two charged disks. Green long dashed – commonly used 1D Coulomb terms, solid red – our Coulomb term, dashed blue – Eq. (A.1) and dotted black $\frac{1}{|x|}$. We find that, for our systems, $\frac{1}{|x|+1}$ most accurately represents the true, 3D, interaction.

accurately represents $v(x)$ is $\frac{1}{|x|+1}$, hence we use this as our interaction term in iDEA.

If we change the interaction term to $\frac{1}{|x|+0.1}$, this corresponds to a 3D nano-wire of diameter 1 a.u. (This is calculated by the same means as above.) This form of the interaction is only used in Chapter 6.

## A.3 Analytical tests

### A.3.1 Converged energy

The many-body ground-state wavefunction is calculated using the imaginary-time propagation of a trial wavefunction. For $t \to -it$ the many-body wavefunction obeys the following equation

$$\Psi(x_1, x_2, x_3, -it) = \Psi_0(x_1, x_2, x_3) e^{-E_0 t} + \Psi_1(x_1, x_2, x_3) e^{-E_1 t} + ..., \tag{A.2}$$

hence, as $t \to \infty$, $\Psi$ converges to the ground-state solution to the Schrödinger equation for our chosen external potential. Therefore, when converged the many-body ground-state energy ($E_0$) can be calculated using the following; for later times

$$\begin{aligned} &\int_{-\infty}^{\infty} \mathrm{d}x_1 \int_{-\infty}^{\infty} \mathrm{d}x_2 \int_{-\infty}^{\infty} \mathrm{d}x_3 \, |\Psi(x_1, x_2, x_3, -it)|^2 \\ &\approx e^{-E_0 t} \int_{-\infty}^{\infty} \mathrm{d}x_1 \int_{-\infty}^{\infty} \mathrm{d}x_2 \int_{-\infty}^{\infty} \mathrm{d}x_3 \, |\Psi_0(x_1, x_2, x_3)|^2, \end{aligned} \tag{A.3}$$

these triple integrals can be labeled as $a$ and $b$ respectively. Therefore,

$$\lim_{t\to\infty} E_0 = \frac{\partial}{\partial t} \ln\left(\frac{b}{a}\right). \tag{A.4}$$

### A.3.2 Time-dependent harmonic well

We begin with the known integral

$$\int_{-\infty}^{\infty} e^{-(z-x)^2} H_n(x)\,\mathrm{d}x = (2z)^n \sqrt{\pi}, \tag{A.5}$$

where $z$ is a constant and $\{H_n(x)\}$ are the set of Hermite polynomials. Expressing the wavefunctions for the three electrons in the shifted well as the superposition of the eigenfunctions of the non-shifted well, where $\psi_k(x,t)$ is the wavefunction of the $k^{\text{th}}$ electron, $\phi_n(x)$ is the $n^{\text{th}}$ eigenfunction of the Hamiltonian of the non-shifted system and $\varepsilon_n$ is the $n^{\text{th}}$ eigenenergy (see Fig. A.3), we get

$$\psi_k(x,t) = \sum_{n=0}^{\infty} c_{k,n}\phi_n(x)e^{-i\varepsilon_n t}. \tag{A.6}$$

Hence, $c_{0,n}$ can be calculated using the overlap integral

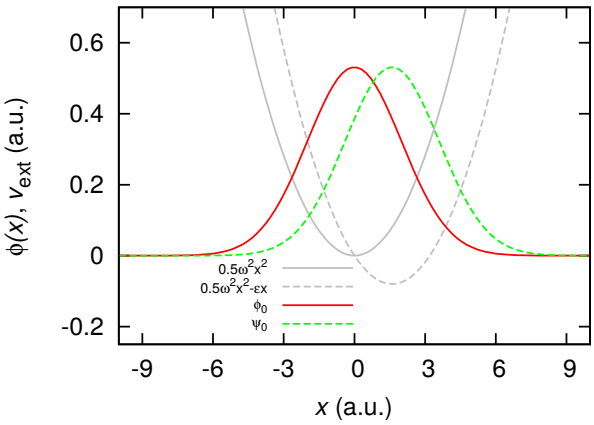


Figure A.3: The harmonic well (grey solid) and the shifted harmonic well (dashed grey). The ground-state ($0^{\text{th}}$) wavefunction for each well. Solid red is the wavefunction that corresponds to the harmonic well, and the dashed green is the wavefunction for the shifted well.

$$\begin{aligned}
c_{0,n} &= \int_{-\infty}^{\infty} \psi_0(x)\,\phi_n^*(x)\,\mathrm{d}x = \sqrt{\frac{\omega}{2^n n!\pi}} \int_{-\infty}^{\infty} e^{-\frac{1}{2}\omega x^2} H_n(y)\, e^{-\frac{1}{2}y^2}\mathrm{d}x, \\
&\text{where} \quad y = \sqrt{\omega}\left(x - \frac{\varepsilon_0}{\omega^2}\right), \Rightarrow \mathrm{d}y = \sqrt{\omega}\mathrm{d}x. \\
&\Rightarrow c_{0,n} = \frac{1}{\sqrt{2^n n!\pi}} \int_{-\infty}^{\infty} e^{-\frac{1}{2}\left(y+\frac{\varepsilon_0}{\sqrt{\omega^3}}\right)^2} H_n(y)\, e^{-\frac{1}{2}y^2}\mathrm{d}y \\
&= \frac{e^{-\frac{\varepsilon_0^2}{4\omega^3}}}{\sqrt{2^n n!\pi}} \int_{-\infty}^{\infty} e^{-\left(y+\frac{\varepsilon_0}{2\sqrt{\omega^3}}\right)^2} H_n(y)\,\mathrm{d}y \\
&= \sqrt{\frac{2^n}{n!}}\left(-\frac{\varepsilon_0}{2\sqrt{\omega^3}}\right)^n e^{-\frac{\varepsilon_0^2}{4\omega^3}} = \sqrt{\frac{2^n}{n!}}(-\alpha)^n e^{-\alpha^2},
\end{aligned} \tag{A.7}$$

where $\alpha = \varepsilon_0/2\sqrt{\omega^3}$. Thus

$$\psi_0(x,t) = \left(\frac{\omega}{\pi}\right)^{\frac{1}{4}} e^{-\frac{1}{2}\omega x^2 - \alpha^2} \sum_{n=0}^{\infty} \frac{1}{n!} (-\alpha)^n H_n(\sqrt{\omega}x) e^{-i\left(n+\frac{1}{2}\right)\omega t}. \tag{A.8}$$

Next we use this result to calculate the first excited state wavefunction for our second electron. Making use of Eq. (A.9), which is a standard relationship between the Hermite polynomials, we derive $c_{1,n}$;

$$H_{n+1}(y) = 2yH_n(y) - 2nH_{n-1}(y), \tag{A.9}$$

hence, as before,

$$c_{1,n} = \int_{-\infty}^{\infty} \psi_1(x)\, \phi_n^*(x)\, \mathrm{d}x = \sqrt{\frac{\omega}{2^n \pi n!}} \int_{-\infty}^{\infty} \sqrt{2\omega} x e^{-\frac{1}{2}\omega x^2} H_n(y)\, e^{-\frac{1}{2}y^2} \mathrm{d}x.$$

Using Eq. (A.9) it follows that

$$\begin{aligned} &\Rightarrow \int_{-\infty}^{\infty} e^{-\frac{1}{2}\omega x^2} H_{n+1}(y)\, e^{-\frac{1}{2}y^2} \mathrm{d}x = 2\int_{-\infty}^{\infty} y e^{-\frac{1}{2}\omega x^2} H_n(y)\, e^{-\frac{1}{2}y^2} \mathrm{d}x \\ &- 2n \int_{-\infty}^{\infty} e^{-\frac{1}{2}\omega x^2} H_{n-1}(y)\, e^{-\frac{1}{2}y^2} \mathrm{d}x. \end{aligned}$$

Substituting in Eq. (A.7) we can find a relationship between our unknown $c_{1,n}$ and the known $c_{0,n}$;

$$c_{1,n} = \sqrt{n+1} c_{0,n+1} + \sqrt{\frac{2}{\omega^3}} \varepsilon_0 c_{0,n} - \sqrt{n} c_{0,n-1}.$$

Substitute in the expression for $c_{0,n}$ we get

$$\begin{aligned} c_{1,n} &= \sqrt{\frac{2^{n+1}}{n!}} \left(-\frac{\varepsilon_0}{\sqrt{2\omega^3}}\right)^{n+1} e^{-\frac{\varepsilon_0^2}{4\omega^3}} + \varepsilon_0 \sqrt{\frac{2^{n+1}}{\omega^3 n!}} \left(-\frac{\varepsilon_0}{\sqrt{2\omega^3}}\right)^{n} e^{-\frac{\varepsilon_0^2}{4\omega^3}} \\ &- \sqrt{\frac{n2^{n-1}}{(n-1)!}} \left(-\frac{\varepsilon_0}{\sqrt{2\omega^3}}\right)^{n-1} e^{-\frac{\varepsilon_0^2}{4\omega^3}} \\ &= \left(\frac{\varepsilon_0}{\sqrt{2\omega^3}} - n\frac{\sqrt{2\omega^3}}{\varepsilon_0}\right) \sqrt{\frac{2^n}{n!}} \left(-\frac{\varepsilon_0}{\sqrt{2\omega^3}}\right)^{n} e^{-\frac{\varepsilon_0^2}{4\omega^3}} = \left(\sqrt{2}\alpha - \frac{n}{\sqrt{2}\alpha}\right) c_{0,n}. \end{aligned} \tag{A.10}$$

Thus, the second, spinless electron obeys

$$\psi_1(x,t) = \left(\frac{\omega}{\pi}\right)^{\frac{1}{4}} e^{-\frac{1}{2}\omega x^2 - \alpha^2} \sum_{n=0}^{\infty} \frac{1}{n!} \left(\sqrt{2}\alpha - \frac{n}{\sqrt{2}\alpha}\right) (-\alpha)^n H_n(\sqrt{\omega}x) e^{-i\left(n+\frac{1}{2}\right)\omega t}. \tag{A.11}$$

Finally we consider the third electron. We begin with

$$c_{2,n} = \int_{-\infty}^{\infty} \psi_2(x)\, \phi_n^*(x)\, \mathrm{d}x = \sqrt{\frac{\omega}{2^{n+1}\pi n!}} \int_{-\infty}^{\infty} (2\omega x^2 - 1) e^{-\frac{1}{2}\omega x^2} H_n(y)\, e^{-\frac{1}{2}y^2} \mathrm{d}x,$$

if we multiply the recurrence relation [Eq. (A.9)] by $x$, it is simple to show that

$$\begin{aligned} &\int_{-\infty}^{\infty} x e^{-\frac{1}{2}\omega x^2} H_{n+1}(y) e^{-\frac{1}{2}y^2} \mathrm{d}x \\ &= 2\sqrt{\omega} \int_{-\infty}^{\infty} xy e^{-\frac{1}{2}\omega x^2} H_n(y) e^{-\frac{1}{2}y^2} \mathrm{d}x - 2n \int_{-\infty}^{\infty} x e^{-\frac{1}{2}\omega x^2} H_{n-1}(y) e^{-\frac{1}{2}y^2} \mathrm{d}x. \end{aligned}$$

From this one can derive $c_{2,n}$ in terms of $c_{1,n}$ and $c_{0,n}$, in a very similar fashion to before for the calculation of $c_{1,n}$. (We note that this can be done indefinitely to find $c_{k,n}$ for any $k$.) Thus we substitute our expressions for $c_{1,n}$ and $c_{0,n}$ (in their integral form) into the above expression and find that

$$c_{2,n} = \sqrt{\frac{n+1}{2}} c_{1,n+1} - \frac{1}{\sqrt{2}} c_{0,n} + \sqrt{2}\alpha c_{1,n} + \sqrt{\frac{n}{2}} c_{1,n-1}.$$

Finally we substitute in our analytical expressions for $c_{1,n}$ and $c_{0,n}$ into the above relationship and find that

$$c_{2,n} = \left( \sqrt{2}(\alpha^2 - n) + \frac{n(n-1)}{2\sqrt{2}\alpha^2} \right) \sqrt{\frac{2^n}{n!}} (-\alpha)^n e^{-\alpha^2}. \tag{A.12}$$

Hence the third electron obeys

$$\psi_2(x,t) = \left(\frac{\omega}{\pi}\right)^{\frac{1}{4}} e^{-\frac{1}{2}\omega x^2 - \alpha^2} \cdot \sum_{n=0}^{\infty} \frac{1}{n!} \left( \sqrt{2}(\alpha^2 - n) + \frac{n(n-1)}{2\sqrt{2}\alpha^2} \right) (-\alpha)^n H_n(\sqrt{\omega}x) e^{-i\left(n+\frac{1}{2}\right)\omega t}. \tag{A.13}$$

The electron density can then be calculated using Eq. (2.11). The current can be calculated using

$$j(x) = -\frac{i}{2} \sum_{k=1}^{N} \left( \psi_k^* \frac{\partial \psi_k}{\partial x} - \psi_k \frac{\partial \psi_k^*}{\partial x} \right). \tag{A.14}$$

This serves as a good test for calculating the current as iDEA uses the continuity equation (*i.e.*, $j$ is calculated directly from $n$ and not the wavefunction).

We now use this analytical solution to test whether the quantum harmonic oscillator has classical characteristics. For the classical harmonic oscillator the position of the electron is definite, and is given by $x = A\cos(\omega t)$, where $A$ is the amplitude of the oscillations. Hence, it is trivial to find the times when the electron has a maximum displacement from the origin; $t = n\pi/\omega$, where $n$ is an integer, as well as the time when the velocity (and therefore the current) is at a maximum; $t = n\pi/(2\omega)$. We find that the quantum harmonic oscillator does have classic properties – this may serve as a test for iDEA also.

# Appendix B

# Density functional development

## B.1 The exact Kohn-Sham potential

We note that any Kohn-Sham equation ($i$), for any number of occupied states, can be rearranged to give the exact Kohn-Sham potential, *i.e.*, $v_{\mathrm{s}} = -\frac{1}{2}\phi_i^{-\frac{1}{2}}\nabla^2\phi_i^{\frac{1}{2}}$. However, obviously this cannot be used in practice as the Kohn-Sham orbital is unknown. However, the form of this term may serve as a useful guide when one is developing approximate functionals.

## B.2 Approximate density functionals for the vector potential

We make the following change of gauge

$$\begin{aligned} v' &\to v + \frac{\partial \chi}{\partial t} \\ \mathbf{A}' &\to \mathbf{A} - \nabla\chi, \end{aligned}$$

without affecting the physical characteristics of the system. Where $\chi = -\int_{-\infty}^{r} \frac{\partial \mathbf{u}}{\partial t} \cdot \mathrm{d}r'$. Hence, $v_{\mathrm{SOA}}(\mathbf{r}, t) = \frac{\nabla^2 n}{4n} - \frac{(\nabla n)^2}{8n^2} - \frac{1}{2}u^2$. In order for the physical characteristics of the system to remain the same, we now require a non-zero Kohn-Sham vector potential; $\mathbf{A}_{\mathrm{SOA}} = -\mathbf{u} = -\frac{\mathbf{j}}{n}$.

The simplicity of this $\mathbf{A}_{\mathrm{SOA}}$ in this gauge is remarkable when one considers that this term is capable of reproducing the effects of nonlocal, dynamic steps in the scalar potential. Because of its simplicity and success at reproducing features present in the exact Kohn-Sham potential, the form of this term should be taken into consideration when one is developing improved, time-dependent approximate functionals.

# Bibliography


[1] P. Hohenberg and W. Kohn. Inhomogeneous electron gas. *Phys. Rev.*, 136:B864–B871, Nov 1964.

[2] W. Kohn and L. J. Sham. Self-consistent equations including exchange and correlation effects. *Phys. Rev.*, 140:A1133–A1138, Nov 1965.

[3] J. P. Perdew and Alex Zunger. Self-interaction correction to density-functional approximations for many-electron systems. *Phys. Rev. B*, 23:5048–5079, May 1981.

[4] B. Walker, B. Sheehy, L. F. DiMauro, P. Agostini, K. J. Schafer, and K. C. Kulander. Precision measurement of strong field double ionization of helium. *Phys. Rev. Lett.*, 73:1227–1230, Aug 1994.

[5] D. Bauer. Two-dimensional, two-electron model atom in a laser pulse: Exact treatment, single-active-electron analysis, time-dependent density-functional theory, classical calculations, and nonsequential ionization. *Phys. Rev. A*, 56:3028–3039, Oct 1997.

[6] Manfred Lein and Stephan Kümmel. Exact time-dependent exchange-correlation potentials for strong-field electron dynamics. *Phys. Rev. Lett.*, 94:143003, Apr 2005.

[7] Aron J Cohen, Paula Mori-Sánchez, and Weitao Yang. Insights into current limitations of density functional theory. *Science*, 321(5890):792–794, 2008.

[8] Max Koentopp, Kieron Burke, and Ferdinand Evers. Zero-bias molecular electronics: Exchange-correlation corrections to Landauer's formula. *Phys. Rev. B*, 73:121403, Mar 2006.

[9] M Koentopp, C Chang, K Burke, and R Car. Density functional calculations of nanoscale conductance. *J. Phys: Condensed Matter*, 20, 2008.

[10] J. D. Ramsden and R. W. Godby. Exact density-functional potentials for time-dependent quasiparticles. *Phys. Rev. Lett.*, 109:036402, Jul 2012.

[11] P. Elliott, J. I. Fuks, A. Rubio, and N. T. Maitra. Universal dynamical steps in the exact time-dependent exchange-correlation potential. *Phys. Rev. Lett.*, 109:266404, Dec 2012.

[12] Erich Runge and E. K. U. Gross. Density-functional theory for time-dependent systems. *Phys. Rev. Lett.*, 52:997–1000, Mar 1984.

[13] Robert van Leeuwen. Mapping from densities to potentials in time-dependent density-functional theory. *Phys. Rev. Lett.*, 82:3863–3866, May 1999.

[14] M. J. P. Hodgson, J. D. Ramsden, J. B. J. Chapman, P. Lillystone, and R. W. Godby. Exact time-dependent density-functional potentials for strongly correlated tunneling electrons. *Phys. Rev. B*, 88:241102, Dec 2013.

[15] Louis de Broglie. *Recherches sur la thorie des quanta*. PhD thesis, Paris, France, Nov 1924.

[16] Max Planck. Ueber die elementarquanta der materie und der elektricitt. *Annalen der Physik*, 309(3):564–566, 1901.

[17] A. Einstein. Über einen die erzeugung und verwandlung des lichtes betreffenden heuristischen gesichtspunkt. *Annalen der Physik*, 322(6):132–148, 1905.

[18] M. Born and R. Oppenheimer. Zur quantentheorie der molekeln. *Ann. Phys.*, 389:457–484, 1927.

[19] Mel Levy. Universal variational functionals of electron densities, first-order density matrices, and natural spin-orbitals and solution of the v-representability problem. *Proceedings of the National Academy of Sciences*, 76(12):6062–6065, 1979.

[20] O. Gunnarsson and B. I. Lundqvist. Exchange and correlation in atoms, molecules, and solids by the spin-density-functional formalism. *Phys. Rev. B*, 13:4274–4298, May 1976.

[21] John P Perdew, Robert G Parr, Mel Levy, and Jose L Balduz Jr. Density-functional theory for fractional particle number: Derivative discontinuities of the energy. *Phys. Rev. Lett.*, 49(23):1691, 1982.

[22] Mel Levy, John P. Perdew, and Viraht Sahni. Exact differential equation for the density and ionization energy of a many-particle system. *Phys. Rev. A*, 30:2745–2748, Nov 1984.

[23] C.-O. Almbladh and U. von Barth. Exact results for the charge and spin densities, exchange-correlation potentials, and density-functional eigenvalues. *Phys. Rev. B*, 31:3231–3244, Mar 1985.

[24] Elliott H Lieb and Stephen Oxford. Improved lower bound on the indirect coulomb energy. *International Journal of Quantum Chemistry*, 19(3):427–439, 1981.

[25] D. M. Ceperley and B. J. Alder. Ground state of the electron gas by a stochastic method. *Phys. Rev. Lett.*, 45:566–569, Aug 1980.

[26] John P. Perdew and Yue Wang. Accurate and simple analytic representation of the electron-gas correlation energy. *Phys. Rev. B*, 45:13244–13249, Jun 1992.

[27] I. N. Remediakis and Efthimios Kaxiras. Band-structure calculations for semiconductors within generalized-density-functional theory. *Phys. Rev. B*, 59:5536–5543, Feb 1999.

[28] A. van de Walle and G. Ceder. Correcting overbinding in local-density-approximation calculations. *Phys. Rev. B*, 59:14992–15001, Jun 1999.

[29] John P. Perdew and Mel Levy. Comment on Significance of the highest occupied Kohn-Sham eigenvalue. *Phys. Rev. B*, 56:16021–16028, Dec 1997.

[30] John P. Perdew, Kieron Burke, and Matthias Ernzerhof. Generalized gradient approximation made simple. *Phys. Rev. Lett.*, 77:3865–3868, Oct 1996.

[31] Paul Ziesche, Stefan Kurth, and John P Perdew. Density functionals from LDA to GGA. *Computational materials science*, 11(2):122–127, 1998.

[32] T. Asada and K. Terakura. Cohesive properties of iron obtained by use of the generalized gradient approximation. *Phys. Rev. B*, 46:13599–13602, Nov 1992.

[33] Charlotte Froese Fischer. Multi-configuration Hartree-Fock Program. Technical report, Univ. of Waterloo, Ont., 1970.

[34] Charlotte Froese Fischer. General Hartree-Fock program. *Computer physics communications*, 43(3):355–365, 1987.

[35] F. Evers, F. Weigend, and M. Koentopp. Conductance of molecular wires and transport calculations based on density-functional theory. *Phys. Rev. B*, 69:235411, Jun 2004.

[36] Kieron Burke, Jan Werschnik, and E. K. U. Gross. Time-dependent density functional theory: Past, present, and future. *The Journal of Chemical Physics*, 123(6), 2005.

[37] ChiYung Yam, Xiao Zheng, GuanHua Chen, Yong Wang, Thomas Frauenheim, and Thomas A. Niehaus. Time-dependent versus static quantum transport simulations beyond linear response. *Phys. Rev. B*, 83:245448, Jun 2011.

[38] G. Vignale. Center of mass and relative motion in time dependent density functional theory. *Phys. Rev. Lett.*, 74:3233–3236, Apr 1995.

[39] Paul Hessler, Jang Park, and Kieron Burke. Several theorems in time-dependent density functional theory. *Phys. Rev. Lett.*, 82:378–381, Jan 1999.

[40] M. A. L. Marques and E. K. U. Gross. A tutorial on density functional theory. In C Fiolhais, F Nogueira, and M.A.L Marques, editors, *A Primer in Density Functional theory*, Lecture Notes in Physics. Springer-Verlag, 2003.

[41] Benoît Braïda, Philippe C Hiberty, and Andreas Savin. A systematic failing of current density functionals: overestimation of two-center three-electron bonding energies. *The Journal of Physical Chemistry A*, 102(40):7872–7877, 1998.

[42] M. Grüning, O. V. Gritsenko, and E. J. Baerends. Improved Description of Chemical Barriers with Generalized Gradient Approximations (GGAs) and Meta-GGAs. *The Journal of Physical Chemistry A*, 108(20):4459–4469, 2004.

[43] Benny G Johnson, Carlos A Gonzales, Peter M W Gill, and John A Pople. A density functional study of the simplest hydrogen abstraction reaction. Effect of self-interaction correction. *Chem. Phys. Lett.*, 221(1-2):100–108, 1994.

[44] Dirk Porezag and Mark R Pederson. Density functional based studies of transition states and barriers for hydrogen exchange and abstraction reactions. *J. Chem. Phys.*, 102(23):9345–9349, 1995.

[45] Sergei Skokov and Ralph A Wheeler. Study of hydrogen abstraction reactions by density-functional methods. *Chem. Phys. Lett.*, 271(4):251–258, 1997.

[46] John P Perdew. Density functional theory and the band gap problem. *International Journal of Quantum Chemistry*, 28(S19):497–523, 1985.

[47] Myrta Grüning, Andrea Marini, and Angel Rubio. Density functionals from many-body perturbation theory: The band gap for semiconductors and insulators. *The Journal of Chemical Physics*, 124(15), 2006.

[48] Myrta Grüning, Andrea Marini, and Angel Rubio. Effect of spatial nonlocality on the density functional band gap. *Phys. Rev. B*, 74:161103, Oct 2006.

[49] John P. Pardew. Density-functional theory and excitation energies. In *Density Functional Methods in Physics*, pages 265–308. Springer, 1985.

[50] M. Grüning, O. V. Gritsenko, S. J. A. van Gisbergen, , and E. J. Baerends. The Failure of Generalized Gradient Approximations (GGAs) and Meta-GGAs for the Two-Center Three-Electron Bonds in $He_2^+$, $(H_2O)^{2+}$, and $(NH_3)^{2+}$. *The Journal of Physical Chemistry A*, 105(40):9211–9218, 2001.

[51] M. Grüning, O. V. Gritsenko, and E. J. Baerends. Exchange-correlation energy and potential as approximate functionals of occupied and virtual Kohn-Sham orbitals: Application to dissociating $H_2$. *The Journal of Chemical Physics*, 118(16):7183–7192, 2003.

[52] R. W. Godby, M. Schlüter, and L. J. Sham. Self-energy operators and exchange-correlation potentials in semiconductors. *Phys. Rev. B*, 37:10159–10175, Jun 1988.

[53] R. W. Godby, M. Schlüter, and L. J. Sham. Accurate exchange-correlation potential for silicon and its discontinuity on addition of an electron. *Phys. Rev. Lett.*, 56:2415–2418, Jun 1986.

[54] Giovanni Onida, Lucia Reining, and Angel Rubio. Electronic excitations: density-functional versus many-body green's-function approaches. *Rev. Mod. Phys.*, 74:601–659, Jun 2002.

[55] M. Shishkin, M. Marsman, and G. Kresse. Accurate quasiparticle spectra from self-consistent *GW* calculations with vertex corrections. *Phys. Rev. Lett.*, 99:246403, Dec 2007.

[56] R. W. Godby, M. Schlüter, and L. J. Sham. Trends in self-energy operators and their corresponding exchange-correlation potentials. *Phys. Rev. B*, 36:6497–6500, Oct 1987.

[57] Hongliang Shi, Hui Pan, Yong-Wei Zhang, and Boris I. Yakobson. Quasiparticle band structures and optical properties of strained monolayer $MoS_2$ and $WS_2$. *Phys. Rev. B*, 87:155304, Apr 2013.

[58] U. Salzner, P. G. Pickup, R. A. Poirier, and J. B. Lagowski. Accurate Method for Obtaining Band Gaps in Conducting Polymers Using a DFT/Hybrid Approach. *The Journal of Physical Chemistry A*, 102(15):2572–2578, 1998.

[59] Paula Mori-Sánchez, Aron J. Cohen, and Weitao Yang. Localization and delocalization errors in density functional theory and implications for band-gap prediction. *Phys. Rev. Lett.*, 100:146401, Apr 2008.

[60] Aron J. Cohen, Paula Mori-Snchez, and Weitao Yang. Fractional spins and static correlation error in density functional theory. *The Journal of Chemical Physics*, 129(12), 2008.

[61] Mariona Sodupe, Juan Bertran, Luis Rodrguez-Santiago, and E. J. Baerends. Ground State of the $(H_2O)^{2+}$ Radical Cation: DFT versus Post-HartreeFock Methods. *The Journal of Physical Chemistry A*, 103(1):166–170, 1999.

[62] Thomas Bally and G. Narahari Sastry. Incorrect Dissociation Behavior of Radical Ions in Density Functional Calculations. *The Journal of Physical Chemistry A*, 101(43):7923–7925, 1997.

[63] Adrienn Ruzsinszky, John P. Perdew, Gbor I. Csonka, Oleg A. Vydrov, and Gustavo E. Scuseria. Spurious fractional charge on dissociated atoms: Pervasive and resilient self-interaction error of common density functionals. *The Journal of Chemical Physics*, 125(19), 2006.

[64] Paula Mori-Snchez, Aron J. Cohen, and Weitao Yang. Many-electron self-interaction error in approximate density functionals. *The Journal of Chemical Physics*, 125(20), 2006.

[65] Kieron Burke. Perspective on density functional theory. *The Journal of Chemical Physics*, 136(15), 2012.

[66] Robert M Metzger, Bo Chen, Ulf Höpfner, MV Lakshmikantham, Dominique Vuillaume, Tsuyoshi Kawai, Xiangli Wu, Hiroaki Tachibana, Terry V Hughes, Hiromi Sakurai, et al. Unimolecular electrical rectification in hexadecylquinolinium tricyanoquinodimethanide. *Journal of the American Chemical Society*, 119(43):10455–10466, 1997.

[67] J Chen, MA Reed, AM Rawlett, and JM Tour. Large on-off ratios and negative differential resistance in a molecular electronic device. *Science*, 286(5444):1550–1552, 1999.

[68] Mark A Reed, C Zhou, CJ Muller, TP Burgin, and JM Tour. Conductance of a molecular junction. *Science*, 278(5336):252–254, 1997.

[69] B. J. van Wees, H. van Houten, C. W. J. Beenakker, J. G. Williamson, L. P. Kouwenhoven, D. van der Marel, and C. T. Foxon. Quantized conductance of point contacts in a two-dimensional electron gas. *Phys. Rev. Lett.*, 60:848–850, Feb 1988.

[70] D A Wharam, T J Thornton, R Newbury, M Pepper, H Ahmed, J E F Frost, D G Hasko, D C Peacock, D A Ritchie, and G A C Jones. One-dimensional transport and the quantisation of the ballistic resistance. *Journal of Physics C: Solid State Physics*, 21(8):L209, 1988.

[71] Rolf Landauer. Spatial variation of currents and fields due to localized scatterers in metallic conduction. *IBM Journal of Research and Development*, 1(3):223–231, 1957.

[72] Giovanni Vignale and Massimiliano Di Ventra. Incompleteness of the Landauer formula for electronic transport. *Phys. Rev. B*, 79:014201, Jan 2009.

[73] Yigal Meir and Ned S. Wingreen. Landauer formula for the current through an interacting electron region. *Phys. Rev. Lett.*, 68:2512–2515, Apr 1992.

[74] C. A. Ullrich. Time-dependent density-functional theory beyond the adiabatic approximation: Insights from a two-electron model system. *The Journal of Chemical Physics*, 125(23), 2006.

[75] Neepa T. Maitra, Fan Zhang, Robert J. Cave, and Kieron Burke. Double excitations within time-dependent density functional theory linear response. *The Journal of Chemical Physics*, 120(13):5932–5937, 2004.

[76] Myrta Grüning and Xavier Gonze. Macroscopic limit of time-dependent density-functional theory for adiabatic local approximations of the exchange-correlation kernel. *Phys. Rev. B*, 76:035126, Jul 2007.

[77] K. J. H. Giesbertz and E. J. Baerends. Failure of time-dependent density functional theory for excited state surfaces in case of homolytic bond dissociation. *Chemical Physics Letters*, 461(4):338–342, 2008.

[78] R. J. Magyar and S. Tretiak. Dependence of spurious charge-transfer excited states on orbital exchange in tddft: large molecules and clusters. *Journal of chemical theory and computation*, 3(3):976–987, 2007.

[79] Max Koentopp, Kieron Burke, and Ferdinand Evers. Zero-bias molecular electronics: Exchange-correlation corrections to landauer's formula. *Physical Review B*, 73(12):121403, 2006.

[80] C. Toher, A. Filippetti, S. Sanvito, and Kieron Burke. Self-interaction errors in density-functional calculations of electronic transport. *Phys. Rev. Lett.*, 95:146402, Sep 2005.

[81] M. Grüning, O. V. Gritsenko, S. J. A. van Gisbergen, and E. J. Baerends. Shape corrections to exchange-correlation potentials by gradient-regulated seamless connection of model potentials for inner and outer region. *The Journal of Chemical Physics*, 114(2):652–660, 2001.

[82] Paul Hessler, Neepa T Maitra, and Kieron Burke. Correlation in time-dependent density-functional theory. *The Journal of chemical physics*, 117(1):72–81, 2002.

[83] David J Tozer and Nicholas C Handy. On the determination of excitation energies using density functional theory. *Physical Chemistry Chemical Physics*, 2(10):2117–2121, 2000.

[84] Christine Jamorski, Mark E. Casida, and Dennis R. Salahub. Dynamic polarizabilities and excitation spectra from a molecular implementation of time-dependent density-functional response theory: $N_2$ as a case study. *The Journal of Chemical Physics*, 104(13):5134–5147, 1996.

[85] Max Koentopp, Connie Chang, Kieron Burke, and Roberto Car. Density functional calculations of nanoscale conductance. *Journal of Physics: Condensed Matter*, 20(8):083203, 2008.

[86] M. Dorogi, J. Gomez, R. Osifchin, R. P. Andres, and R. Reifenberger. Room-temperature Coulomb blockade from a self-assembled molecular nanostructure. *Phys. Rev. B*, 52:9071–9077, Sep 1995.

[87] Ronald P Andres, Thomas Bein, Matt Dorogi, Sue Feng, Jason I Henderson, Clifford P Kubiak, William Mahoney, Richard G Osifchin, and R Reifenberger. Coulomb staircase at room temperature in a self-assembled molecular nanostructure. *Science*, 272(5266):1323–1325, 1996.

[88] LA Bumm, JJ Arnold, MT Cygan, TD Dunbar, et al. Are single molecular wires conducting? *Science*, 271(5256):1705, 1996.

[89] Gianluca Stefanucci and Stefan Kurth. Steady-state density functional theory for finite bias conductances. *Nano letters*, 15(12):8020–8025, 2015.

[90] I. D'Amico, J. P. Coe, V. V. França, and K. Capelle. Quantum mechanics in metric space: Wave functions and their densities. *Phys. Rev. Lett.*, 106:050401, Feb 2011.

[91] P. M. Sharp and I. D'Amico. Metric space formulation of quantum mechanical conservation laws. *Phys. Rev. B*, 89:115137, Mar 2014.

[92] Thomas F Gallagher. Rydberg Atoms (Cambridge monographs on atomic, molecular and chemical physics), 1994.

[93] YO Dudin and A Kuzmich. Strongly interacting rydberg excitations of a cold atomic gas. *Science*, 336(6083):887–889, 2012.

[94] Mark E Casida. Time-dependent density-functional theory for molecules and molecular solids. *Journal of Molecular Structure: THEOCHEM*, 914(1):3–18, 2009.

[95] Mark E Casida, Kim C Casida, and Dennis R Salahub. Excited-state potential energy curves from time-dependent density-functional theory: A cross section of formaldehyde's 1a1 manifold. *International journal of quantum chemistry*, 70(4-5):933–941, 1998.

[96] David J Tozer and Nicholas C Handy. Improving virtual Kohn-Sham orbitals and eigenvalues: Application to excitation energies and static polarizabilities. *The Journal of chemical physics*, 109(23):10180–10189, 1998.

[97] Mark E Casida. Jacob's ladder for time-dependent density-functional theory: Some rungs on the way to photochemical heaven. In *ACS Symposium Series*, volume 828, pages 199–220. Washington, DC; American Chemical Society; 1999, 2002.

[98] Sébastien Hamel, Mark E Casida, and Dennis R Salahub. Exchange-only optimized effective potential for molecules from resolution-of-the-identity techniques: Comparison with the local density approximation, with and without asymptotic correction. *The Journal of chemical physics*, 116(19):8276–8291, 2002.

[99] Andreas Dreuw, Jennifer L Weisman, and Martin Head-Gordon. Long-range charge-transfer excited states in time-dependent density functional theory require non-local exchange. *The Journal of chemical physics*, 119(6):2943–2946, 2003.

[100] Mark E Casida and Tomasz A Wesołowski. Generalization of the Kohn-Sham equations with constrained electron density formalism and its time-dependent response theory formulation. *International journal of quantum chemistry*, 96(6):577–588, 2004.

[101] Mark E Casida, Christine Jamorski, Kim C Casida, and Dennis R Salahub. Molecular excitation energies to high-lying bound states from time-dependent density-functional response theory: Characterization and correction of the time-dependent local density approximation ionization threshold. *The Journal of chemical physics*, 108(11):4439–4449, 1998.

[102] G. F. Bertsch, J.-I. Iwata, Angel Rubio, and K. Yabana. Real-space, real-time method for the dielectric function. *Phys. Rev. B*, 62:7998–8002, Sep 2000.

[103] John Hubbard. Electron correlations in narrow energy bands. In *Proceedings of the Royal Society of London A: mathematical, physical and engineering sciences*, volume 276, pages 238–257. The Royal Society, 1963.

[104] Johanna I. Fuks, Mehdi Farzanehpour, Ilya V. Tokatly, Heiko Appel, Stefan Kurth, and Angel Rubio. Time-dependent exchange-correlation functional for a Hubbard dimer: Quantifying nonadiabatic effects. *Phys. Rev. A*, 88:062512, Dec 2013.

[105] L. Mancini, J. D. Ramsden, M. J. P. Hodgson, and R. W. Godby. Adiabatic and local approximations for the Kohn-Sham potential in time-dependent Hubbard chains. *Phys. Rev. B*, 89:195114, May 2014.

[106] N. Metropolis and S. Ulam. The Monte Carlo Method. *Journal of the American Statistical Association*, 44(247):335–341, 1949.

[107] Ariel Gordon, Robin Santra, and Franz X. Kärtner. Role of the Coulomb singularity in high-order harmonic generation. *Phys. Rev. A*, 72:063411, Dec 2005.

[108] J. Crank and P. Nicolson. A practical method for numerical evaluation of solutions of partial differential equations of the heat-conduction type. *Proceedings of the Cambridge Philosophical Society*, 43:50–67, 1947.

[109] R. van Leeuwen and E. J. Baerends. Exchange-correlation potential with correct asymptotic behavior. *Phys. Rev. A*, 49:2421–2431, Apr 1994.

[110] John F. Dobson. Harmonic-potential theorem: Implications for approximate many-body theories. *Phys. Rev. Lett.*, 73:2244–2247, Oct 1994.

[111] M. Taut. Two electrons in an external oscillator potential: Particular analytic solutions of a Coulomb correlation problem. *Phys. Rev. A*, 48:3561–3566, Nov 1993.

[112] Darwin W Smith, Salem Jagannathan, and George S Handler. Density functional theory of atomic structure. i. exchange and correlation potentials for two-electron atoms. *International Journal of Quantum Chemistry*, 16(S13):103–110, 1979.

[113] M. J. P. Hodgson, J. D. Ramsden, T. R. Durrant, and R. W. Godby. Role of electron localization in density functionals. *Phys. Rev. B*, 90:241107, Dec 2014.

[114] D. M. Ceperley and B. J. Alder. Ground state of the electron gas by a stochastic method. *Phys. Rev. Lett.*, 45:566–569, Aug 1980.

[115] R.M. Dreizler and E.K.U. Gross. *Density Functional Theory: An Approach to the Quantum Many-Body Problem*. Springer Berlin Heidelberg, 2012.

[116] R.G. Parr and W. Yang. *Density-Functional Theory of Atoms and Molecules*. International Series of Monographs on Chemistry. Oxford University Press, USA, 1994.

[117] Manfred Lein, E. K. U. Gross, and John P. Perdew. Electron correlation energies from scaled exchange-correlation kernels: Importance of spatial versus temporal nonlocality. *Phys. Rev. B*, 61:13431–13437, May 2000.

[118] O. V. Gritsenko, S. J. A. Van Gisbergen, A. Görling, E. J. Baerends, et al. Excitation energies of dissociating $H_2$: A problematic case for the adiabatic approximation of time-dependent density functional theory. *J. Chem. Phys*, 113(19):8478–8489, 2000.

[119] Neepa T. Maitra, Kieron Burke, and Chris Woodward. Memory in time-dependent density functional theory. *Phys. Rev. Lett.*, 89:023002, Jun 2002.

[120] Daniele Varsano, Andrea Marini, and Angel Rubio. Optical saturation driven by exciton confinement in molecular chains: A time-dependent density-functional theory approach. *Phys. Rev. Lett.*, 101:133002, Sep 2008.

[121] Robert O Jones and Olle Gunnarsson. The density functional formalism, its applications and prospects. *Reviews of Modern Physics*, 61(3):689, 1989.

[122] Warren E. Pickett. Pseudopotential methods in condensed matter applications. *Computer Physics Reports*, 9:115 – 197, Apr 1989.

[123] X. Gonze, Ph. Ghosez, and R. W. Godby. Density-functional theory of polar insulators. *Phys. Rev. Lett.*, 78:294–297, Jan 1997.

[124] M. Di Ventra, S. T. Pantelides, and N. D. Lang. First-principles calculation of transport properties of a molecular device. *Phys. Rev. Lett.*, 84:979–982, Jan 2000.

[125] Max Koentopp, Connie Chang, Kieron Burke, and Roberto Car. Density functional calculations of nanoscale conductance. *Journal of Physics: Condensed Matter*, 20:083203, Feb 2008.

[126] N. Helbig, J. I. Fuks, M. Casula, M. J. Verstraete, M. A. L. Marques, I. V. Tokatly, and A. Rubio. Density functional theory beyond the linear regime: Validating an adiabatic local density approximation. *Phys. Rev. A*, 83:032503, Mar 2011.

[127] Luke Shulenburger, Michele Casula, Gaetano Senatore, and Richard M Martin. Spin resolved energy parametrization of a quasi-one-dimensional electron gas. *J. Phys. A*, 42(21):214021, 2009.

[128] Michele Casula, Sandro Sorella, and Gaetano Senatore. Ground state properties of the one-dimensional Coulomb gas using the lattice regularized diffusion Monte Carlo method. *Phys. Rev. B*, 74:245427, Dec 2006.

[129] Thomas E. Baker, E. Miles Stoudenmire, Lucas O. Wagner, Kieron Burke, and Steven R. White. One-dimensional mimicking of electronic structure: The case for exponentials. *Phys. Rev. B*, 91:235141, Jun 2015.

[130] Gao Xianlong, Marco Polini, M. P. Tosi, Vivaldo L. Campo, Klaus Capelle, and Marcos Rigol. Bethe ansatz density-functional theory of ultracold repulsive fermions in one-dimensional optical lattices. *Phys. Rev. B*, 73:165120, Apr 2006.

[131] Lee A. Cole and J. P. Perdew. Calculated electron affinities of the elements. *Phys. Rev. A*, 25:1265–1271, Mar 1982.

[132] Randolph Q. Hood, M. Y. Chou, A. J. Williamson, G. Rajagopal, R. J. Needs, and W. M. C. Foulkes. Quantum monte carlo investigation of exchange and correlation in silicon. *Phys. Rev. Lett.*, 78:3350–3353, Apr 1997.

[133] Min-Cheol Kim, Eunji Sim, and Kieron Burke. Understanding and reducing errors in density functional calculations. *Phys. Rev. Lett.*, 111:073003, Aug 2013.

[134] T.R. Durrant, M.J.P. Hodgson, J.D. Ramsden, and R.W. Godby. Electron localization in static and time-dependent systems. *arXiv:1505.07687*, 2015.

[135] John F Dobson. Interpretation of the Fermi hole curvature. *J. Chem. Phys.*, 94(6):4328–4333, 1991.

[136] A. D. Becke and K. E. Edgecombe. A simple measure of electron localization in atomic and molecular systems. *The Journal of Chemical Physics*, 92(9):5397–5403, 1990.

[137] Maria Hellgren and E. K. U. Gross. Discontinuities of the exchange-correlation kernel and charge-transfer excitations in time-dependent density-functional theory. *Phys. Rev. A*, 85:022514, Feb 2012.

[138] M. J. P. Hodgson, J. D. Ramsden, and R. W. Godby. Origin of static and dynamic steps in exact Kohn-Sham potentials. *Phys. Rev. B*, 93:155146, Apr 2016.

[139] Daniel Vieira, Klaus Capelle, and Carsten A Ullrich. Physical signatures of discontinuities of the time-dependent exchange–correlation potential. *Physical Chemistry Chemical Physics*, 11(22):4647–4654, 2009.

[140] S. Kurth, G. Stefanucci, E. Khosravi, C. Verdozzi, and E. K. U. Gross. Dynamical Coulomb Blockade and the Derivative Discontinuity of Time-Dependent Density Functional Theory. *Phys. Rev. Lett.*, 104:236801, Jun 2010.

[141] Jian Wang and Alexei A Stuchebrukhov. DFT calculation of electron tunneling currents: Real-space (grid) molecular orbitals vs. Gaussian-type molecular orbitals. *International Journal of Quantum Chemistry*, 80(4-5):591–597, 2000.

[142] Yan Zhao and Donald G Truhlar. Density functional for spectroscopy: no long-range self-interaction error, good performance for Rydberg and charge-transfer states, and better performance on average than B3LYP for ground states. *The Journal of Physical Chemistry A*, 110(49):13126–13130, 2006.

[143] Andreas Savin, Reinhard Nesper, Steffen Wengert, and Thomas F Fässler. ELF: The electron localization function. *Angew. Chem. Int. Ed.*, 36(17):1808–1832, 1997.

[144] Bernard Silvi and Andreas Savin. Classification of chemical bonds based on topological analysis of electron localization functions. *Nature*, 371(6499):683–686, 1994.

[145] Walter Kohn and Ann E Mattsson. Edge electron gas. *Phys. Rev. Lett.*, 81(16):3487, 1998.

[146] Feng Hao, Rickard Armiento, and Ann E Mattsson. Using the electron localization function to correct for confinement physics in semi-local density functional theory. *J. Chem. Phys.*, 140(18):18A536, 2014.

[147] Jianwei Sun, Adrienn Ruzsinszky, and John P. Perdew. Strongly constrained and appropriately normed semilocal density functional. *Phys. Rev. Lett.*, 115:036402, Jul 2015.

[148] T. R. Durrant, M. J. P. Hodgson, J. D. Ramsden, and R. W. Godby. Electron localization in static and time-dependent systems. *arXiv preprint arXiv:1505.07687*, 2015.

[149] Eduard Matito, Bernard Silvi, Miquel Duran, and Miquel Solà. Electron localization function at the correlated level. *J. Chem. Phys.*, 125(2):024301, 2006.

[150] Stefano Pittalis, Alain Delgado, and Carlo Andrea Rozzi. Same-spin dynamical correlation effects on the electron localization. *arXiv preprint arXiv:1509.04089*, 2015.

[151] Carl O Almbladh and Ulf von Barth. Density-functional theory and excitation energies. In *Density Functional Methods in Physics*, pages 209–231. Springer, 1985.

[152] S. J. A. Van Gisbergen, P. R. T. Schipper, O. V. Gritsenko, E. J. Baerends, J. G. Snijders, B. Champagne, and B. Kirtman. Electric field dependence of the exchange-correlation potential in molecular chains. *Phys. Rev. Lett.*, 83(4):694, 1999.

[153] X. Gonze, Ph. Ghosez, and R. W. Godby. Density-polarization functional theory of the response of a periodic insulating solid to an electric field. *Phys. Rev. Lett.*, 74:4035–4038, May 1995.

[154] M. van Faassen, P. L. de Boeij, R. van Leeuwen, J. A. Berger, and J. G. Snijders. Ultranonlocality in time-dependent current-density-functional theory: Application to conjugated polymers. *Phys. Rev. Lett.*, 88:186401, Apr 2002.

[155] M Van Faassen, PL De Boeij, R Van Leeuwen, JA Berger, and JG Snijders. Application of time-dependent current-density-functional theory to nonlocal exchange-correlation effects in polymers. *J. Chem. Phys.*, 118(3):1044–1053, 2003.

[156] D. Torelli. Functionals for TDDFT description of electron transport in nanostructures. Master's thesis, University of Bologna, Bologna, July 2016.

[157] Robert van Leeuwen, Oleg Gritsenko, and EvertJan Baerends. Step structure in the atomic Kohn-Sham potential. *Zeitschrift für Physik D Atoms, Molecules and Clusters*, 33(4):229–238, 1995.

[158] N. Helbig, I. V. Tokatly, and A. Rubio. Exact Kohn-Sham potential of strongly correlated finite systems. *The Journal of Chemical Physics*, 131(22), 2009.

[159] Oleg V. Gritsenko and Evert Jan Baerends. Effect of molecular dissociation on the exchange-correlation Kohn-Sham potential. *Phys. Rev. A*, 54:1957–1972, Sep 1996.

[160] Kai Luo, Peter Elliott, and Neepa T. Maitra. Absence of dynamical steps in the exact correlation potential in the linear response regime. *Phys. Rev. A*, 88:042508, Oct 2013.

[161] Zeng-hui Yang, John R. Trail, Aurora Pribram-Jones, Kieron Burke, Richard J. Needs, and Carsten A. Ullrich. Exact and approximate Kohn-Sham potentials in ensemble density-functional theory. *Phys. Rev. A*, 90:042501, Oct 2014.

[162] M. Fuchs, Y.-M. Niquet, X. Gonze, and K. Burke. Describing static correlation in bond dissociation by Kohn-Sham density functional theory. *The Journal of Chemical Physics*, 122(9), 2005.

[163] John P. Perdew and Mel Levy. Physical Content of the Exact Kohn-Sham Orbital Energies: Band Gaps and Derivative Discontinuities. *Phys. Rev. Lett.*, 51:1884–1887, Nov 1983.

[164] Adi Makmal, Stephan Kümmel, and Leeor Kronik. Dissociation of diatomic molecules and the exact-exchange Kohn-Sham potential: The case of LiF. *Phys. Rev. A*, 83:062512, Jun 2011.

[165] Fabio Della Sala and Andreas Görling. Asymptotic Behavior of the Kohn-Sham Exchange Potential. *Phys. Rev. Lett.*, 89:033003, Jun 2002.

[166] Jianmin Tao, John P. Perdew, Viktor N. Staroverov, and Gustavo E. Scuseria. Climbing the Density Functional Ladder: Nonempirical Meta-Generalized Gradient Approximation Designed for Molecules and Solids. *Phys. Rev. Lett.*, 91:146401, Sep 2003.

[167] David G Tempel, Todd J Martinez, and Neepa T Maitra. Revisiting molecular dissociation in density functional theory: a simple model. *Journal of chemical theory and computation*, 5(4):770–780, 2009.